

ALTERATION MAPPING BY REMOTE SENSING: APPLICATION TO
HASANDAĞ – MELENDİZ VOLCANIC COMPLEX

A THESIS SUBMITTED TO
THE GRADUATE SCHOOL OF NATURAL AND APPLIED SCIENCES
OF
THE MIDDLE EAST TECHNICAL UNIVERSITY

BY

ERDEM YETKİN

IN PARTIAL FULFILLMENT OF THE REQUIREMENTS FOR THE DEGREE OF
MASTER OF SCIENCE
IN
THE DEPARTMENT OF GEOLOGICAL ENGINEERING

SEPTEMBER 2003

Approval of the Graduate School of Natural and Applied Sciences

Prof. Dr. Canan ÖZGEN
Director

I certify that this thesis satisfies all the requirements as a thesis for the degree of
Master of Science.

Prof. Dr. Asuman G. TÜRKMENOĞLU
Head of Department

This is to certify that we have read this thesis and that in our opinion it is fully
adequate, in scope and quality, as a thesis for the degree of Master of Science.

Assist. Prof. Dr. M. Lütfi SÜZEN
Co-Supervisor

Assoc. Prof. Dr. Vedat TOPRAK
Supervisor

Examining Committee Members

Assoc. Prof. Dr. Vedat TOPRAK

Assist. Prof. Dr. Mustafa Türker

Assist. Prof. Dr. M. Lütfi SÜZEN

Dr. Arda ARCASOY

Dr. Mesut SOYLU

ABSTRACT

ALTERATION MAPPING BY REMOTE SENSING: APPLICATION TO HASANDAĞ – MELENDİZ VOLCANIC COMPLEX

Yetkin, Erdem

M.Sc., Department of Geological Engineering

Supervisor: Assoc. Prof. Dr. Vedat Toprak

Co-Supervisor: Assist. Prof. Dr. M. Lütfi Szen

September 2003, 94 pages

Certain alteration minerals are used to identify the hydrothermally altered rocks. Potassic, phyllic (sericitic), propylitic, argillic and silicification are main alteration types observed in volcanic rocks. The role of remote sensing in alteration mapping is the differentiation of the minerals that are unique for different alteration types.

In this study, Landsat TM 5 images are used. General alteration trend in the area is mapped by conventional methods of color composite, band rationing, principal component analysis and multi-linear regression analysis.

Detailed mineral mapping carried on by using the United States Geological Survey (USGS) spectral library data. Spectral reflectances of selected minerals are analyzed according to the TM band intervals and appropriate band ratios are selected. TM bands 1,2,3,4,5 and 7 are used. Outputs of mineral maps are investigated for zonal distribution.

Mineral maps that are obtained by the mineral separation method reveal that the youngest volcanic complex Hasandağ is poorly altered. Instead, Keçiboyduran, Melendiz and Tepeköy volcanic complexes are found to be highly altered with the pattern of clay dominant in the center and increasing oxidation towards flanks. Also the alteration along the previously mapped buried faults is a proof that the method can provide information about the alteration source.

Key Words: Remote sensing, alteration mapping, spectral library, Cappadocian Volcanic Province.

ÖZ

UZAKTAN ALGILAMA İLE ALTERASYON HARİTALAMASI: HASANDAĞ – MELENDİZ VOLKANİK KOMPLEKSİNE UYGULANMASI

Yetkin, Erdem

Yüksek Lisans, Jeoloji Mühendisliği Bölümü

Tez Yöneticisi: Doç. Dr. Vedat Toprak

Ortak Tez Yöneticisi: Y. Doç. Dr. M. Lütfi Süzen

Eylül 2003, 94 sayfa

Kayaçlarda hidrotermal sıvıların neden olduğu alterasyonun belirlenmesinde belli başlı alterasyon mineralleri kullanılır. Potassik, fillik (serizitik), propilitik, arjillik, gelişmiş arjillik, silisleşme, volkanik kayaçlarda görülen belli başlı alterasyon tipleridir., Alterasyon haritalamasında uzaktan algılamanın rolü, her tipin kendine has olan alterasyon minerallerinin ayıklanmasıdır.

Bu çalışmada Landsat TM 5 uydusunun görüntüleri kullanılmıştır. Genel alterasyon haritalamasında renk kompozisyonu, bant oranlaması, temel bileşenler analizi ve multilineer regresyon gibi konvansiyonel yöntemler uygulanmıştır.

Ayrıntılı mineral haritalaması ‘United States Geological Survey’ (USGS) spektral kütüphane datası kullanılarak yapılmıştır. Seçilen minerallerin spektrumları Landsat TM’in bant aralıklarına göre detaylı bir şekilde incelenmiş ve buna uygun bant oranları seçilmiştir. Elde edilen mineral haritaları daha sonra alansal dağılım açısından incelenmiştir.

Uygulanan mineral ayıklama yöntemi ile elde edilen mineral haritaları göstermiştir ki, en genç volkanik kompleks olan Hasandağ kompleksi alterasyon açısından en bakir alandır. Bunun yanında Keçiboyduran ve Melendiz kompleksleri merkezde kil ağırlıklı, eteklere doğru oksitçe zengin bir alterasyon zonlanması gösterir. Bölgede önceki çalışmalardan tesbit edilmiş gömülü fay doğrultuları boyunca gözlenen alterasyon da yöntemin, bozunma kaynağı ile ilgili yorumlara da katkı sağlayabileceğinin göstergesidir.

Anahtar kelimeler : Uzaktan algılama, alterasyon haritalaması, spektral kütüphane, Kapadokya Volkanik Provensi.

To my beloved family members

ACKNOWLEDGEMENTS

For the endless energy he has in supporting, motivating and teaching me I am very grateful and very lucky to have worked with my supervisor Assoc. Prof. Dr. Vedat Toprak.

I would like to thank to my co-supervisor Assist. Prof. Dr. Lutfi Szen for his guidance in the dark valleys of altered images.

I would like to thank to Dr. Arda Arcasoy for his valuable comments at the critical stages of the thesis.

I would like to express my appreciation to Dr. Mesut Soylu for changing my point of view in geology.

Also I would like to thank to Deniz Gerek for helping me dealing with the script writing.

I would like to express my sincere thanks to my family for their un-writable tolerance and support.

TABLE OF CONTENTS

ABSTRACT	iii
ÖZ.....	v
DEDICATION	vii
ACKNOWLEDGEMENTS	viii
TABLE OF CONTENTS	ix
LIST OF TABLES	xiii
LIST OF FIGURES.....	xiv
LIST OF ABBREVIATIONS	xvii
CHAPTER	
1. INTRODUCTION	1
1.1. Purpose and Scope.....	1
1.2. Study area	2
1.3. Method of Study.....	3
1.4. Organization of thesis.....	3
2. REGIONAL GEOLOGY.....	5
2.1. Previous Works	5
2.2. Geological Setting	8
2.3. Rock Units.....	10
2.3.1. Volcaniclastics.....	10
2.3.2. Volcanic complexes	12

2.3.3.	Volcanic cone fields	12
2.3.4.	Plio-Quaternary continental deposits	13
2.4.	Tectono-Volcanic Framework.....	13
2.4.1.	Faults	13
2.4.2.	Volcanic Activity	14
2.5.	Geology of “Hasandağ-Melendiz Volcanic Complex”	17
2.5.1.	Basalts	17
2.5.2.	Andesitic basalts and andesites	17
2.5.3.	Volcanic cone breccias.....	17
2.5.4.	Tuff Breccias	18
2.5.5.	Radial ash flow of Hasandağ complex	18
2.5.6.	Ash formation of Hasandağ complex.....	19
2.5.7.	Ash flow tuffs of Hasandağ.....	19
2.5.8.	Volcanic agglomerate and conglomerates of Keçiboyduran volcanic complex.....	19
2.5.9.	Pyroclastic formation of Melendiz complex	19
2.5.10.	Viterous tuffs of Melendiz volcanic complex	20
2.5.11.	Agglomerates of Melendiz volcanic complex.....	20
3.	ALTERATION MAPPING BY USING REMOTE	21
3.1.	Alteration of Rocks	21
3.2.	Alteration Types	22
3.3.	Techniques of Remote Sensing in Alteration Mapping	23
3.3.1.	Remote Sensing Technology.....	23
3.3.1.1.	The Landsat Satellites	25
3.3.2.	Present Techniques in Alteration Mapping.....	30
3.3.2.1.	Color Composites	30

3.3.2.2.	Band Rationing.....	33
3.3.2.3.	Principal Component Analysis.....	36
3.3.2.4.	Least Squares Fitting Method.....	41
3.3.3.	Mineral Mapping by using Spectral Reflectance Data.....	43
4.	DATA AND ANALYSIS.....	47
4.1.	Data	47
	Laboratory Reflectance Spectra	48
4.1.1.	Preprocessing.....	49
4.1.2.	Methodology	52
4.2.	Conventional Analyses.....	52
4.2.1.	Color Composites	52
4.2.2.	Band Rationing.....	56
4.2.3.	Crosta Technique.....	61
4.2.3.1.	Hydroxyl Mapping	61
4.2.3.2.	Iron Oxide Mapping	63
4.2.3.3.	H + F Mapping	65
4.2.3.4.	Color Composite of H, H+F and F images.....	65
4.2.4.	Least Squares Fitting Method.....	67
4.3.	Spectral Library Analysis.....	69
4.3.1.	Kaolinite Mapping.....	70
4.3.2.	Illite Mapping.....	71
4.3.3.	Montmorillonite Mapping	72
4.3.4.	Pyrophyllite Mapping.....	73
4.3.5.	Alunite Mapping.....	74
4.3.6.	Orthoclase Mapping	75

4.3.7.	Quartz Mapping.....	76
4.3.8.	Epidote Mapping	77
4.3.9.	Chlorite Mapping	78
4.3.10.	Hematite Mapping.....	79
4.3.11.	Goethite Mapping.....	80
4.3.12.	Jarosite Mapping	81
4.3.13.	Vegetation Mapping for Accuracy Assessment	82
5.	DISCUSSION AND CONCLUSIONS.....	86
5.1.	Data	86
5.2.	Conventional Techniques of Alteration Mapping	87
5.3.	Mineral mapping by using spectral reflectance data	88
5.4.	Further Recommendations	91
REFERENCES		92

LIST OF TABLES

TABLE

3.1. Alteration types and representing minerals, used during this study.....	23
3.2. Remote sensing systems for mineral exploration.....	26
3.3. Spectral Properties of Landsat TM 5.....	27
3.4. Summary of the literally known color composites.....	32
3.5. Summary of literally known band ratio composites.....	36
3.6. Coefficients and constants of the sixth order polynomial equation.	42
3.7. Descriptive statistics of illite for TM band1 interval.	45
3.8. Limiting values of the Illite spectral reflectance that are used in the filtering of TM band ratios.	45
3.9. Limiting values of band ratios that are calculated from the spectral reflectance data of Illite.	46
4.1. Haze values of TM Bands that are removed.	51
4.2. Eigenvector Loadings for Hydroxyl Mapping	63
4.3. Eigenvector Loadings for Iron-Oxide Mapping.....	63
4.4. Eigenvector Loadings for H + F Mapping	65
4.5. Coefficients and the constants of the sixth order polynomial function.	67
4.6. Accuracy assessment matrix	84

LIST OF FIGURES

FIGURE

1.1. Location and topography map of the study area..	3
2.1. Geological setting of the Cappadocian Volcanic Province.	10
2.2. Simplified geological map of Cappadocian volcanic province (CVP)..	11
2.3. Development of CVP during (a) pre-Mid Miocene, (b) Mid-Miocene to early Pliocene and (c) Late Pliocene to Quaternary.	15
2.4. Detailed geological map of Hasandağ-Melendiz volcanic complex	18
3.1. Spectral reflectance curves of argillic alteration minerals.	28
3.2. Spectral reflectance curves of advanced argillic alteration minerals.	28
3.3. Spectral reflectance curves of propylitic alteration minerals.	29
3.4. Spectral reflectance curves of iron oxide minerals.	29
3.5. Additive colors.	30
3.6. Visual construction of the principal components from original data.	38
3.7. Flow chart of the mineral mapping technique.	44
4.1 RGB display of TM Bands 3, 2, 1 respectively.	48
4.2. Linear contrast stretched RGB display of TM Bands 3, 2, 1	49
4.3. Spectral reflectance curves of 4 different kaolinite samples.	50
4.4. Band correlation graph between band 1 and 7.	51
4.5. Flow chart of the study.	53

4.6. Color composites a. RGB of 472, b. RGB of 476, c. RGB of 754, d. RGB of 475.	56
4.7. Band ratio color composites.	58
4.8. Hydroxyl Map.	62
4.9. Iron Oxide Map.	64
4.10. Hydroxyl + Iron Oxide Map.....	66
4.11 Color composite image of H: H+F: F.....	66
4.12. LS-Fit. Output Map.	68
4.13. Spectral reflectance curve of kaolinite (USGS library).....	70
4.14. Band4/Band1 ; Band4/Band7 ; Band5/Band7 are filtered.	70
4.15. Spectral reflectance curve of illite (USGS library).	71
4.16. Band5/Band4, Band1/Band7, Band2/Band7 are filtered.....	71
4.17. Spectral reflectance curve of montmorillonite (USGS library).....	72
4.18. Band5/Band4, Band1/Band7, Band4/Band1 are filtered.....	72
4.19. Spectral reflectance curve of pyrophyllite (USGS library).	73
4.20. Band5/Band4 and Band4/Band7 is filtered.	73
4.21. Spectral reflectance curve of alunite (USGS library).....	74
4.22. Band5/Band4, Band4/Band7, Band5/Band7, Band2/Band7 are filtered....	74
4.23. Spectral reflectance curve of orthoclase (USGS library).	75
4.24. Band7/Band1, Band3/Band1, Band4/Band1 are filtered.....	75
4.25. Spectral reflectance curve of quartz (USGS library).....	76
4.26. Band1/Band3 and Band5/Band7 is filtered.	76
4.27. Spectral reflectance curve of epidote (USGS library).....	77
4.28. Band5/Band1 and Band3/Band1 is filtered.	77
4.29. Spectral reflectance curve of chlorite (USGS library).	78

4.30. Band3/Band1, Band4/Band5, Band5/Band7, Band5/Band1, Band4/Band1 are filtered.....	78
4.31. Spectral reflectance curve of hematite (USGS library).....	79
4.32. Band4/Band3 is filtered, when haze is removed.	79
4.33. Spectral reflectance curve of goethite (USGS library).....	80
4.34. Band2/Band1 is filtered, when haze is removed.	80
4.35. Spectral reflectance curve of jarosite (USGS library).....	81
4.36. Band1/Band7 and Band1/Band5 are filtered.....	81
4.37. Reference data..	83
4.38. Spectral analysis data..	84
5.1. Color composite of Crosta H, H+F and F as RGB.....	87
5.2. Color composite of residual bands 3, 7 and 1 as RGB.....	88
5.3. Ironoxide-rich areas obtained by spectral library analysis.	89
5.4. Close up views of ironoxide-rich pixels.....	89
5.5. Clay minerals-rich areas obtained by spectral library analysis.	90
5.6. Close up views of clay-rich pixels.	90
5.7. Areas that are both clay and iron oxide altered.	91

LIST OF ABBREVIATIONS

Landsat TM: Landsat Thematic Mapper
USGS: United States Geological Survey
CVP: Cappadocian Volcanic Province
Ma: Million Ages
DEM: Digital Elevation Model
CACC: Central Anatolian Crystalline Complex
AVIRIS: Airborne Visible/Infrared Imaging Spectrometer
NASA: National Aeronautics and Space Administration
IR: Infra Red
NIR: Near Infra Red
SWIR: Short Wave Infra Red
LSFit: Least Squares Fitting
RGB: Red Green Blue
FCC: False Color Composite
BV: Brightness Value
PCA: Principal Component Analysis
PC: Principal Component
DN: Digital Number
SD: Standard Deviation
XRD: X-Ray Diffractometer
ALI: Advanced Land Imager

CHAPTER 1

INTRODUCTION

Use of remote sensing technologies in various geological applications has considerably increased in the recent years due to the fruitful results provided by the analysis. Two main reasons for this increase are: 1) new methods and interpretation techniques are suggested by researchers that tend to extract reliable information from satellite images, and 2) new satellite images with better spatial and spectral resolutions are available that provide more information to the user about the investigation area. Developments in the software technology should also be considered as a positive contribution to such studies.

The most common applications of remote sensing in geological analysis are mapping rock units and structural elements. Identification of special geological features such as alteration minerals, other economic rock types, landslides, karstic features global monitoring are some of the new trends in remote sensing studies.

1.1. Purpose and Scope

The aim of this study is to apply remote sensing techniques for the mapping of alteration products which could form a preliminary basis of an exploration project in the study area. The area is selected from Cappadocian Volcanic Province (CVP), which covers several composite volcanoes and is a promising area for alteration minerals.

The scope of the thesis is limited with the identification of major alteration minerals. A complete list of these minerals will be given later in Chapter 3. Two sets of methods will be applied during analysis. The first set includes application of well-known algorithms and methods compiled from the literature. The second set analysis involve mapping of individual minerals in accordance with their spectral properties as publicized in the United States Geological Survey (USGS) spectral library.

1.2. Study area

The study area is included within the Cappadocian Volcanic Province between Niğde and Aksaray (Figure 1.1). It covers the central portion of the province from Hasandağ to Melendiz Mountain (Figure 1.2.), the 1:100.000 scaled map sections of L32, L33, M32 and M33. In the figure, the coordinates in black, are Universal Transverse Mercator (UTM) zone 36 coordinates with European 1950 datum; red ones are longitude and latitude geographical coordinates. This corresponds to a mountain belt that extends almost in E-W direction. Total length of the area is 45 km and the width is 30 km. The highest peak of the area is Hasandağ with an elevation of 3227 m. Average elevation of the plains surrounding the belt is about 1000 m. The relief map clearly displays that the Hasandağ, Keçiboyduran and Melendiz volcanic complexes have very high topographic relief easily distinguished from the low lying background.

The main reasons in the selection of this area are:

- 1) The area is totally covered by volcanic rocks in the form of composite volcanoes. These rocks are the target areas for alteration minerals,
- 2) Alteration mineral potential of the area is known from the literature. The area, however, is not investigated by any study that involves remote sensing techniques.
- 3) Surface geology of the area is well known that simplifies interpretations of the results.

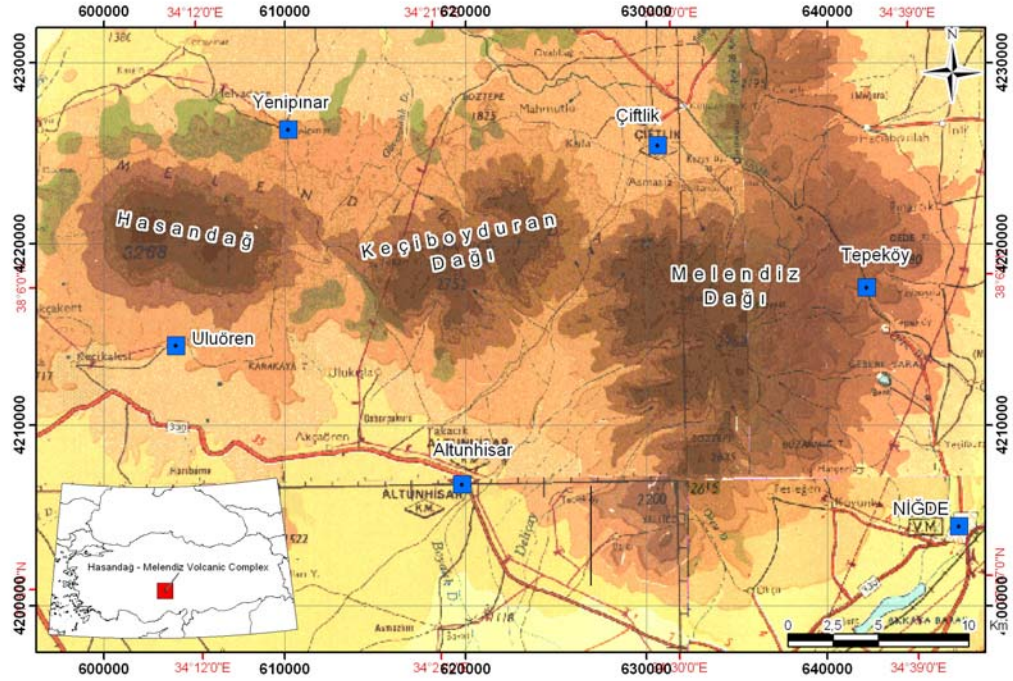


Figure 1.1. Location and topography map of the study area. Elevation of basal plain is about 1000 m. The highest elevation is peak of Hasandağ (3270 m). Volcanic bodies are in circular form and correspond to, from left to right, Hasandağ, Keçiboyduran and Melendiz Mountains.

1.3. Method of Study

The study is mostly carried out as office work, starting with literature survey, continued with the image processing application; method development and ended up with analyzing the results. During all types of image processing TNT-Mips v6.3 software is used; for statistical computations SPSS v11.0 and Microsoft Excel is used; for cartographic applications and map preparation Arcview GIS 8.3 and FreeHand 10.0 are used.

1.4. Organization of thesis

This thesis includes five chapters, each of which deals with the separate part of the whole subject and highly linked. A brief description of each chapter is as follows:

Chapter 1 is the introduction to thesis title and includes information about what will be given in the proceeding chapters.

Chapter 2 is the geology chapter. Regional setting, rock units, tectonic setting and volcanic complexes that are present in the study area are explained briefly. Also the previous geological studies are listed in this chapter.

Chapter 3 gives the background information about the technical details about what is meant by ‘alteration mapping by remote sensing techniques’. This chapter is divided into two parts, one of which summarizes the literally known methods in alteration mapping and the other introduces the proposed mineral mapping technique.

Chapter 4 introduces data and provides the analysis results of the techniques that are applied in the same order with the Chapter 3. Alteration maps produced both by conventional methods and the proposed methods are discussed in detail.

Chapter 5 states the reliability of the outcome of this study and makes recommendations for further studies.

CHAPTER 2

REGIONAL GEOLOGY

This chapter describes general geological characteristics of the study area and surrounding regions. The chapter is divided into five sections as follows: 1) Previous studies about the geology of the area, 2) Geological Setting of the Cappadocian Volcanic Province (CVP), 3) Rock units existing within the CVP, 4) Tectonic elements of the CVP, and 5) Geology of the “Hasandağ-Melendiz Volcanic Complex”.

2.1. Previous Works

The previous studies that will be mentioned here summarize the literature about the geology of the area.

The study area is a part of Cappadocian Volcanic Province (CVP). There is a rich literature on various geological aspects of the CVP. Major geological characteristics of the region will be given in the next chapter. Therefore, in this section, the studies related to the main theme of this thesis (Hasandağ – Melendiz volcanic complex and tectonic features of the area) will be considered. The studies are briefly explained below in chronological order.

Beekman (1966) mapped Hasandağ-Melendiz Dağ region at 1/25.000 scale which is the first detailed work carried out within the investigation area. He distinguished eruption centers of the main volcanic bodies and mapped the “vent material” separately. These rocks are the target regions in this study.

Pasquaré (1968) mapped Nevşehir area at 1/25.000 scale. This is the first study on the stratigraphy and nomenclature of the ignimbrites in the region. He measured type sections of all individual ignimbrites and suggested a depositional area for them.

Innocenti *et al.* (1975) study stratigraphy, chemical composition and geochronology of the tephra succession around Nevşehir. The volcanism in the region is determined to be calcalkaline in nature. Age determinations from different ignimbrites indicate that the main phase of volcanic activity is Middle-Late Miocene to Pliocene.

Besang *et al.* (1977) assigned an age 5.4 Ma to a sample collected from eastern margin of the Melendiz volcanic complex. This is the first age determination published in the literature. Accordingly, the age of Melendiz volcanics is Late Miocene-Pliocene.

Pasquare *et al.* (1988) divides the volcanism in Central Anatolia into three main activity periods. Accordingly, first period is represented by a mostly andesitic effusive activity; second period is represented by the emplacement of numerous pyroclastic flow deposits. Melendiz Dağ volcanic complex (which is the investigated area in this thesis) is formed during this period. During the third period andesitic-basaltic stratovolcanoes and acid monogenic centers developed. The relationship between the volcanic activity and the tectonism is stated by the main fault systems present in Central Anatolia.

Ercan *et al.* (1990; 1992) studied volcanic activity around Hasandağ-Karacadağ area. They concentrated on the origin and evolution of volcanism in the area. They also determined ages of several volcanic eruptions including Hasandağ volcano. Although the ages of basaltic volcanics exposed at lower elevations are very young (35.000 to 60.000 years), age of lava flows from Hasandağ volcano dates back to 270.000 years.

Göncüoğlu and Toprak (1992) mapped the volcanic rocks in the close vicinity of the area into nine volcanic complexes: These are 1. Keçikalesi volcanics, 2. Kızılçın volcanics, 3. Tepeköy volcanics, 4. Çınarlı volcanics, 5. Melendiz volcanics, 6. Keçiboyduran volcanics, 7. Göllüdağ volcanics, 8. Hasandağ

volcanics, 9. Karataş volcanics. With the exception of Karataş volcanics which is composed of basaltic lava flows all other rocks correspond to either strato-volcano or caldera.

Toprak and Göncüoğlu (1993) defined a major fault in the region and named it as “Keçiboyduran – Melendiz fault”. This fault passes through eruption centers of two strato-volcanoes which are target areas of alteration minerals in this study. The fault was active during Late Miocene – Pliocene and is buried beneath the volcanoes today.

Le Pennec *et al.* (1994) established the stratigraphic succession of the ignimbrites for the whole volcanic province. Various field data are collected and measured to locate the source of ignimbritic eruptions. Accordingly, the source area for the major ignimbrites of the Nevşehir plateau is inferred as Derinkuyu basin extending between Nevşehir and the Melendiz Dağ volcanic complex.

Toprak (1994) stated that the northern margin of Central Anatolian Volcanic Province depression is defined by a major fault zone named as Central Kızılırmak Fault Zone. Most of the ignimbrites are emplaced within the basin (Ürgüp basin) to the south of this fault zone being intercalated with continental clastics. The fault zone strikes almost in an E-W direction.

Aydar *et al.* (1994) investigated petrological characteristics and volcano-structural characteristics of the Cappadocian Volcanic Province in the area between Hasandağı and Erciyes volcanoes.

Toprak (1996) described the origin and the evolution of Quaternary aged basins within the volcanic province. He suggested three origins for these depressions as tectonic, tectono-volcanic and volcanic origin. Some of these basins are located around the study area (e.g., Tuzgölü basin, Çiftlik basin, Derinkuyu basin and Niğde-Bor basin).

Temel *et al.* (1998) presented the petrology and the geochemistry of the ignimbrite units in the area in detail. The origin of the volcanic units is found to be related with fractional crystallization of a mantle-derived magma. Geochemistry results showed a transition from collisional to extensional tectonics.

Deniel *et al.* (1998) studied volcanic evolution of Hasandağı volcano. Three stages of edifice construction have been identified for this volcano: Paleovolcano, Mesovolcano and Neovolcano. Most samples from Hasandağı volcano are calc-alkaline and define an almost complete trend from basaltic andesite to rhyolite. However, the more recent Neovolcano mafic samples are alkaline basalts. The mineralogical and geochemical characteristics of the oldest lavas (13 Ma) and Paleo-Hasandağı (7 Ma) are significantly different from those of the younger lavas Meso- and Neo-Hasandağı (1 Ma) .

Froger *et al.* (1998) studied possible sources of widespread tephra deposits in the volcanic province. According to them the tephra sequence is composed of 10 Neogene ignimbrites. The associated calderas have been partly dismantled and buried by subsequent tectonic and sedimentary processes and, therefore, cannot be readily recognized in the field. Using various field data they suggested Derinkuyu basin and surrounding areas for potential sites of the buried calderas.

Toprak (1998) analyzed the distribution of polygenetic and monogenetic volcanoes and linked this distribution to the faults existing in the area. He concluded that most of the cones are concentrated along the major faults of the region, namely Tuzgölü and Ecemiş fault zones. Other concentrations correspond to buried faults particularly in the western part of the area, around Melendiz volcanics and around Acıgöl-Göllüdağ volcanics.

Dhont *et al.* (1998) investigated regional tectonic features of the Cappadocian volcanics with particular emphasis on the major eruption centers. They used Synthetic Aperture Radar SAR scenes of the European Remote Sensing ERS satellite and Digital Elevation Models DEMs, complemented by field structural analysis to understand the relationships between tectonics and volcanism since the late Miocene 10 Ma in Central Anatolia.

2.2. Geological Setting

Cappadocian Volcanic Province (CVP) extends as a belt in NE-SW direction for a length of 250-300 km situated in Central Anatolia (Figure 2.1). The volcanism of the CVP has been investigated by several researchers who mainly concentrated on the chronology, petrographical and geochemical characteristics,

and ignimbrite emplacement (Pasquare, 1968; Innocenti *et al.*, 1975; Pasquare *et al.*, 1988; Ercan *et al.*, 1990, 1992; Aydar *et al.*, 1994; Le Pennec *et al.*, 1994). The CVP is a calc-alkaline volcanic province whose formation is attributed to the convergence between Eurasian and Afro-Arabian plates occurring in the eastern Mediterranean (Toprak, 1996).

Six major rock associations surround the CVP (Figure 2.1). The following paragraphs briefly describe these units.

Tuzgölü basin is located within the system of depressions of central Anatolia. It was initiated during the late Cretaceous as a fore-arc basin along a northeasterly dipping Neotethyan subduction zone. Superimposition of continental units onto marine deposits occurred and the basin is filled with mainly lacustrine to fluvial deposits during the late Miocene - Late Pliocene. The basin is still active.

Sivas basin is developed between two major tectonic belts of Turkey, the Anatolides and the Pontides. It was initiated during the closure of the northern branch of Neotethys in the early Tertiary and is filled with dominantly continental deposits of Eocene to Miocene age.

Ulukışla basin is composed of arc volcanics of L. Cretaceous to E. Tertiary intercalated with flyschoidal sequences. The basin is believed to be a product of a northerly subduction that occurred between Anatolides and Taurides.

Tauride Belt constitutes a major tectonic belt extending mainly in the E-W direction. The belt is divided into seven tectonic sub-units on the basis of different stratigraphic and structural characteristics.

Known as the basement rocks, Niğde massif, exposed in the north of CVP and Kırşehir massif, exposed in the south belongs to the Central Anatolian Crystalline Complex (Toprak, 1996). These basement rocks are composed of Palaeozoic-Mesozoic medium to high-grade metamorphic rocks, Upper Cretaceous ophiolites and Upper Cretaceous-Palaeocene granitoids (Toprak and Göncüoğlu, 1993).

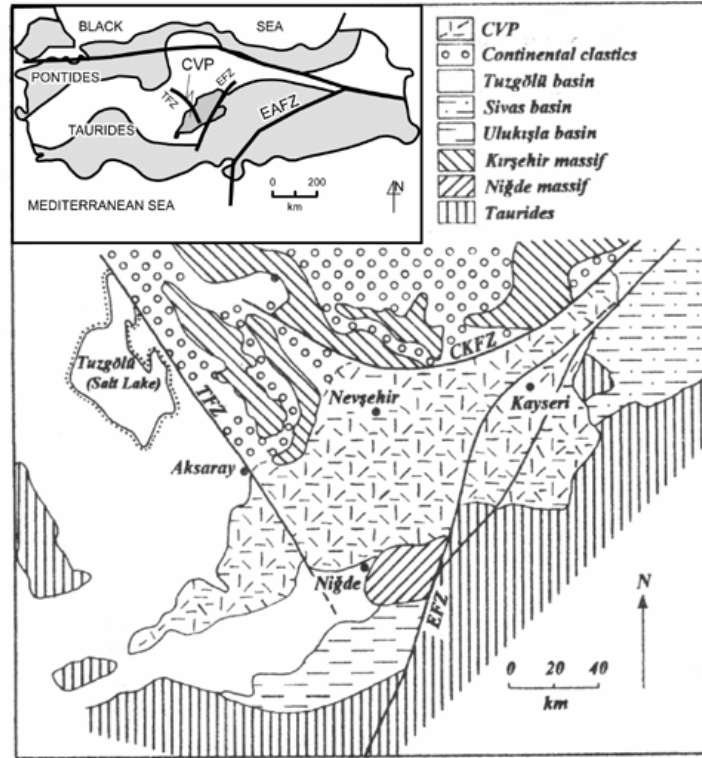


Figure 2.1. Geological setting of the Cappadocian Volcanic Province (Toprak and Göncüoğlu, 1993).

2.3. Rock Units

Rock units existing around CVP are described in previous section. In this section the rock units within the CVP will be explained which are grouped into four major categories. These are Mio-Pliocene volcanoclastics, Miocene-Quaternary volcanic complexes, Plio-Quaternary continental clastics and Quaternary cinder cone fields (Figure 2.2).

2.3.1. Volcaniclastics

Volcaniclastic rocks are dominantly composed of tephra deposits (ignimbrites) and are intercalated with the lacustrine-fluvial deposits. The formation has a thickness of more than 400 m and extends throughout the CVP. It is studied by numerous researches due to the presence of extensive ignimbrites within the formation (Pasquaré; 1968; Innocenti *et al.*, 1975; Pasquaré *et al.*, 1988; Le Pennec *et al.*, 1994; Temel *et al.*, 1998). Accordingly, the ignimbritic activity of CVP occurred between 11 and 1 Ma (Innocenti *et al.*, 1975).

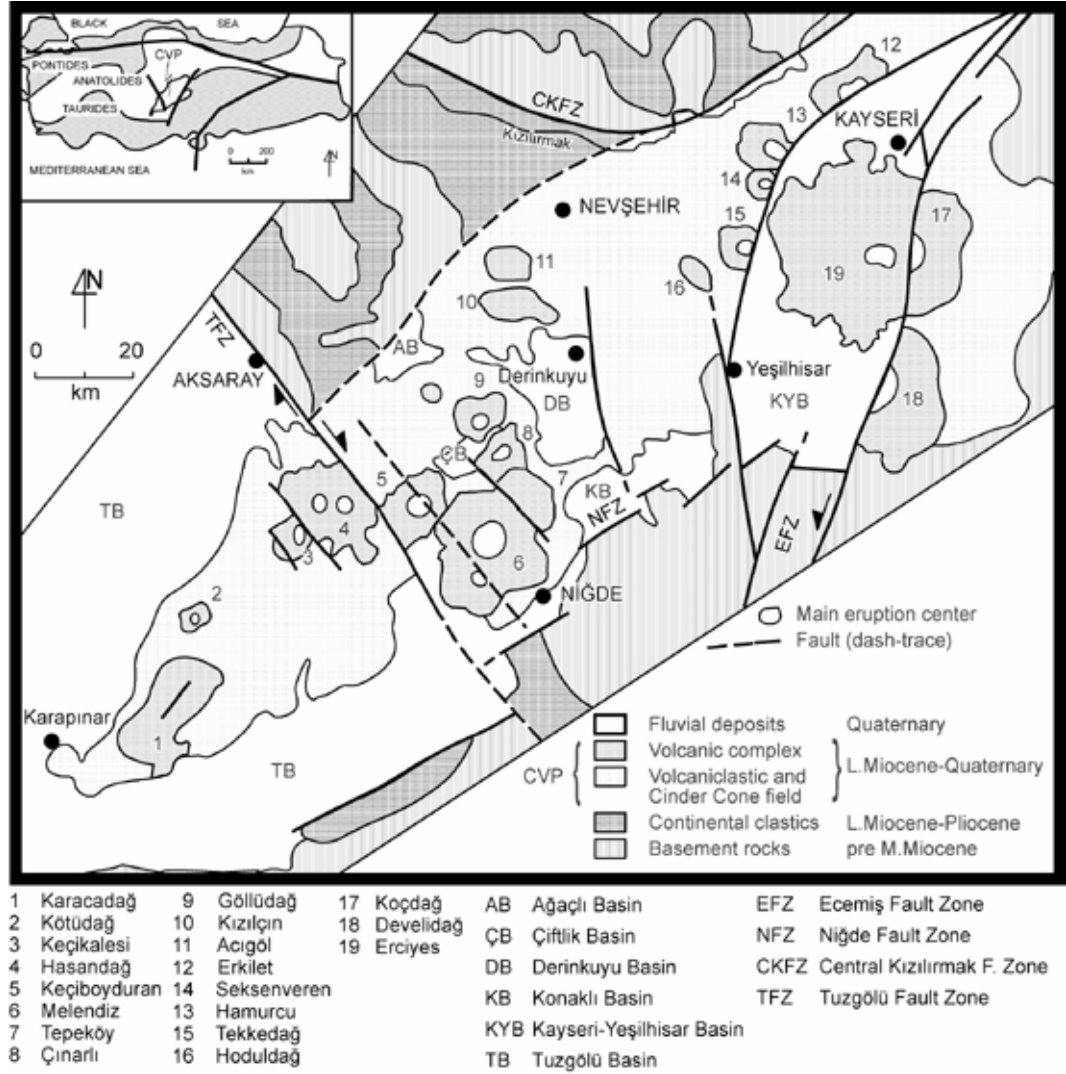


Figure 2.2. Simplified geological map of Cappadocian volcanic province (CVP). Modified after Toprak, 1998.

First attempt to locate the vent for the ignimbrites is made by Pasquaré *et al.*, (1988) who proposed Quaternary Çiftlik Basin (north of Melendiz complex) as “Çiftlik Caldera” and an ignimbrite source for the area. Later studies show that this basin is not a caldera and therefore the source should be in another place in the region (Göncüoğlu and Toprak, 1992, Le Pennec *et al.*, 1994). Based on various field data the source area for the major ignimbrites of the Nevşehir plateau is proposed as Derinkuyu basin extending between Nevşehir and the Melendiz Dağ volcanic complex.

The sedimentary units within the volcaniclastics are relatively poorly studied compared to ignimbrites. These sedimentary units are characterized by volcanic conglomerates and pelitic rocks at the base, by marls and fine-grained slightly

tuffaceous sandstones in the middle part and by clay, marls and lacustrine limestones at the top. In this sequence, six fossil mammal deposits are recognized in different stratigraphic positions. The palaeontological data show an age between Maeotian (Late Miocene) and Pontian (Late Miocene-Pliocene) times (Pasquaré, 1968). This age is conformable with the radiometric ages of the associated ignimbritic units (Innocenti *et al.*, 1975).

2.3.2. Volcanic complexes

Volcanic complexes correspond to the major eruptive centers in the province and form huge topographic masses. Nineteen volcanic complexes are identified within the province (Figure 2.2). Although some of the complexes are studied in detail, most of them are still poorly known. Most of them are polygenetic volcanoes; others are in the form of either a dome or a caldera (Table 2.1). The complexes are aligned in NE-SW direction, more or less, parallel to the long axis of the volcanic belt. The dominant lithologies of the complexes are changing from andesite, dacite, rhyolite, rhyo-dacite to basaltic andesite. Size, degree of erosion, type, form (circular, subcircular) and age change from place to place without a certain trend in any direction.

This thesis is carried out on four of these volcanic complexes. Details of these complexes will be given in the next chapter.

2.3.3. Volcanic cone fields

Volcanic cone fields are composed of monogenetic (parasitic) eruptions and their associated lava flows. They are scattered throughout the study area being concentrated in certain parts.

Most of these volcanoes are in the form of cinder cones although some exist as rhyolitic or andesitic domes and maars (Pasquare, 1968). The cinder cones have a basal diameter of a few tens of meters to 1-1.5 kilometers with a height of a few ten meters to a few hundred meters. They are all associated with basaltic lava flows and are Late Quaternary in age (Ercan *et al.*, 1990b; 1992). Rhyolitic domes are common around the Acıgöl caldera (no: 11 in Figure 2.2) and are characterized with the large basal diameters reaching up to 5 km. They are

Quaternary in age. Andesitic domes, on the other hand, are mostly observed in the area between Nevşehir, Derinkuyu and Yeşilhisar. They range in age from Late Miocene to Quaternary.

2.3.4. Plio-Quaternary continental deposits

Plio-Quaternary continental deposits cover large areas within the CVP. These deposits are exposed within isolated basins developed under the influence of tectonic and volcanic structures existing in the area. Toprak (1996) distinguished 7 basins (Figure 2.2) and classified them according to their mode of origin. The basins are all developed within the main depression of the CVP and are filled with mostly fluvial clastics. The ages of these depressions are assigned relative to the age of the youngest unit of Ürgüp Formation. Accordingly, they have an age of Plio-Quaternary with minor variations from place to place.

2.4. Tectono-Volcanic Framework

Tectonic activity and volcanism are two processes that coexist within the CVP. In this section first the major faults existing in the area will be explained followed by major volcanic activities during Miocene to recent.

2.4.1. Faults

Two fault systems of different age and nature are recognized within the CVP (Toprak and Göncüoğlu, 1993a). These are (1) Tuzgölü-Ecemiş fault system, and (2) CVP fault system.

(1) Tuzgölü-Ecemiş system is a fault swarm located between the conjugate Tuzgölü fault in the west and the Ecemiş fault in the east (Fig. 2.2). The Tuzgölü fault, with a length of more than 150 km and a vertical offset of more than 300 m, defines the eastern margin of the Tuzgölü basin. Ecemiş fault with a total length of about 600 km cuts across the CVP in its eastern part. Other major faults within this system are Keçiboyduran-Melendiz (Toprak and Göncüoğlu, 1993a, b) and Derinkuyu faults.

(2) CVP faults strike NE-SW, parallel to the long axis of the CVP. Two major faults of this system are Central Kızılırmak (Toprak, 1994) and Niğde faults

which define the northern and southern margin of the volcanic depression, respectively (Fig. 2.2).

2.4.2. Volcanic Activity

The development of the CVP is explained on the basis of the ages of the exposed volcanic products and the fault systems recognized in the area (Pasquare *et al.* 1988, Toprak and Göncüoğlu 1993, Toprak 1998). Three periods suggested by Pasquare *et al.* (1988) corresponds to the Pre-Mid Miocene, Mid Miocene-Early Pliocene and Late Pliocene-Quaternary periods suggested by Toprak and Göncüoğlu (1993).

Pre-Mid Miocene: In this period only the Tuzgölü-Ecemiş fault system is active. The region was being deformed mainly by the conjugate faults of this system (Figure 2.3a). The initiation age of the Tuzgölü fault zone can be dated back to the Late Cretaceous and that of the Ecemiş fault zone is said to be Palaeocene-Eocene (Toprak and Göncüoğlu 1993). The nature of the faults before the Miocene is still not known but they are thought to be originated because of the N-S compression in the area due to the convergence in the eastern Mediterranean. Pasquare *et al.* (1988) states that this period represented mainly by the activity of effusive monogenic centers of andesitic composition and the data in Table 2.1 (Toprak 1998) agrees with this behavior of volcanism during this period.

Middle Miocene-Early Pliocene: CVP faults are the characteristic unit of this period. A short-term tensional period in NW-SE direction produced CVP faults. The oldest volcanics, Keçikalesi and Kızılçın are the oldest products of the CVP with Mid-Late Miocene age. The ages of Tepeköy and Çınarlı indicate that these volcanic complexes are also generated in this period. The initial volcanic activity is proposed to be started in a belt extending in NE-SW direction. Faults parallel to this direction most of which are thought to be buried are shown as a proof of the mechanism (Toprak and Göncüoğlu 1993). The movement along the CVP faults has lead to the formation of an extensional basin in the region (Figure 2.3b). Thick sequence of fluvial to lacustrine sediments intercalated with volcanoclastics filled the depression. The Central Kızılırmak and Niğde fault

zones define the northern and southern margins of the depression today. During this period Ecemiş-Tuzgölü fault system was also active contemporaneously with CVP fault system. The Keçiboyduran and Melendiz volcanic complexes are formed during this period. Pasquare *et al.* (1988) proposed that basaltic centers were active in the area north and northeast of Ürgüp.

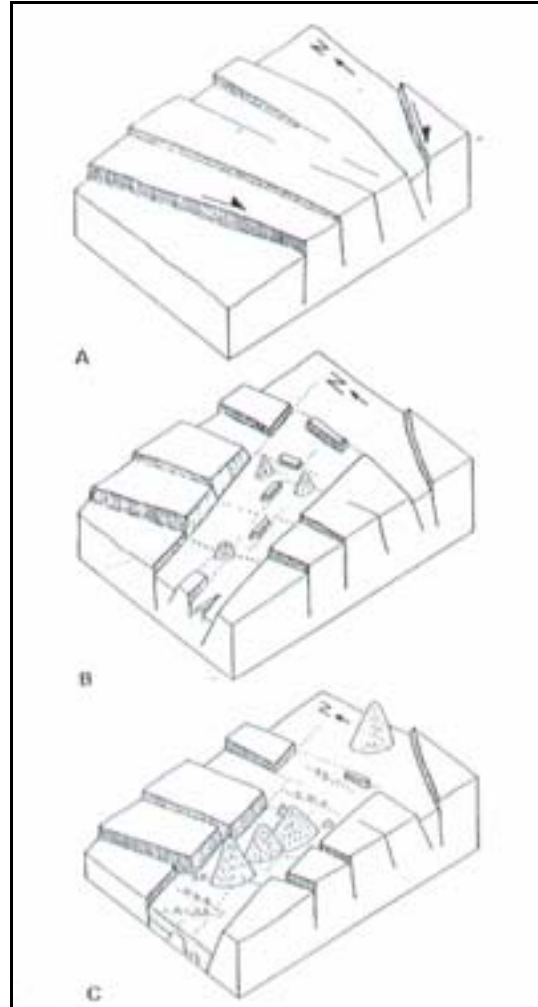


Figure 2.3. Development of CVP during (a) pre-Mid Miocene, (b) Mid-Miocene to early Pliocene and (c) Late Pliocene to Quaternary (Toprak and Göncüoğlu 1993).

Late Pliocene-Recent: In this period the activity of CVP fault system nearly stops. Most of the faults in the system are buried beneath the volcanics and sedimentary deposits. Thus, most of the deformation in the CVP during this period is caused by the Tuzgölü-Ecemiş fault system (Figure 2.3c). Dextral Tuzgölü fault, sinistral Ecemiş fault, normal Derinkuyu fault was active; Keçiboyduran-Melendiz and Göllüdağ faults were inactive during this period. Toprak and Göncüoğlu (1993) suggested that the CVP fault system was displaced by the Tuzgölü-Ecemiş fault zone in this period. Great central volcanoes like Hasandağ and Erciyes; numerous monogenic centers and cinder cones are developed in this period.

Table 2.1. General characteristics and available age data of the volcanic complexes exposed within the CVP (Toprak 1998).

Number	Name	Age(Ma)	Age	Type	Dominant lithology
1	Karacadağ		Mid-Late Miocene	stratovolcano	andesite
2	Kötüdağ		Mid-Late Miocene	dome	andesite
3	Keçikalesi	13.7-12.4	Middle Miocene	caldera	basaltic andesite
4	Hasandağ	0.78-0.277	Plio-Quaternary	stratovolcano	basaltic andesite-andesite
5	Keçiboyduran		Early Pliocene	stratovolcano	andesite-basaltic andesite
6	Melendiz	6.5-5.1	Early Pliocene	stratovolcano	andesite-basaltic andesite
7	Tepeköy		Mid-Late Miocene	stratovolcano	andesite, dacite
8	Çınarlı		Late Miocene	Stratovolcano	andesite
9	Göllüdağ	1.15-0.86	Early Quaternary	dome	rhyolite, rhyodacite
10	Kızılçın	13.7-6.5	Middle Miocene	stratovolcano	andesite, dacite
11	Acıgöl	0.4-0.019	Late Quaternary	caldera	rhyolite
12	Erkilet		Mio-Pliocene	stratovolcano	andesite
13	Hamurcu		Mio-Pliocene	stratovolcano	andesite
14	Seksenveren		Mio-Pliocene	stratovolcano	andesite
15	Tekkedağ	5.1	Mio-Pliocene	stratovolcano	andesite
16	Hoduldağ		Mio-Pliocene	dome?	andesite
17	Koçdağ		Mio-Pliocene	stratovolcano	andesite
18	Develidağ		Mio-Pliocene	stratovolcano	andesite
19	Erciyes	2.59-1.43	Plio-Quaternary	stratovolcano	andesite, rhyo-dacite

2.5. Geology of “Hasandağ-Melendiz Volcanic Complex”

In this section detailed geology of the Hasandağ-Melendiz volcanic complex is explained within the portion of the study area (Fig. 2.4). The geology of Hasandağ-Melendiz volcanic complex includes 11 lithological units (Beekman, 1966). The numbers in the parenthesis are the corresponding numbers in the legend. These are, **1) Basalts** (No:5), **2) Andesitic basalts and andesites** (No:9), **3) Volcanic breccias** (No:10), **4) Tuff breccias** (No:13), **5) Radial ash flow of Hasandağ** (No:7), **6) Hasandağ ash formation** (No:8), **7) Hasandağ ash flow tuffs** (No:6), **8) Volcanic agglomerates and conglomerates of Keçiboyduran complex** (No:11), **9) Pyroclastic formation of Melendiz complex** (No:16), **10) Vitreous tuffs of Melendiz complex** (No:14), **11) Agglomerates of Melendiz complex** (No:12) (Numbers represent the legend). The detailed descriptions of these units are given in the following sections, respectively.

2.5.1. Basalts

Basalt flows, around Hasandağ and in the north of Melendiz complex, are the extrusion products of the volcanic cinder cones and Melendiz volcanic series. They are grouped in 3 petrographic groups. a) Augite-hyperstene basalts mostly found in Melendiz and Keçiboyduran complexes. b) Hornblende-hyperstene basalts found in Hasandağ complex. c) Olivine basalts of volcanic activity in the plain areas (Fig. 2.4, No:5).

2.5.2. Andesitic basalts and andesites

Majority of these andesitic basalts and andesites are outcropped only in deep wall rock structures of Keçiboyduran and Melendiz volcanic complexes. Volcanic activity in the plain areas have only basaltic characteristic. Andesitic basalts are transition rocks both physically and petrographically. Andesitic parts have hyperstene and augite in composition (Fig. 2.4, No:9).

2.5.3. Volcanic cone breccias

Cone breccias are found in Melendiz and Keçiboyduran complexes locally. These massive, unsorted breccias consisting basaltic block fragments are all

covered with brown colored limonite and purple colored manganese deposition (Fig. 2.4, No:10).

2.5.4. Tuff Breccias

Outcrops of tuff breccias are located in the north, east and south of Altunhisar. This unit consists of angular pumice, lava slag and lava fragments in a vitreous and compact matrix (Fig. 2.4, No:13).

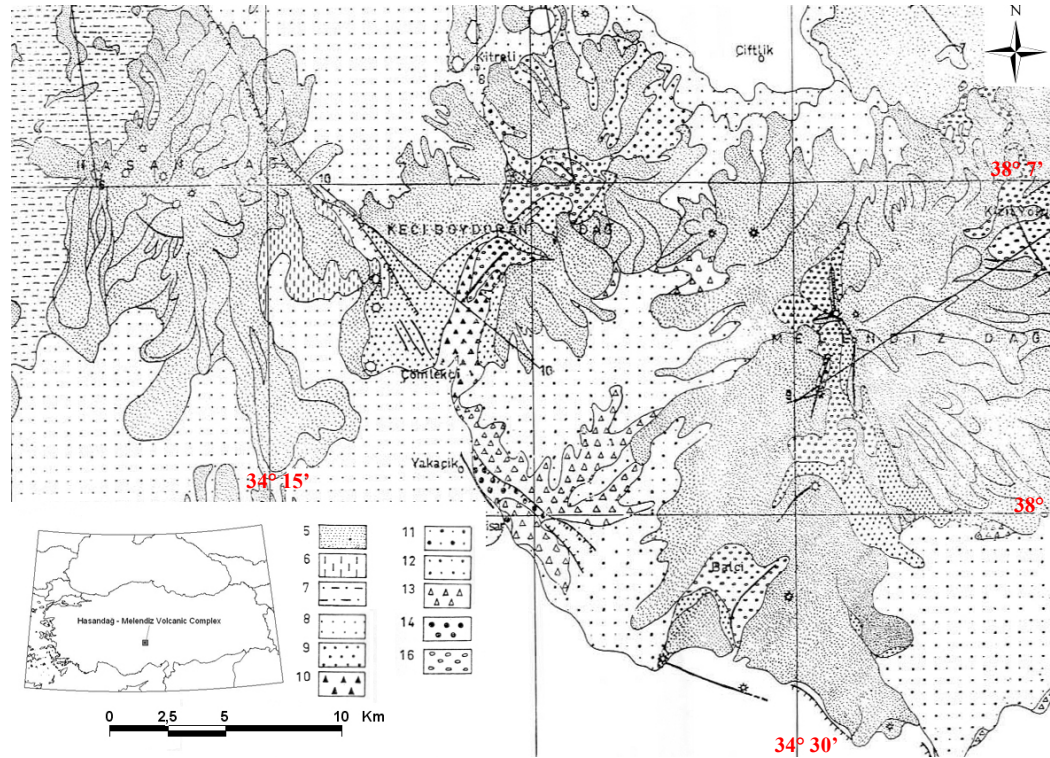


Figure 2.4. Detailed geological map of Hasandağ-Melendiz volcanic complex (Beekman, 1966). 5) Basalts, 6) Hasandağ ash flow tuffs, 7) Radial ash flow of Hasandağ, 8) Hasandağ ash formation, 9) Andesitic basalts and andesites, 10) Volcanic breccias, 11) Volcanic agglomerates and conglomerates of Keçiboyduran complex, 12) Agglomerates of Melendiz complex, 13) Tuff breccias, 14) Vitreous tuffs of Melendiz complex, 16) Pyroclastic formation of Melendiz complex.

2.5.5. Radial ash flow of Hasandağ complex

The deposit is characterized by light colored ash, slag, lapilli tuffs and andesite blocks with volcanic ash, sand and gravel in the matrix. This unit is outcropped steep sloped stream beds in the northwest flanks of Hasandağ complex (Fig. 2.4, No:7).

2.5.6. Ash formation of Hasandağ complex

The formation covers the wide areas north, west and south of Melendiz and Hasandağ volcanic complexes. 3 different types of depositions are a) homogeneous, b) layered, and c) mixed deposits.

Homogeneous ash and lapilli deposits are found in south and southwest of Hasandağ complex. Layered and sorted pumice outcrops in Göllüdağ region. Mixed type deposits of unlayered ashes, lava and tuff blocks of varying sizes are found in the north and northwest of Hasandağ (Fig. 2.4, No:8).

2.5.7. Ash flow tuffs of Hasandağ

These tuffs are found in southwest part of Hasandağ complex. The formation includes banded and non-welded tuffs. The colored bands are composed of plagioclase, quartz and biotite grains with different concentrations. The variety of these bands is linked with the selective erosion of the unit (Fig. 2.4, No:6).

2.5.8. Volcanic agglomerate and conglomerates of Keçiboyduran volcanic complex

This unit includes various sizes of mixed lava and tuff fragment in tuffaceous matrix and found in the valleys of northern flanks of Keçiboyduran mountain (Fig. 2.4, No:11). High andesitic content is observed.

2.5.9. Pyroclastic formation of Melendiz complex

This tuff formation outcrops only in Melendiz complex (Kızılyokuş caldera – Tepeköy region) and in volcanic center of Keçiboyduran complex. Whole formation is limonitized (iron oxidized) and some thin tuff layers are silicified. Undoubtedly, these volcanic centers are exposed to strong hydrothermal activity. Mineralization other than limonite and silica like large areas of sulphur deposition is an important evidence for intense hydrothermal activity. Rocks with colors of yellow, green, brown and purple observed. However, limonite and manganese deposits are observed between tuff layers, mostly they are deposited as disseminations and thin layers in the tuff. The matrix structures of agglomerates and tuff-breccias are in brown and purple for this reason

(dissemination). The hydrothermal fluid circulation also affected the large basaltic rock fragments that are separated from agglomerates. It is observed that these basalt fragments turned into soft tuff-like rock (clay altered rock) (Fig. 2.4, No:16).

2.5.10. Vitreous tuffs of Melendiz volcanic complex

The outcrop of this unit is restricted with Altunhisar region. Small fragments of pumice and lava pieces are light colored and loosely disseminated in compact tuff. Faint purple and brown colors are because of the thin disseminated limonite and manganese deposition (Fig. 2.4, No:14).

2.5.11. Agglomerates of Melendiz volcanic complex

This agglomeratic unit outcrops around Melendiz. Lower portions of the facies are recognizably layered but the upper portion lacks layering. Lower portion is characterized by volcanic conglomerate. In the upper portion of the facies is made up of mixed fragments of varying sizes. Not only andesites and basalts but also tuffs and ignimbrites are present in this upper portion, layered in a pebbly and sandy matrix (Fig. 2.4, No:12).

CHAPTER 3

ALTERATION MAPPING BY USING REMOTE SENSING

3.1. Alteration of Rocks

Hydrothermal alteration is defined as the reflection of response of pre-existing , rock-forming minerals to physical and chemical conditions different than those under which they originally formed, especially by the action of hydrothermal fluids (Beane, 1982).

The nature of the alteration products depends on 1) the character of the wall rock, 2) the character of the invading fluid, which defines such factors as Eh, pH, vapor pressure of various volatile species, anion-cation composition, and degree of hydrolysis, and 3) the temperatures and pressures at which the reactions take place (Guilbert and Park, 1986).

Alteration may result from 1) diagenesis in sediments, 2) regional processes, such as metamorphism, 3) postmagmatic or post-volcanic processes associated with cooling, and 4) direct mineralization processes.

Reactions that are important to alteration are of many times: 1) hydrolysis, 2) hydration-dehydration, 3) alkali or alkali-earth metasomatism, 4) decarbonation, 5) silication, 6) silicification, 7) oxidation-reduction and finally, a number of addition-removal interactions such as carbonatization, desulfidation, sulfidation, and fluoridation.

3.2. Alteration Types

The principle alteration assemblages and associates found in aluminosilicate rocks are explained below.

Potassic or biotite-orthoclase alteration, also known as K-silicate, involves the presence of introduced or recrystallized K-feldspar in a rock with or without biotite and sericite, commonly with traces of any of the characterizing calcium salt accessory minerals anhydrite, apatite, fluorite, calcite and scheelite also chalcopyrite, molybdenite, pyrite, magnetite or hematite.

Phyllic or sericitic alteration is characterized by the dominance of the phyllosilicate sericite, a name reserved for fine-grained white mica (muscovite) which results from alteration and metamorphism. All primary rock-forming silicates such as feldspars, micas and mafic minerals are converted to sericite plus quartz.

Propylitic alteration involves the alteration-generation of epidote, chlorite, and carbonates typically replacing plagioclase (epidote, chlorite, calcite) and hornblende-biotite (chlorite, epidote, montmorillonite).

Argillic assemblages are formed by the dominance of kaolinite after plagioclase, montmorillonite after the amphiboles and plagioclase. K-feldspar is metastable and not affected, but alkali and alkali-earth leaching and removal are substantial, except for potassium.

Advanced argillic represents low K^+ / H^+ and Na^+ / H^+ through both low activities of the alkalies and strongly acid, high H^+ fluids. Strong leaching of all alkalies occurs. At higher temperatures above about 300 °C, pyrophyllite or pyrophyllite-andalusite occurs; at lower temperatures, kaolinite and dickite prevail. Quartz is abundant, and alunite, topaz, tourmaline and other hydro-chloro-fluoro-boro-aluminosilicates also occur.

The alteration types that are used in this study and the representing minerals are shown in Table 3.1.

Table 3.1. Alteration types and representing minerals, used during this study.

Alteration Types	Representing Minerals
Potassic	Orthoclase
Propylitic	Epidote, Chlorite
Argillic	Kaolinite, Illite, Montmorillonite
Advanced Argillic	Pyrophyllite, Alunite
Oxidation (Fe)	Hematite, Goethite, Jarosite
Silicification	Quartz

3.3. Techniques of Remote Sensing in Alteration Mapping

Remote sensing is the science of gathering, analyzing and understanding of images and other data received from satellites and aircrafts that record the relation and interaction between matter and electromagnetic energy.

Hydrothermally altered rocks are characterized by unusually colorful rocks. The various colorful rocks are the host rocks of those mineral deposits with the colors representing the results of chemical interaction with the surrounding hydrothermal fluids. The hydrothermal fluid processes altering the mineralogy and chemistry of the host rocks can produce distinctive mineral assemblages which vary according to the location, degree and duration of those alteration processes. When these alteration products expose at the surface, sometimes it can be mapped at a zonal pattern, theoretically concentric around a core of highest grade alteration and greatest economic interest. The importance of the recognition of such spatial patterns of alteration makes the remote sensing techniques as one of the standard procedure in exploration geology, due to its speed and price.

One of the key idea of remote sensing techniques in exploration geology is that it is applied to rocks, minerals, and structures associated with a particular ore, and not the ore itself. There are very logical reasons for this procedure. The ore is not always exposed at the surface, and it often is not as spectrally unique or as widely disseminated as the minerals and rocks that are associated with the ore body (Vincent 1997).

3.3.1. Remote Sensing Technology

Materials on the earth's surface interact with the electromagnetic waves that are emitted from the sun and recorded by the remote sensing systems.

Therefore spectral reflectance curve of every material gives a unique signature. The reflectance curves of the minerals used in this study are presented in Chapter 4.

As the electromagnetic spectrum includes a wide range of wavelength, only a portion of it can be 'sensed' by the remote sensing systems. So called 'bandwidth' is one of the important features that identifies a remote sensing system's sensitivity to the electromagnetic waves. The sensitivity of an imaging remote sensing system operating in the visible and infrared spectral regions is measured by means of its spatial, spectral and radiometric resolution.

Spatial resolution is basically the area of the sensor that is covered on an instantaneous view. Digital images are represented by a single cell or pixel referring to the unit area that is recorded. Simply the pixel size defines the spatial resolution. Spatial resolution increases with the decreasing area represented by one pixel, which is 30 m x 30 m for Landsat 5 TM.

The term spectral resolution refers to the width of the spectral bands that the remote sensing systems are designed to be sensitive in recording the multispectral images. The width of the spectral bands is not the only important feature in the satellite imagery, the position of these bands in the spectrum and the number of these bands is also very important. Narrow bandwidth means high spectral resolution but also there should be enough number of spectral bands to successfully identify the targets on the images.

Radiometric resolution refers to the number of digital levels used to express the recorded data by the sensor. The amount of the detail visible on the image increases with the increasing number of binary digits. The multispectral images of Landsat 5 TM are recorded with the radiometric resolution of 8-bit, making the 256 brightness levels, where 0 for black and 255 for white.

There is no one aspect that makes a remote sensing system sensitive and accurate only by itself. Spatial, spectral and radiometric resolutions all together identify the power of the system. According to the type of the information desired different combinations of these elements become important. Large scale investigations like continental drifting require low spatial and spectral

resolution. Mineral mapping on the controversy requires high spatial, spectral and radiometric resolutions.

Conventional multispectral scanning systems, such as Landsat TM and SPOT XS, record up to 10 spectral bands with bandwidths on the order of 0.10 μm . Hyperspectral scanners are a special type of multispectral scanner that record many tens of bands with bandwidths on the order of 0.01 μm . Many minerals have distinctive spectral reflectance patterns at visible wavelengths and especially at reflected IR wavelengths. Under favorable conditions, many minerals may be identified on suitably processed hyperspectral data. The Airborne Visible/Infrared Imaging Spectrometer (AVIRIS) which is a hyperspectral system carried on high altitude aircraft by NASA records the spectral region covered by the 224 spectral bands (Rowan *et al.*, 2000). The advantages of both hyperspectral and broad band scanners (Landsat TM) can be integrated for detailed mapping purposes (Ferrier *et al.*, 2002).

Table 3.2 summarizes the characteristics of the principal remote sensing systems that are currently used for mineral exploration. Some systems like Landsat, SPOT, Aster, Ikonos are deployed only on satellites. Other systems like hyperspectral analyzers are generally deployed on aircraft. Radar systems are deployed on both satellites and aircraft. Images acquired by satellite systems have the following advantages: 1) archive of worldwide data is readily available; 2) images cover large areas on the ground; 3) prices per square kilometer are generally lower. Disadvantages of satellite images are: 1) the latest hyperspectral technology is currently available only from aircraft; 2) aircraft missions can be configured to match the requirements of a project.

3.3.1.1. The Landsat Satellites

Landsat satellites have been launched by NASA. Two generations of Landsat satellites have acquired valuable remote sensing data for mineral exploration and other applications. These were the generations which are placed in sun-synchronous orbits that provide repetitive images of the entire earth, except for the extreme polar regions. The first generation Landsats 1, 2, and 3 operated from 1972 to 1985 and is essentially replaced by the second generation. Table

3.2 lists some characteristics of the second generation Landsats 4, 5 and 7, which began in 1982 and continues to the present.

Table 3.2. Remote sensing systems for mineral exploration

	Characteristic	Landsat 4, 5 thematic mapper (TM)	Landsat 7 enhanced (ETM)	SPOT multispectral scanner (XS)	SPOT panchromatic (Pan)	Advanced Land Imager (ALI)	AVIRIS hyperspectral scanner	Hyperion
Spectral region	Visible and reflected IR	0.45 to 2.35 μm	0.45 to 2.35 μm	0.50 to 0.89 μm	-	0.45 to 2.35 μm	0.40 to 2.50 μm	0.40 to 2.50 μm
	Panchromatic	-	0.52 to 0.90 μm	-	0.51 to 0.73 μm	0.48 to 0.69 μm	-	-
	Thermal IR	10.5 to 12.5 μm	-	-	-	-	-	-
Spectral bands		7	8	3	1	10	224	220
Terrain coverage	East to west	185 km	185 km	60 km	60 km	37 km cross-track	10.5 km cross-track	7.5 km
	North to south	170 km	170 km	60 km	60 km	-	-	100 km
Ground resolution cell	Visible and reflected IR	30 by 30 m	30 by 30 m	20 by 20 m	-	30 m	20 m	30 m
	Panchromatic	-	15 by 15 m	-	10 by 10 m	10 m	-	-
	Thermal IR	120 by 120 m	60 by 60 m	-	-	-	-	-

Landsat 6 of the second generation was launched in 1993, but failed to reach orbit. The second generation of Landsat continued with Landsat 7, launched in April, 1999, with an enhanced TM system. A panchromatic band 8 0.52 to 0.90 μm with spatial resolution of 15 m is added. Band 8 can be combined with the visible and reflected IR bands 30 m resolution to produce a color image with an apparent resolution of 15 m. Spatial resolution of the thermal IR band 6 is improved from 120 m to 60 m.

Solar energy that is reflected from the earth's surface is separated by a spectrometer into narrow wavelength intervals called spectral bands. Each band is recorded as a separate image. Spectral reflectance curves that are shown in Figure 3.1 also display the band intervals of Landsat 5 TM. The vertical axis shows the percentage of incident sunlight that is reflected by the materials. The horizontal axis shows wavelengths of energy for the visible spectral region 0.4 to 0.7 μm and the reflected portion 0.7 to 3.0 μm of the infrared IR region. Reflected IR energy consists largely of solar energy reflected from the earth at wavelengths longer than the sensitivity range of the eye. The thermal portion of

the IR region 3.0 to 1000 μm consists of radiant, or heat, energy and is not shown in Figure 3.1. The TM system records three wavelengths of visible energy blue, green, and red and three bands of reflected IR energy, which are indicated in Figure 3.1. These visible and reflected IR bands have a spatial resolution of 30 m. Band 6, which is not shown on Fig. 3.1, records thermal IR energy 10.5 to 12.5 μm with a spatial resolution of 120 m (Table 3.3). Each TM scene records 170 by 185 km of terrain. The image data are telemetered to earth receiving stations (Sabins, 1999).

Table 3.3. Spectral Properties of Landsat TM 5.

Band	Wavelength μm	Properties
1	0.45 – 0.52	Blue and green, diffusion to water, vegetation - soil separation
2	0.52 – 0.60	Green, highly sensitive to green reflectance of vegetation
3	0.63 – 0.69	Red, Chlorophyll sensitive
4	0.76 – 0.90	Reflected IR, Identification of Biomass content and coastal line
5	1.55 – 1.75	Reflected IR, Moisture content of soil and vegetation, diffusion through thin layers of cloud, identification of vegetation types
6	10.40 – 12.50	Thermal IR, Moisture content of soil
7	2.08 – 2.35	Reflected IR, Sensitive to the absorption of the hydroxyl ions in the minerals

The minerals that have similar origins do have similar peaks and troughs in their spectral curves.

According to the alteration types the spectral reflectance of minerals show similar characteristics. Argillic and advanced argillic alteration minerals relatively have high reflectance values in TM band intervals of 2, 3, 4 and 5; low in band 7 (Fig. 3.1, 3.2). Propylitic alteration minerals have low reflectance in visible region of spectrum (TM 1,2,3) and higher in the short wave infrared region (TM 5,7) (Fig. 3.3). Iron oxide minerals have very low reflectance in band 1, reach to a temporal peak in band 3 and are maximum in bands 5 and 7 (Fig. 3.4).

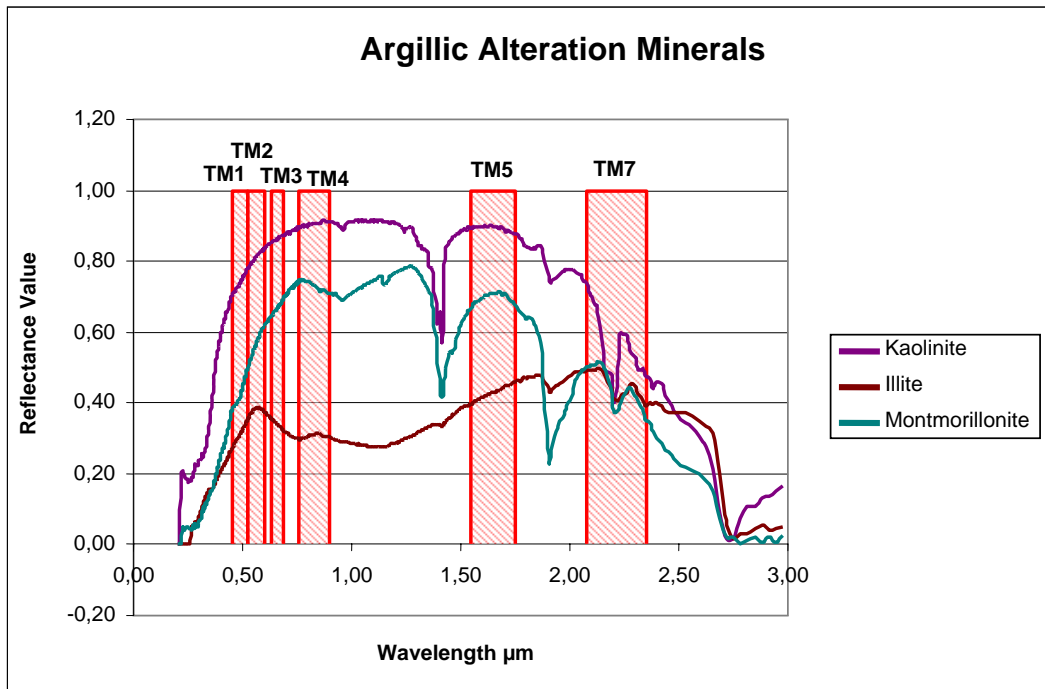


Figure 3.1. Spectral reflectance curves of argillic alteration minerals.

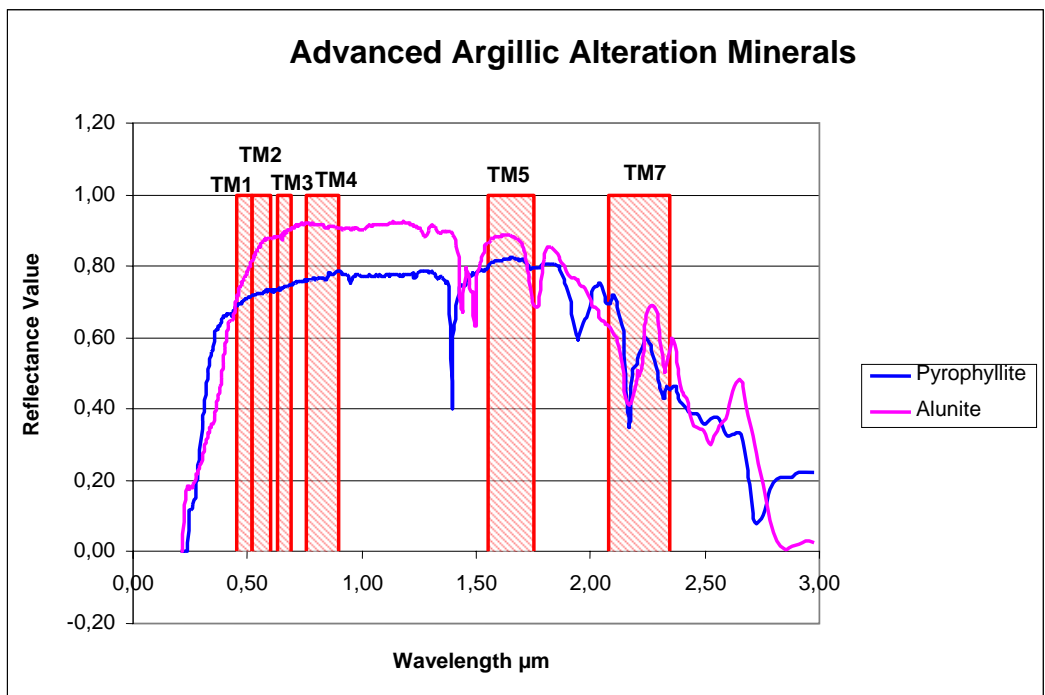


Figure 3.2. Spectral reflectance curves of advanced argillic alteration minerals.

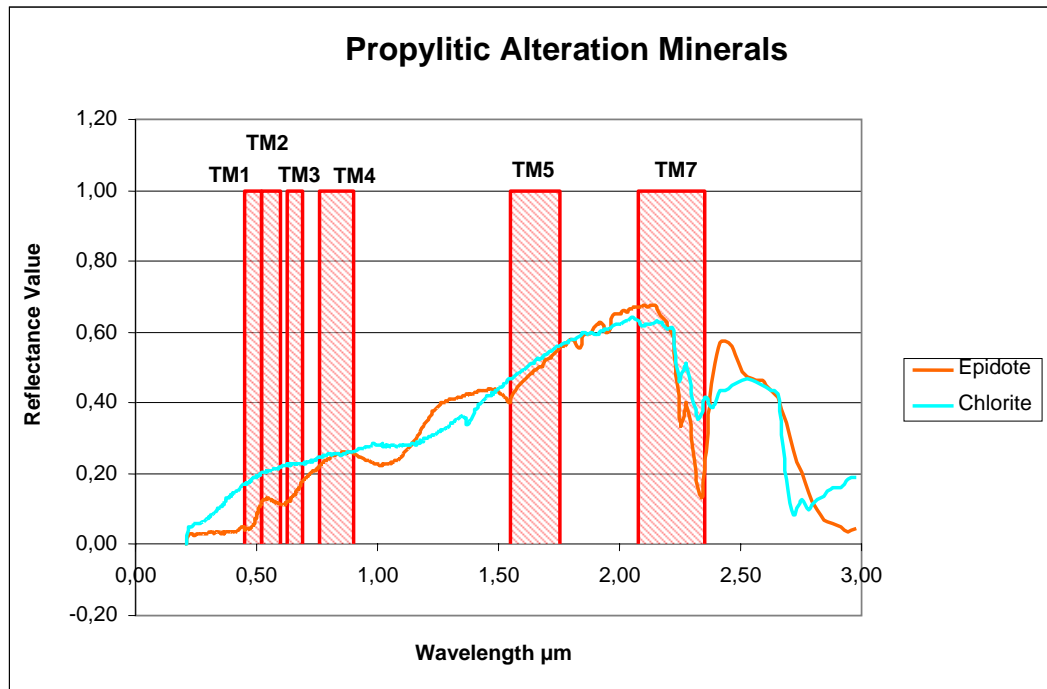


Figure 3.3. Spectral reflectance curves of propylitic alteration minerals.

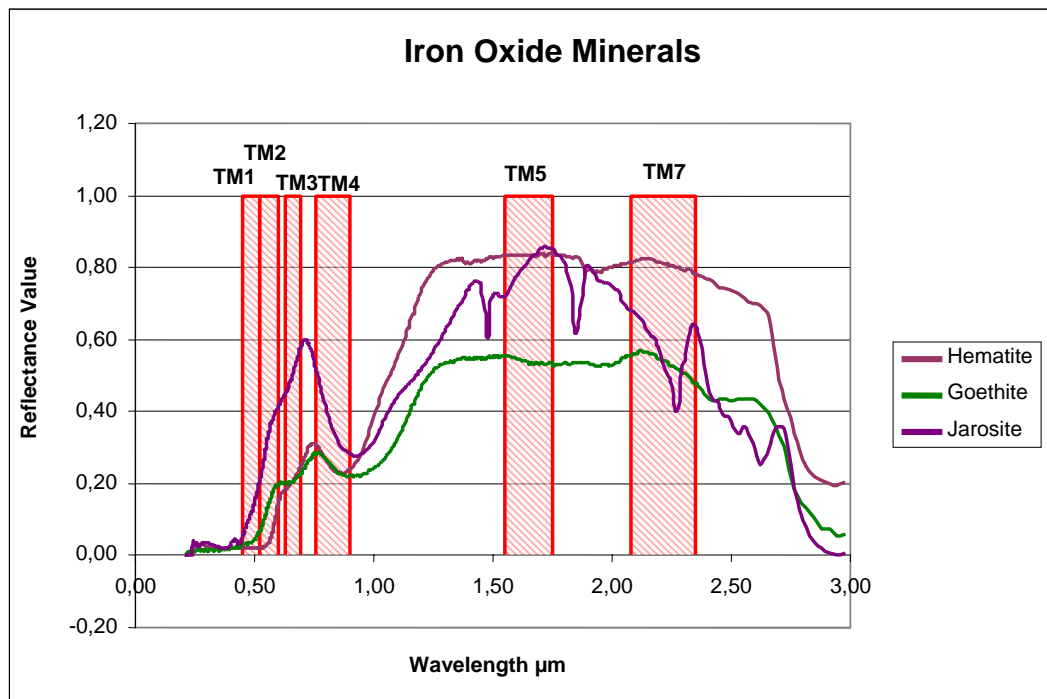


Figure 3.4. Spectral reflectance curves of iron oxide minerals.

3.3.2. Present Techniques in Alteration Mapping

Remote Sensing techniques have been applied for years and new methodological perspectives are still being developed by using this high technology. Color composites, band rationing, Crosta Technique and Least Squares Fitting Method are the well known and practiced conventional methods.

3.3.2.1. Color Composites

The idea behind this technique is to combine the multispectral information with the visible wavelength region, in order to make it visible to the human eye.

Every object in nature has unique reflectance values at different wavelengths. The colors that the human eye can see, is the combination of the reflectance at red, green and blue portions of visible wavelength region. The display devices imitate the human eye, by displaying the visible wavelength region.

Technically, most common type of color display in computer systems is the additive display, which means that the white light can be produced from the addition of three additive primary colors; red (0,6 - 0,7 μm), green (0,5 - 0,6 μm) and blue (0,4 - 0,5 μm) (Fig. 3.5). That is why RGB composition of Landsat 5 TM bands Band3, Band2 and Band1 is called True Color Composition (TCC), as it displays the image most likely as it is seen in nature to the human eye. All the other band compositions displayed as RGB are called False Color Composition (FCC) (Vincent, 1997).

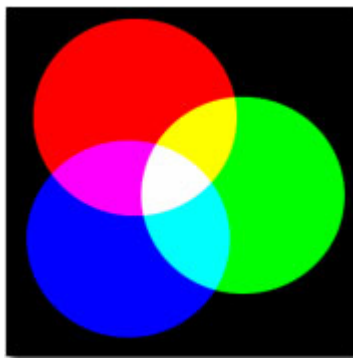


Figure 3.5. Additive colors.

The color composition, in fact, is the basis of the other techniques, because the results can be easily interpreted in detail with color composites by assigning the desired spectral band to the desired RGB channel.

Literature survey returned a large number of studies concerned on the best combination of bands to display the maximum information about the surface mineralogy.

A discriminant analysis was performed using all the seven TM bands, to compare the band interaction for enhancement of desired information (Faruqi, 1991). All possible 3 x 3 variance – covariance matrices are ranked corresponding to 3 dimensional subspace within n-dimensional data space, where n is equal to 7 in Landsat TM case. This determinant is considered as a measure of the volume of the 3-channel ellipsoid in a multispectral image entropy with the best 3 bands having the highest volume of all possible combinations. The best combination of TM bands according to this criteria, is found to be with color assignment of RGB in the sequence of 4, 5, 3. Another meaningful group is selected according to the spectral properties of bands. Band4 is selected for displaying NIR (Near Infrared) reflections, Band7 is selected to differentiate clay alteration zones and Band6 is used to differentiate the silicate rocks. RGB sequence of Bands 4, 7, and 6 displayed structural delineation by Band4, hydrothermal alteration haloes by Band7, temperature contrasts in older and younger phase of volcanism by Band6.

Statistical methods are found to be defective in a way that they ignore the distinction between geologically significant variance (color differences between or within rock types) and non-geological factors (differences in topography and shadow for surfaces with high and albedo, and differences between rock, vegetation, alluvium etc.). It is found to be better to assess each band individually by eye and choose the best three having the likely diagnostic features (Rothery, 1987).

Most of the previous studies are agreed to have the hydroxyl absorption band, which is Band7 and a general reflectance high band which is Band5. The bands, 7, 5 and 4 are combined in RGB were decided as the most informative image. Pillow lavas are observed in magenta and dykes in orange whereas gabbros have a distinct green tone. Faults and hydrothermally altered areas and intrusions are displayed as red (Rothery, 1987).

RGB color composites of TM bands 741, 541 and 531 are selected according to the index of optimum band selection criteria. Also for discriminating the clay minerals, TM742 and TM475 are selected. TM Band1 is substituted by Band2 because the visible blue wavelength is more affected by the atmospheric scattering. Bands 5 and 7 are used to discriminate clay minerals. Radiometric enhancement is found to be very important in visual analysis of RGB color composites which is performed by different methods like, linear contrast stretching, histogram equalization and decorrelation stretching (Chica-Olmo *et al.*, 2002).

RGB display of bands 7, 4 and 2 clearly makes the structural elements identifiable and allows discrimination of surficial units like sedimentary and volcanic rocks. Light reddish brown color represents granites and grayish-green color represent monzogranite (Abdelhamid and Rabba, 1994).

Based on the statistical results of average factoring, standard deviations and interband correlations of TM bands 2,3,4,5 and 7; combination of bands 4,7,2 and 4,7,3 are selected for color composite in RGB order of channels. Color composite of bands 4(R), 7(G), 2(B) displayed iron oxides as yellow green and the background as pink; 4(R), 7(G), 3(B) composite displayed again iron oxides as yellow green but the background as orange red (Jingyuan and Xucman, 1991).

The color composites discussed in the literature can be summarized in a table with the RGB color display correspondents (Table 3.4).

Table 3.4. Summary of the literally known color composites.

RGB display of respective TM bands	Red correspondent	Green correspondent	Blue correspondent	Extra	Reference
4 : 7 : 6	Structural lineament differentiation	Hydrothermal alteration	Temperature contrast		Rothery 1987
7 : 5 : 4	Hydrothermal alteration and intrusives	Gabbro	Vegetation		Rothery 1987
7 : 4 : 2	Clay minerals are brighter than the others	Vegetation		Radiometric correction is important	Chica-Olmo 2002
4 : 7 : 5	Vegetation	Clay minerals are brighter	Clay minerals are brighter	Radiometric correction is important	Chica-Olmo 2002
7 : 4 : 2	Granites, FeO, MnO displayed as reddish brown areas	Monzogranite in grayish-green	Sedimentary units in bluish-grey	Sedimentary and volcanic units are separated	Abdelhamid & Rabba 1994
4 : 7 : 2	Background is pink	FeO is yellow-green			Jingyuan & Xucman, 1991
4 : 7 : 3	Background is orange-red	FeO is yellow-green			Jingyuan & Xucman, 1991

3.3.2.2. Band Rationing

Band rationing is a multispectral image processing method that includes the division of one spectral band by another. This division results in the ratio of spectral reflectance measured in the one spectral band to the spectral reflectance measured in another spectral band.

Identical surface materials can give different brightness values because of the topographic slope and aspect, shadows, or seasonal changes in sunlight illumination angle and intensity. These variances affect the viewer's interpretations and may lead to misguided results. That is the band rationing operation which transforms the data and reduces the effects of such environmental conditions. In addition, rationing may also provide unique information not available in any single band which is very useful for disintegrating the surface materials (Jensen, 1996).

The band rationing is expressed mathematically as;

$$BV_{i,j,r} = \frac{BV_{i,j,k}}{BV_{i,j,l}}$$

Where $BV_{i,j,r}$ is the output ratio for the pixel at row i , column j ; $BV_{i,j,k}$ is the brightness value at the same location in band k , and $BV_{i,j,l}$ is the brightness value in band L . The range of $BV_{i,j,r}$ is theoretically from 0 to ∞ . But in fact, the range is from 1/255 to 255.

To represent the outcome of this function the resulting ratio matrix, is encoded to a standard 8-bit format by the help of normalizing functions like linear stretching.

Band ratios of 1.65 / 2.2 μm , 0.66 / 0.56 μm and 0.83 / 1.65 μm which correspond to Band5 / Band7, Band3 / Band2 and Band4 / Band5; are selected for the red, green and blue channels while displaying. Iron oxide-rich areas are displayed as green due to the presence of ferric iron charge transfer band in the ultraviolet, and clay-rich areas are displayed as red, due to the presence of the

hydrous minerals absorption band near 2.2 μm . Yellow or orange areas represent the areas where both clay and iron oxide minerals are present (Abrams *et al.*, 1983).

After the filtering process the contrast between the resulting images displayed dark-toned unaltered rocks, in shades of blue and green, and hydrothermally altered rocks, displayed in bright yellow to orange, coinciding with the preliminary mapped phyllic-potassic zones. However, discrimination between phyllic and potassic alteration zones couldn't be made. Granite outcrops are mapped as reddish – orange areas (Abrams *et al.*, 1983).

A set of ratios are selected reflecting the spectral behavior of iron oxides, minerals containing OH, H₂O, CO₃ and SO₄ molecules and vegetation. Band ratio 4/3 displays vegetation in bright tones caused by the high reflectance of mesostructure in the NIR band in contrast to the steep fall-off of reflectance towards the visible (TM 3) due to intense chlorophyll absorption (Kaufmann, 1988).

Clay minerals containing water (bound or unbound), micas, carbonates, sulphates and hydrates are enhanced by the band ratio 5/7. The ferric and ferrous iron is best enhanced by the band ratios 7/4, 7/1 or 5/4, and 5/1 due to major electronic transition bands in NIR (at $\sim 0.87 \mu\text{m}$) and the visible, charge transfer bands in ultraviolet and the unaffected SWIR range. Mostly used band ratio 3/1 often fails because the difference between bands 3 and 1 is much less than the combinations with SWIR bands with bands 1 or 4.

Spectral variations are enhanced while albedo differences are suppressed by rationing the bands but the technique is not capable of suppress the nonlinearities and non-periodic loss of rows.

The color composite created by band ratio 7/4, 4/3 and 5/7 displayed as RGB respectively. Consequently red color represents the minerals containing iron ions, green represents the vegetated zones and blue represents OH/ H₂O-, SO₄- or CO-bearing minerals (rocks and soils) (Kaufmann, 1988).

Non detectable alteration centers with color composite images are revealed by using TM band ratio image of 5/7. But it is observed that the ratio of 5/7 is

sensitive also to vegetated areas. To filter out the vegetation mapped, band ratio of 4/3 is subtracted from the band ratio of 5/7 and both are then weighted to optimize the result. This technique revealed alteration, otherwise undetectable because of vegetation around it (Amos and Greenbaum, 1989).

The proportions of kaolinite, illite and free iron increase from the contact towards the granite intrusion, while the proportions of chlorite and smectite decrease. Laboratory reflectance spectra of soil samples demonstrate that with the increase of the proportion of kaolinite, illite and free iron and the decrease of chlorite ratios of TM bands 2/3, 2/5, 2/7 decrease while the ratios of bands 3/4, 4/7 and 5/7 increase. Stepwise masking of various band ratio images are used to distinguish pixels that correspond with kaolinitic soils by eliminating of other pixels. Basically, the pixels with the highest values for TM2/TM7 are equalized to zero. As the chlorite-rich samples returns higher values than the kaolinite-rich soils, chlorite is masked revealing only the kaolinite-rich soils mapped on the image. Masking can be formulized as:

If (Band2 / Band7) x (Scaling factor) is less than (Upper Limit Value) than assign that pixel to 0

Else assign that pixel to 1

The final map therefore will display the kaolinite-rich soils as black pixels and the others will appear as white. Also masking the vegetation and iron-rich soils are performed in the same way (Goossens and Kroonenberg, 1994).

RGB image produced by respectively band 3/4, 5 and 5/7 is found successful displaying the iron oxides as apricot yellow and the background as sky-blue (Jingyuan and Xucman, 1991).

Band ratio of TM5/TM7 is found very effective in highlighting clay minerals, TM5/TM4 and TM3/TM1 enhanced the areas with iron minerals and ferric oxides, respectively. RGB composite of TM5/TM7, TM5/TM4 and TM3/TM1 revealed the main geological features of the region (Chica-Olmo *et al.*, 2002).

Ratio images are advantageous in enhancing the features in shadows in mountainous terrains. The RGB color composite of ratio images respectively, 5/7, 3/1 and 5/4 maps the granite and the volcanics in dark-blue to blue and

violet-blue colors, reflecting the presence of Fe and Mn-oxides. Also the color composite of TM 3/1, 5/7 and 4/5 band ratios assigned to RGB channels respectively, with histogram equalization, clearly displays the distribution of highly altered zones in dark-blue to violet-blue colors (Abdelhamid and Rabba, 1994).

The color composites with band ratios that are literally known are summarized in the Table 3.5.

Table 3.5. Summary of literally known band ratio composites.

RGB display of respective TM band Ratios	Red correspondent	Green correspondent	Blue correspondent	Extra	Reference
5/7 : 3/2 : 4/5	Clay-rich areas	FeO rich areas		Yellow, orange areas both clay and FeO rich	Abrams et al. 1983
7/4 : 4/3 : 5/7	Minerals containing iron ions	Vegetated zones	OH/ H ₂ O-, SO ₄ - or CO-bearing minerals		Kaufmann 1988
3/4 : 5 : 5/7				FeO as apricot yellow and the background as sky-blue	Jingyuan & Xucman, 1991
5/7 : 5/4 : 3/1	Clay minerals	Iron minerals	Ferric oxides		Chica-Olmo 2002
3/1 : 5/7 : 4/5				Highly altered zones dark-blue to violet-blue	Abdelhamid & Rabba 1994

3.3.2.3. Principal Component Analysis

The Principal Components process uses the principal components transformation technique for reducing dimensionality of correlated multispectral data. The technique is used widely with a few to many correlated rasters to create a lesser number of objects.

Information from six bands of thematic mapper (TM) imagery is transformed to three processed images that contain virtually all of the variance from the set of input objects in this method. The three output bands can be displayed simultaneously as components of an RGB display, which is easier to interpret than the raw data. Also, transformation sometimes enables you to see details that were obscured in the raw data.

Principal components analysis consist the translation of the origin and rotation of the data axes to better fit the brightness values of input objects. Each input object is a coordinate axis and each output object is a principal components axis.

Principal component transformation consists of two-step process. In the first step n histograms of the scene to be imaged are used as inputs to the principal component algorithm. This algorithm calculates n principal components, which are actually orthogonal vectors in n -dimensional space that are oriented along directions of maximum remaining variance. The projection coefficients of the n spectral bands onto the final n principal components are the result of the first step with the help of the equation:

$$P_k = \sum_{i=1}^n a_{i,k} DN(i)$$

Here P_k is the k th principal component value for a given pixel, $DN(i)$ is the digital number of the i th spectral band (out of total n bands) for a given pixel, and $a_{i,k}$ give the projection coefficients calculated by the principal component algorithm for projecting digital numbers from the n spectral bands onto the n principal component vectors.

Most of the variability in the information in the input objects is found in two or three of the objects. The other input objects contain decreasing amounts of the variance in the information set.

In a scatter plot of the brightness values from two objects that contain most of the variability in the information set, the data resembles an ellipse and the original axes and origin do not fit the distribution very well (Fig. 3.6). Moving the origin to the location of the mean values of the two sets of data will surely give the axes a better fit to the data. Data is then translated, that is rotated, the major axis using this new origin. The first principal component axis extends along the major (longest) axis of the ellipse and encompasses most of the variability in the information set. The minor axis, which is the second principal component axis, is orthogonal to the major axis, and it is aligned along the maximum remaining variance. The variances of the principal components are called eigenvalues. Therefore, the maximum amount of remaining variance; which becomes smaller as the order of the principal component increases, is

removed by each subsequent principal component, orthogonal to all the other principal components. Consequently, the n th component, contains all of the remaining variance and separates the most spectrally unique pixels from the rest of pixels in the image. The total variance of all principal components sum up to 100% of the total variance of the data; with the first three PCs usually accounting the majority (50% - 95%) of the variance, when $n > 3$.

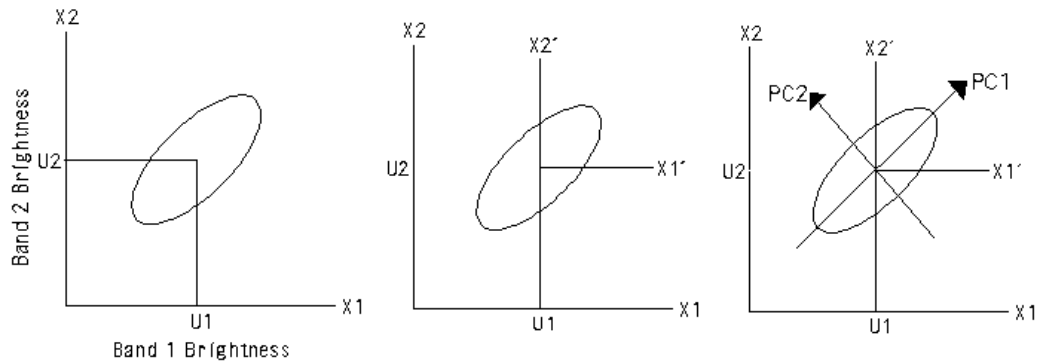


Figure 3.6. Visual construction of the principal components from original data.

The second step consists of the transformation of the image to principal component space. Using the equation n principal component values for each pixel is calculated. The resulting PCs include information from all other bands. The first principal component displays the greatest variance, and highlights sunlit slopes rather than shadowed areas. The n th principal component image usually gives the homogeneous image, interrupted by a few bright and dark pixels that are spectrally unique for that image scene.

It is possible to create a color composite by using the desired 3 of the n PCs, when $n > 3$. As the most of the variance is represented by the first three principal components, they are used as a color composite to observe boundaries between terrain units. Color composites of the higher order principal component images, including the n th one, makes it possible for the small areas on the ground that are spectrally outrageous to be identifiable (Vincent, 1997).

Crosta Technique

Reducing the number of spectral bands input for principal component analysis ensures that certain materials will not be mapped and increases the likelihood that others will be unequivocally mapped into only one of the principal component images. The methodology is called Crosta Technique. The method does not require detailed knowledge of the spectral properties of target materials; also no atmospheric or radiometric correction is needed. PCA on raw, unstretched data is found to be effective in all cases. Resulting images produced by PCA were judged and found to be accurate in delineating alteration zones.

The magnitude and sign of eigenvector loadings (eigenvalues) give information about which spectral properties of vegetation, rocks and soils are responsible for the statistical variance mapped into each PC, and this is the basis of the Crosta technique.

The method is applied to 6 TM bands (1, 2, 3, 4, 5 and 7) and the results made it clear that in any case it is not possible to separate the mineral classes into any single principal component image. Therefore, the number of input channels is reduced to avoid a particular spectral contrast and the chances of defining a unique principal component for a specific mineral class will be increased.

Selective PCA can be used to both reduce the dimensionality of a data set, while minimizing the loss of information and to enhance and map the spectral contrast between two different spectral regions. The degree of correlation between two TM bands is related to the amount of spectral contrast between them. Higher correlation between the spectral bands means less contrast and the lower correlation means more contrast (Chavez and Kwarteng, 1989). Feature Oriented Principal Components Selection is based on the examination of PCA eigenvector loadings to decide which of the principal component will extract information directly related to the theoretical spectral signatures of specific targets. The methodology relies specifically on the selective input of only four image bands for PCA. This technique performed by using four selected TM bands in order to highlight the spectral response of iron-oxide minerals (absorption in visible TM bands 1 & 2 and higher reflection in TM3) and hydroxyl-bearing (clay) minerals (absorption in TM7, higher reflectance in TM5).

In hydroxyl mapping TM bands 1, 4, 5 and 7 are used. To avoid mapping the iron-oxides TM bands 2 and 3 are not considered, but instead of TM1, either of them could substitute. The analysis showed that the albedo (reflectance) is mapped by PC1, and the spectral difference between shortwave-infrared and visible ranges is mapped by PC2. PC3 is found to be responsible for displaying the vegetation as brightest and PC4 highlights hydroxyl-bearing minerals as dark pixels in the PC image. To map the hydroxyls in bright pixels PC4 is negated (multiplied by -1) and called Crosta hydroxyl (H) image (Loughlin, 1991).

One very important property of this H image is the fact that it has a negative contribution from vegetation in TM4 (when negated) and therefore vegetated areas are not highlighted and separated (Tangestani and Moore, 2002).

Similarly the iron-oxide map is obtained by using the unstretched TM bands of 1, 3, 4, and 5. The substitution of TM5 with TM7 results with little effect. The principal components can be interpreted as; albedo in PC1, difference between SWIR and visible spectral ranges in PC2, vegetation in PC3 and iron-oxide minerals in PC4 as bright pixels after negated. So, PC4 of this transformation is called Crosta iron-oxide image (F). Iron-oxides could also be mapped in PC2 with hydroxyls, therefore the eigenvector loadings of the iron-oxide and hydroxyl sensitive bands (TM1, 3 and 5) should be checked considering with the vegetation band of TM4 (Tangestani and Moore (2002).

The information stored on the H and F images are combined to produce a map displaying the pixels with anomalous concentrations of both hydroxyls and iron-oxides as the brightest. This new image is called H+F image. This merging of the two images is also achieved by PCA; such as the principal component having positive eigenvalues from both input bands is selected.

By using the Crosta H, H+F and F images, where they are stretched, in desired combinations, color composites are prepared. Respectively displaying the Crosta images of H, H+F and F in RGB channels returns a dark bluish color composite image on which alteration zones are unusually bright. White pixels within alteration zones are the areas where both iron-stained and argillized. Bright reddish to orange zones are more argillized than iron-stained; and bright cyan to bluish zones are more iron-stained than argillized (Loughlin, 1991).

Although the PC images in initially stretched forms provided brighter images and distinction for lithological units, they are found very similar to those of unstretched data and a disturbance of other features prevented the enhancement of the alteration.

3.3.2.4. Least Squares Fitting Method

Assuming that a sample of variables y_i and x_i are included in the data of interest and the value of y_i is not known. The least squares fitting method allows the calculation of the estimates of y_i , written \hat{y}_i , where the corresponding x_i is given, using a function of the form,

$$\hat{y}_i = a_0 + a_1 x_i$$

Each unknown value of the variable y_i is to be estimated given the corresponding known value of the variable x_i . The terms a_0 and a_1 are called least-squared coefficients. They are computed from the sample values of x and y , and have the property that the sum of the squared differences between the true (usually unknown) values y_i and the values \hat{y}_i , which is estimated from the equation, is a minimum for all possible value of a_0 and a_1 . These least squared differences are called residuals. Therefore the equation should be revised as,

$$\hat{y}_i = a_0 + a_1 x_i + r_i$$

The equation gets complicated when there are more than one predictor variable. When there are 6 bands as the predictor bands, number of coefficients are 7. Therefore, the sixth order polynomial function represents the equation (Mather, 1987).

The technique assumes that the bands used as input values are behaving as the variables of a linear expression. And the 'y' value of the equation, namely the predicted band information, gives us a calculated output value. This predicted band is what that band should be according to the linear equation. The problem of having vegetation responsible of some reflectance in the bands that are used to map clay minerals, can therefore be omitted by using this technique. The vegetation is mapped in the predicted band with the values that are calculated just by using the reflectance information in the other bands. The minerals which are sensitive to a specific band are then differentiated from the features which are reflective to the

other bands as well; just by taking the difference between the predicted values and the original values. Calling this difference, the residual, color composites are displayed with the specific anomalously reflective features and then interpreted (Clark *et al.*, 1993).

Table 3.6 represents the coefficients and constants obtained as a result of the multiple regression analysis. The formulae can be summarized as:

$$\text{Predicted Band} = a_1*B_1 + a_2*B_2 + a_3*B_3 + a_4*B_4 + a_5*B_5 + \text{Constant}$$

$B_1 \dots n$: independent or predictor variable

$a_1 \dots n$: least-squares coefficient for $B_1 \dots n$

Table 3.6. Coefficients and constants of the sixth order polynomial equation.

Raster	Constant	band1	band2	band3	band4	band5	band7
band1 =	36,9442		1,5459	-0,0956	-0,0489	-0,0795	0,1542
band2 =	-1,0507	0,2244		0,395	0,0378	-0,0061	-0,0254
band3 =	-14,6677	-0,0583	1,6583		-0,0439	0,0276	0,1049
band4 =	27,9649	-0,2649	1,4088	-0,3905		0,7986	-0,9609
band5 =	12,7783	-0,2956	-0,1552	0,168	0,548		1,4506
band7 =	-5,7889	0,2046	-0,2322	0,2283	-0,2354	0,518	

By using the residual band3, residual band 7 and residual band 1 we can map hematite, clay and goethite. Here, it should be important to use Visible bands when calculating the residuals for these bands and to use IR bands when calculating the residuals of these bands. So it should be better to use Bands 1,2,3 for residuals of these bands and Bands 4,5,7 for residuals in the linear equations. It is stated that using the residual band 3, residual band 7 and residual band 1 respectively in RGB display we interpret the followings:

White : Goethite + Hematite + Clay

Orange : Hematite + Clay

Cyan : Goethite + Clay

Purple: Hematite + Goethite

Red : Hematite

Green : Clay

Blue : Goethite

3.3.3. Mineral Mapping by using Spectral Reflectance Data

The technique is purely based on the band rationing process. More than the band selection criteria, a filtering script based on the statistical calculations is developed. The technique can be summarized as in a flow chart in Figure 3.7.

Spectral reflectance data of the alteration minerals is statistically processed according to the TM band intervals. Descriptive statistics like the minimum, maximum, mean and standard deviation are calculated for the TM band intervals separately for every mineral (Table 3.7).

P-P and Q-Q plots are analyzed to obtain information about the distribution type of the data belonging to the band intervals for every mineral. Generally data is found to be normally distributed. For all of the data it is therefore assumed to be normally distributed, although it is not an accurate assumption for the whole data.

Two standard deviations are added to the mean value to have the upper limit and subtracted to have the lower limit of the mineral mask that is used to filter the band ratios.

Reflectance data is sorted according to the wavelength intervals of TM bands; 0.45 – 0.52 for band1, 0.52 – 0.60 for band2, 0.63 – 0.69 for band3, 0.76 – 0.90 for band4, 1.55 – 1.75 for band5 and 2.08 – 2.35 μm for band7. The technique is applied to spectral reflectance data for illite and explained as an example.

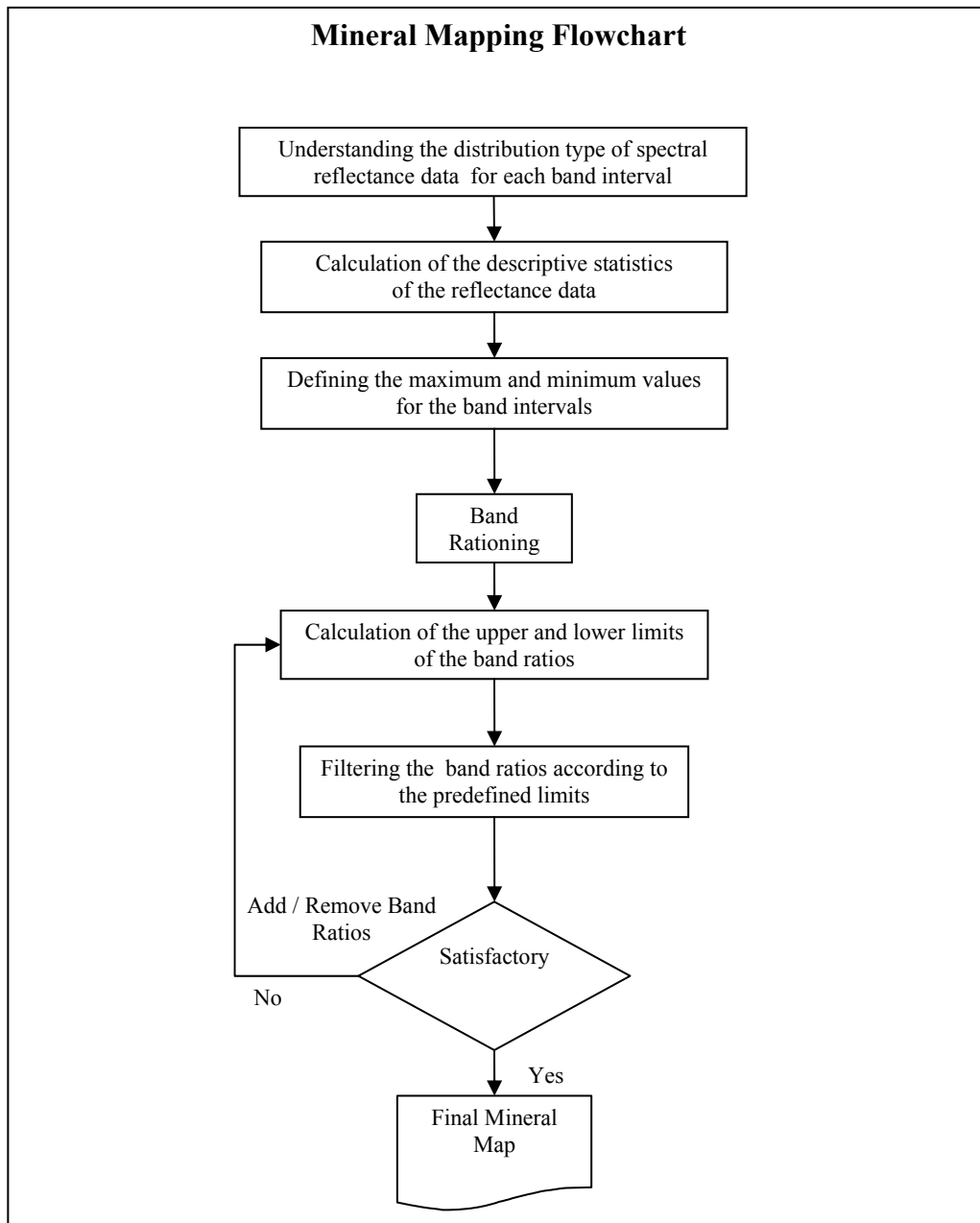


Figure 3.7. Flow chart of the mineral mapping technique.

Table 3.7. Descriptive statistics of illite for TM band1 interval.

Descriptive Statistics of Reflectance Value for Band1			
		Statistic	Std. Error
Mean		0,306706571	0,003749428
95% Confidence Interval for Mean	Lower Bound	0,299086817	
	Upper Bound	0,314326326	
5% Trimmed Mean		0,306382063	
Median		0,30469	
Variance		0,000492037	
Std. Deviation		0,022181916	
Minimum		0,27222	
Maximum		0,34724	
Range		0,07502	
Interquartile Range		0,03929	
Skewness		0,232904983	0,397694044
Kurtosis		-1,100219708	0,777794391

Having calculated the mean value (μ) and the standard deviation (SD), by using the following algebra,

$$\mu + (2 \times SD) = \text{Maximum} \quad \mu - (2 \times SD) = \text{Minimum}$$

upper and lower limits for the filtering function of band1 is calculated as:

Maximum: 0,351070403

Minimum: 0,26234274

The same procedure is followed for the rest of the bands and results are tabulated in Table 3.8.

Table 3.8. Limiting values of the Illite spectral reflectance that are used in the filtering of TM band ratios.

	Maximum	Minimum
Band1	0,35107	0,26234
Band2	0,39603	0,35595
Band3	0,35970	0,32084
Band4	0,31592	0,29506
Band5	0,46474	0,39175
Band7	0,51549	0,37939

These limiting values for all of the band ratio combinations are calculated. Simply the ratio of the minimum of a band in the nominator to the maximum of a band in the denominator gives the lower limit of this ratio. Vice versa, the ratio of the maximum of a band in the nominator to the minimum of a band in the denominator gives the upper limit of the same ratio.

$$\begin{aligned} \text{Band1_Max} / \text{Band2_Min} &= \text{UpperLimit} \\ \text{Band1_Min} / \text{Band2_Max} &= \text{LowerLimit} \end{aligned}$$

The limiting values for all of the possible band ratios are calculated in the same manner and tabulated in Table 3.9.

Table 3.9. Limiting values of band ratios that are calculated from the spectral reflectance data of Illite.

Limiting Values for all combinations of band ratios according to Illite spectra						
Band Ratios	Upper Limit	Lower Limit		Band Ratios	Upper Limit	Lower Limit
Band1/Band2	0,986286402	0,662436973		Band4/Band1	1,204210164	0,840446448
Band1/Band3	1,094216397	0,729335108		Band4/Band2	0,887524122	0,745040323
Band1/Band4	1,189843806	0,83041983		Band4/Band3	0,984646492	0,820280399
Band1/Band5	0,896162591	0,564495285		Band4/Band5	0,806424903	0,634885683
Band1/Band7	0,925343152	0,508919539		Band4/Band7	0,832683454	0,572379854
Band2/Band1	1,509577577	1,013904275		Band5/Band1	1,771493981	1,11586894
Band2/Band3	1,234336257	0,989576202		Band5/Band2	1,305622297	0,989197298
Band2/Band4	1,342209232	1,12672994		Band5/Band3	1,448497437	1,08909428
Band2/Band5	1,010920675	0,765918292		Band5/Band4	1,575086708	1,24004107
Band2/Band7	1,043837952	0,690512029		Band5/Band7	1,224947083	0,759954311
Band3/Band1	1,371111838	0,913896011		Band7/Band1	1,964947153	1,080680176
Band3/Band2	1,010533598	0,81015201		Band7/Band2	1,448200695	0,958003106
Band3/Band4	1,219095326	1,015592914		Band7/Band3	1,606678286	1,054749851
Band3/Band5	0,918194153	0,690370569		Band7/Band4	1,747091538	1,200936557
Band3/Band7	0,948092099	0,622402138		Band7/Band5	1,31586858	0,816361796

The tabulated limiting values are then used in the filtering formula which lets the pixels having the values between these upper and lower limits after rationing process. The formula used is as follows, where the limiting values are highlighted in Table 3.9.

$$\begin{aligned} &\text{if } (1.5751 < (\text{band5} / \text{band4}) > 1.2400) \text{ and} \\ & (0.5089 < (\text{band1} / \text{band7}) > 1.5089) \text{ and} \\ & (1.0438 < (\text{band2} / \text{band7}) > 0.6965) \\ & \text{output} = 1 \\ & \text{else} \\ & \text{output} = 0 \end{aligned}$$

Therefore, the pixels having values between the limits will be displayed as white, the others as black, and the resulting image will be statistically a map of illite.

CHAPTER 4

DATA AND ANALYSIS

4.1. Data

Thematic Mapper (TM) images of Landsat 5 satellite are used throughout the analysis. As the focused area of interest is divided between the images with orbit and section numbers of 176/33 (covering north) and 176/34 (covering south), 2nd quadrant of the 176/34 image is selected in order to cover the Hasandağ-Keçiboyduran and Melendiz volcanic complexes. As long as the images are known to be recorded on the same day, the image mosaicking is not preferred to avoid data distortion. Therefore, no geometric correction is applied by means of georeferencing to the image while processing. Because, during the mosaicking procedure pixels are resampled and assigned to new values, study area is selected restrictedly to avoid this procedure.

TM bands of 1,2,3,4,5 and 7 are used extensively in most of the processes and the Thermal Infrared band of 6 is used only in a color composite. The whole image having 2984 lines and 4320 columns of pixels is extracted to have a subscene of the study area having 1172 lines and 1996 columns; in order to minimize the disturbance of the unrelated pixels. Figure 4.1 displays the RGB composition of TM Bands 3,2,1 for this extracted raw image.

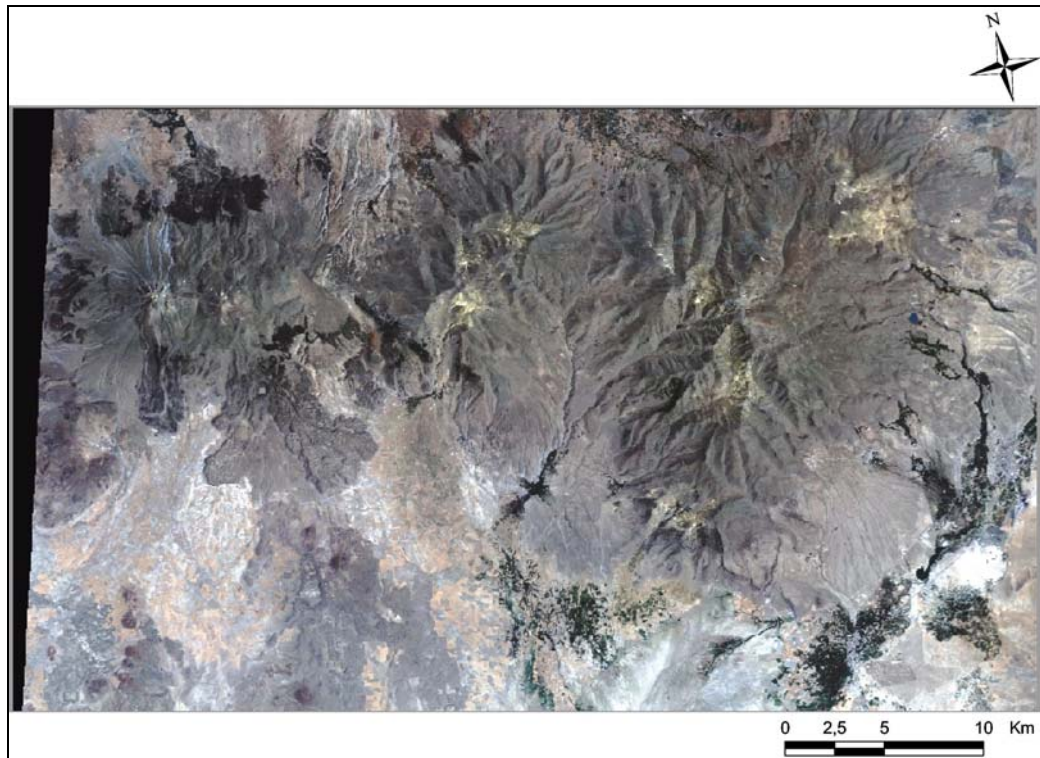


Figure 4.1 RGB display of TM Bands 3, 2, 1 respectively.

Furthermore, the volcanic units mapped in the area are separated from the surrounding units to better highlight the intended output maps. Geological map prepared by Toprak (1997) (Fig. 2.2) used as the reference guide for masking out the non-volcanic units. The boundary between the volcanics and fluvial deposits is drawn manually as a polygon. The units outside this polygon are simply cropped by using the TNT Mips software. Figure 4.2 displays the RGB composite of TM 3,2,1 respectively.

The laboratory spectrum data for the minerals are gathered from USGS spectral library. As there are many spectrum data available for a specific mineral, the one which represents the other spectrums tried to be selected.

Laboratory Reflectance Spectra

Apart from the Landsat 5 TM image, the laboratory spectra for the previously selected minerals are gathered from USGS spectral library (<http://speclab.cr.goc/>). The spectral reflectance of these minerals are analyzed in the laboratory conditions. The samples have descriptions about their location,

homogeneity, physical and chemical properties compositions with XRD (X-ray diffractometer) analysis results attached to the reflectance data.

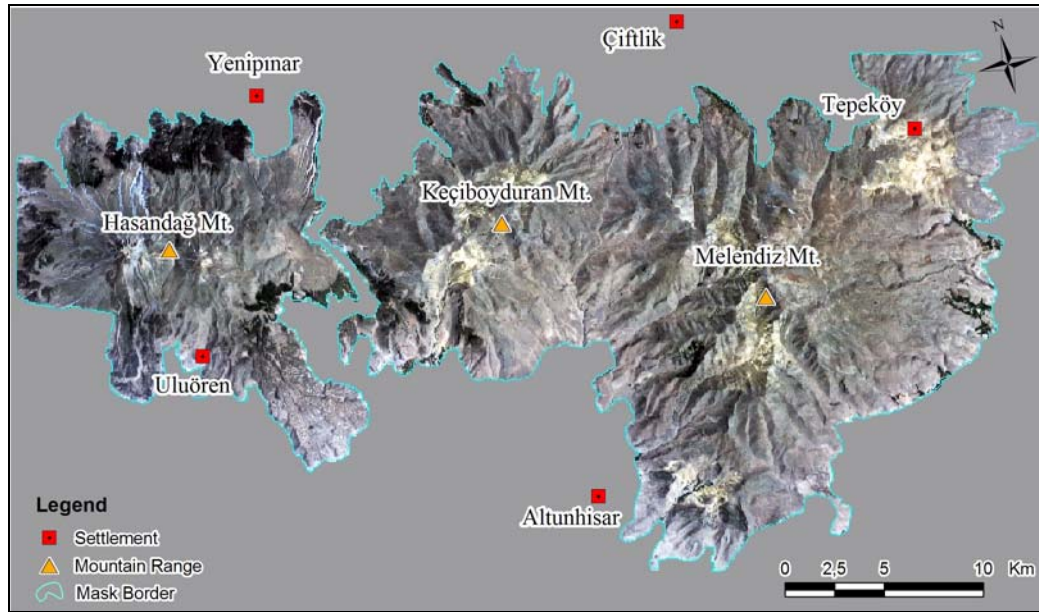


Figure 4.2. Linear contrast stretched RGB display of TM Bands 3, 2, 1 respectively. Non-volcanic units are masked out.

In the USGS data set, as it acts like a database, there are many samples gathered from different localities having different ingredients. This variety results in slight chemical differences in the sample, hence yielding in different intensities in reflectance or even resulting different spectral curves. However, all of the samples are proved to belong to same mineral so the majority of different samples are showing characteristic spectral trends. Based on this property a single laboratory spectrum showing the general trends of the selected mineral is chosen. Figure 4.3 shows the plots of 4 different kaolinite samples and the one that is chosen for the use in processes as red (Kaolinite CM3).

4.1.1. Preprocessing

Radiometric and geometric corrections are the preprocessing techniques used in order to compensate the atmospheric or equipment related errors recorded on the image.

On a remotely-sensed image, a value at any pixel location is not a record of the ground-leaving radiance at that point. The ground-leaving signal is degraded by absorption and its directional properties are altered by scattering. Atmosphere does not behave as hundred percent transparent, it reflects and also absorbs the sun rays before and after they arrive to the target on the ground. The multispectral bands in the $0.4 - 2.4 \mu\text{m}$ region of the spectrum therefore is subject to this signal alteration with variable amounts (Fig. Jensen 1996, pg.112). This atmospheric effect is known as the haze, and it is removed by means of correlating the bands that are less sensitive with the more sensitive bands (Mather, 1987 and Jensen, 1996).

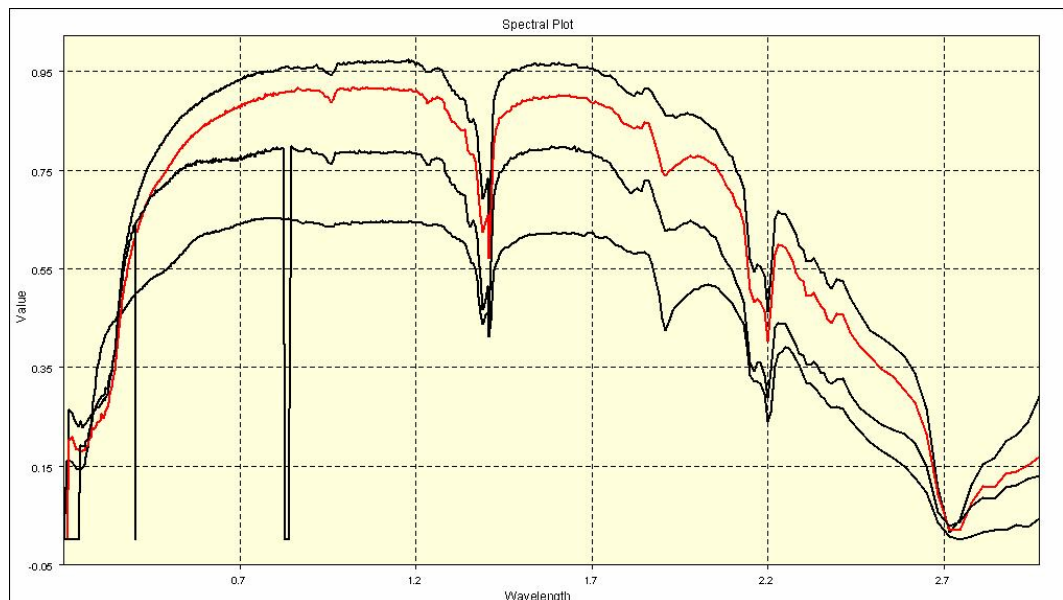


Figure 4.3. Spectral reflectance curves of 4 different kaolinite samples. The red one is selected and used in the processes.

TM bands 1,2 and 3 are correlated with the band 7 and the haze amounts are decided (Fig. 4.4). In the graph x-axis is the band1 and y-axis is the band7 grey levels. Band 7 values start from very near to 0 whereas band 1 values start from 52, showing that the pixels are displayed over-reflectant by this much, which known as a radiometric error caused by the atmospheric transmission. Two bands are highly correlated after the grey level of 52. This amount is subtracted from the band 1 reflectance data to remove this error.

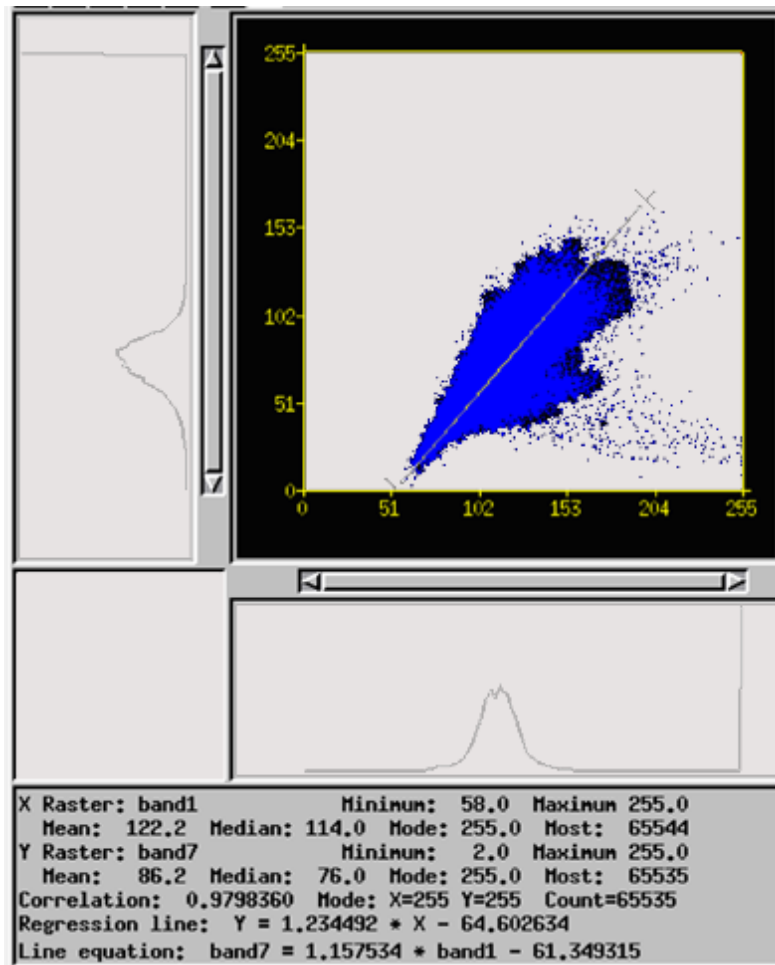


Figure 4.4. Band correlation graph between band 1 and 7.

Accordingly, the haze amounts that are removed are tabulated in Table 4.1.

Table 4.1. Haze values of TM Bands that are removed.

TM Band No.	Removed value as Haze
Band 1	52
Band 2	17
Band 3	12
Band 4	No haze removal
Band 5	No haze removal
Band 7	No haze removal

Geometric corrections are performed to eliminate the systematic and non-systematic distortions related with the physical and geometric conditions of the scanning devices. The remote sensor data that is commercially available is

already systematic error removed, however non-systematic error remains in the image (Jensen, 1996). The image data is accepted as free from geometric errors.

4.1.2. Methodology

During the analysis a simple to complex step-wise path is followed. Each analysis result is compared with the previous one. Color composites, several band rationing techniques, principle components analysis (PCA) and least squares fitting (multilinear regression) are applied to the original unregistered raw data. The resulting images are considered to be the potential alteration maps. If the results display any convergence with the data acquired from previous works then the final (combination) map of all techniques is registered and processed and prepared for the ground truth. The geology of the area is gathered from the published maps and mostly forms the basis of the ground truth data. Lastly according to the ground-truth study the applied techniques are criticized to have the final conclusion (Fig. 4.5).

4.2. Conventional Analyses

The following sections include the image processing techniques that are literally found to map the information regarding the alteration of rocks. These conventional well-known methods include color composite method, band rationing method, principal component analysis and least squares fitting method (Chapter 3).

Principal component analysis is to gather information from the correlation between the bands to highlight the spectrally unique features.

Least squares fitting method is the multi-linear regression analysis which accepts the correlation between the input bands as linear.

4.2.1. Color Composites

Color composite method is simply the decision of the order of bands to be displayed in red, green and blue channels. The concept surely forms the basis of the other methods.

ALTERATION MAPPING FLOWCHART

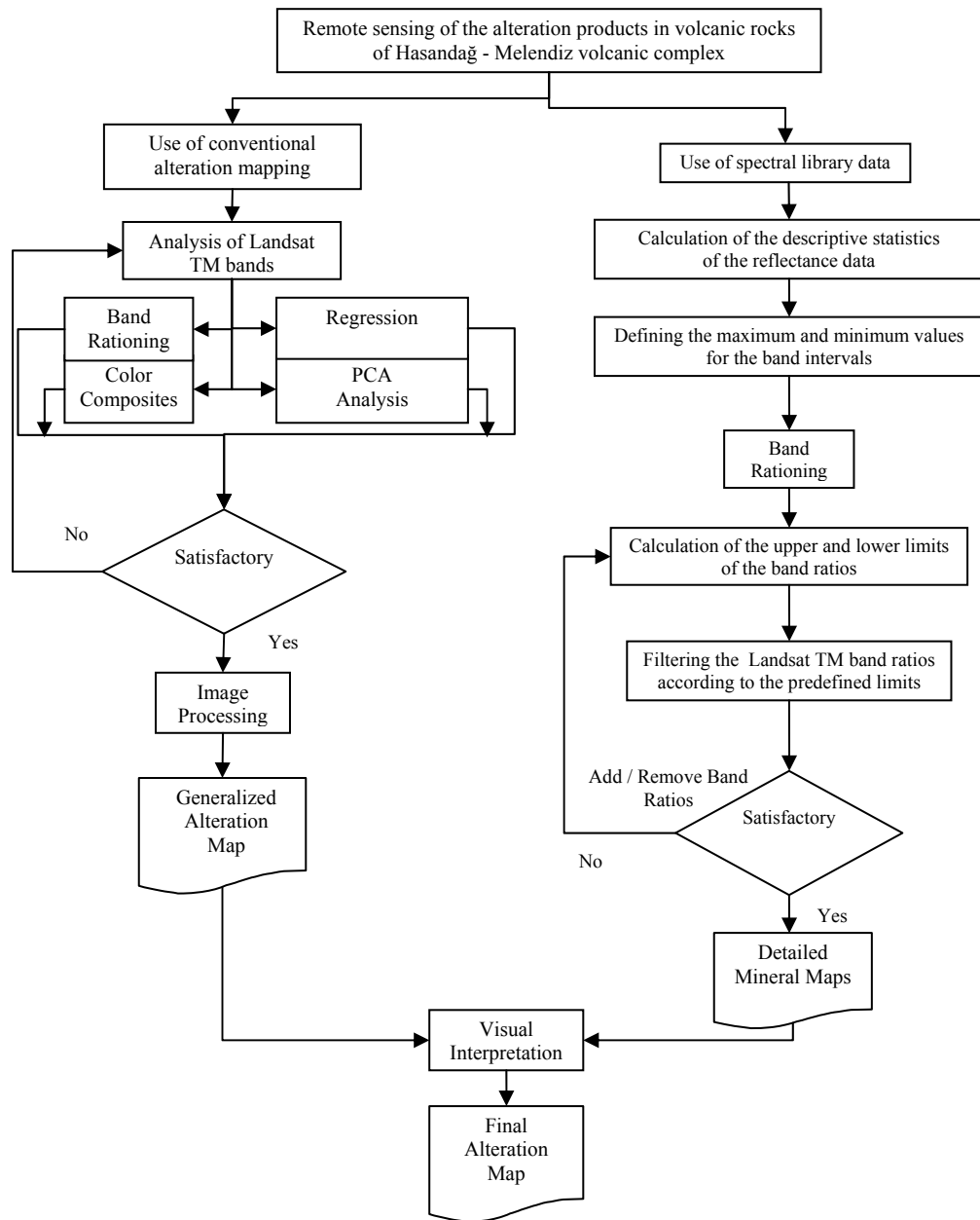


Figure 4.5. Flow chart of the study.

The results of the color composite combinations that are explained in the previous chapter are discussed in this section. No image correction has been made prior to the processes. Images that are selected to be displayed as a composite are normalized type contrast stretched. Visually, normalized contrast enhancement gives better results than linear contrast stretching. That is because the stretching transformation is performed varyingly according to the histogram density in normalizing contrast enhancement.

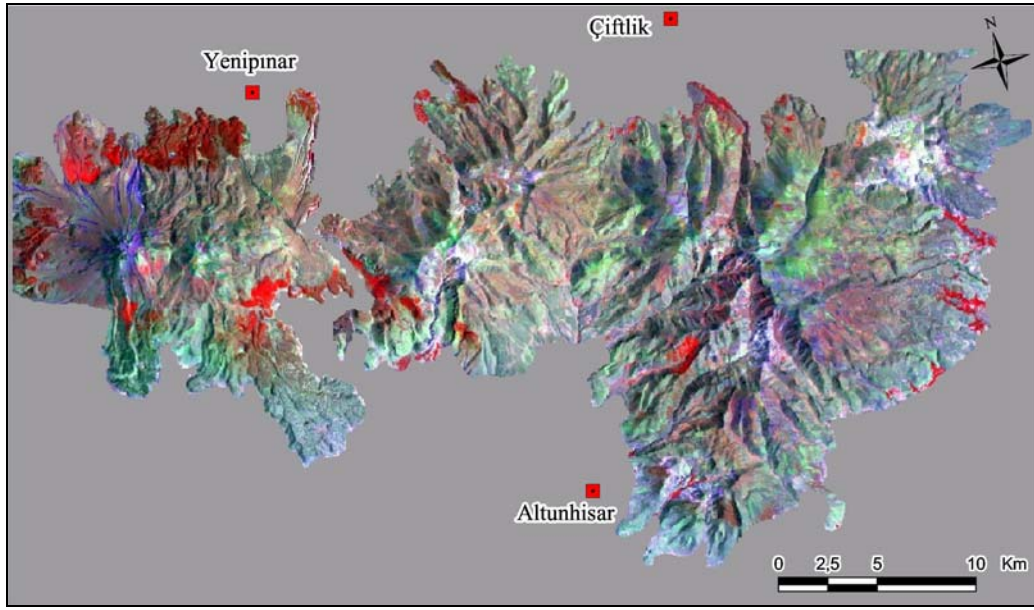
Color composite display of bands 4, 7 and 2 respectively in the red, green and blue channels is shown in Figure 4.6a. The red areas are vegetated as the band 4 is sensitive to vegetation. Band 7 is responsible for moderate reflectance for clay minerals and is displayed in green. It is easy to say that band 7 could not recognize the clay altered zones as there are various wide green areas in the image. However, yellow-green areas between Melendiz and Tepeköy volcanics are iron-oxidized more than clay altered. White areas including the volcanic centers point both clay and iron-oxide altered areas.

Composite image of 476 is the only image having the thermal infrared band 6. Yellow-green areas can be interpreted as altered areas incapable of differentiating the type. Blue displayed areas are the response to thermal infrared band 6. Light-dark blue outline of the study area therefore is the unaltered rocks, blue changes to greenish yellow around the main volcanic centers indicating the relation of the alteration with the distance to center (Fig. 4.6b).

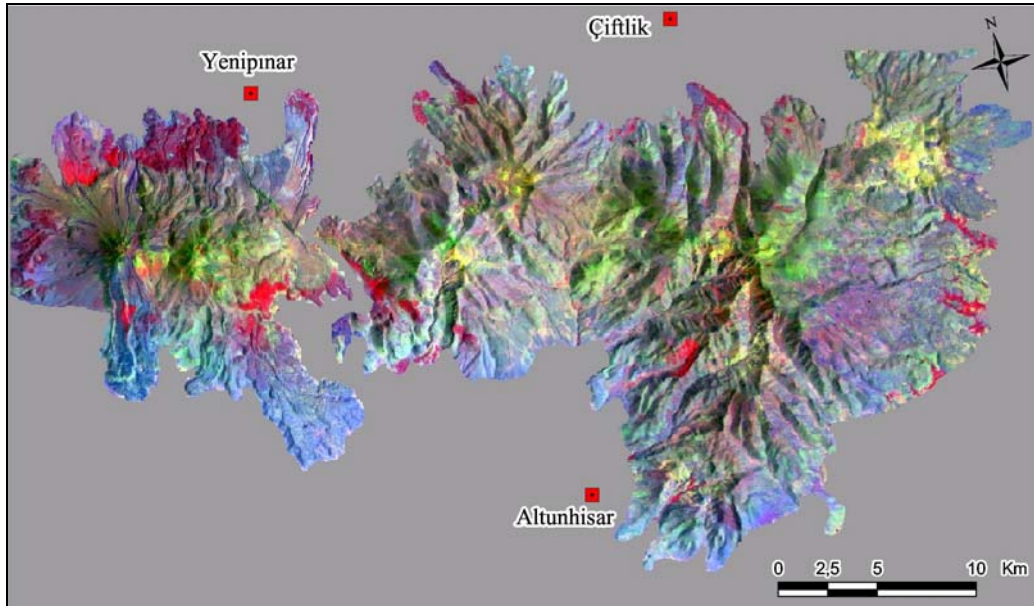
Using the bands 7 and 5 in red and green channels and band 4 in the blue channel produced an image having clay altered areas displayed as white and iron-oxidized areas as brown-yellow tones. Iron-oxides relatively have same amount of reflectance in bands 5 and 7, leading yellow-brown tones in the image. Both vegetation and hydroxyls are reflective in band 4 interval. Thus, blue areas are the vegetated and white areas are clay dominant altered regions (Fig. 4.6c).

Different combination with the same bands of 4,7 and 5 with previous image, clearly demonstrates how the same data can be used to give a different output. Vegetation is mapped as red this time and the iron oxides as green-cyan. The whitish pixels represent like in the previous, clay-rich areas. Tepeköy complex is mapped as clay-rich area in both of the composites (Fig. 4.6d).

As it is clearly observed, the color composite method is a fast but not that detailed enough to map the certain borders for alteration types. Only general information is mapped. The procedure of assigning the bands to the display channels is the same in the other methods, changing the input bands to be displayed.

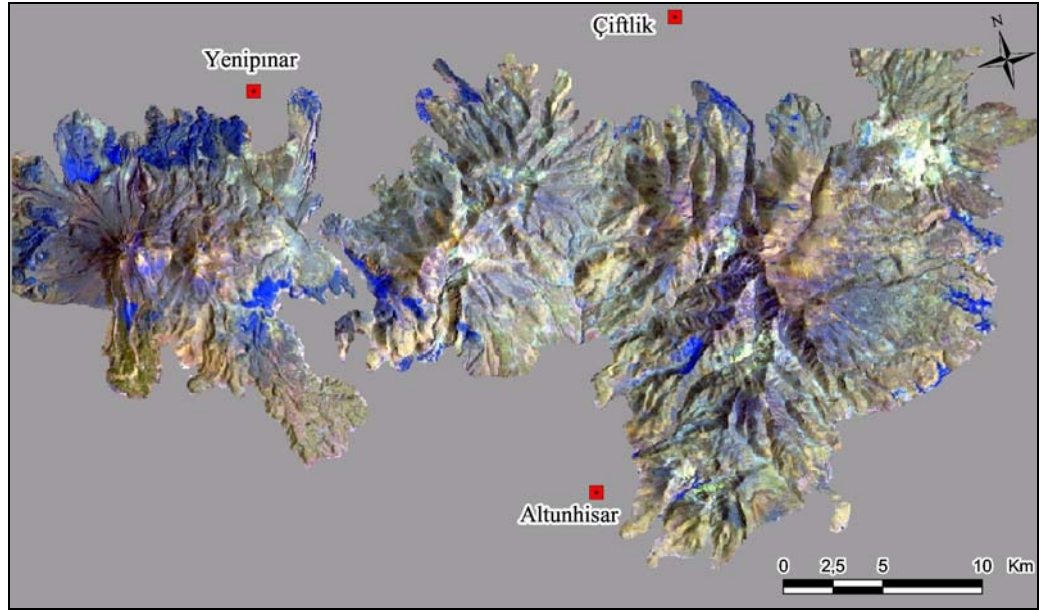


a. RGB of 472.

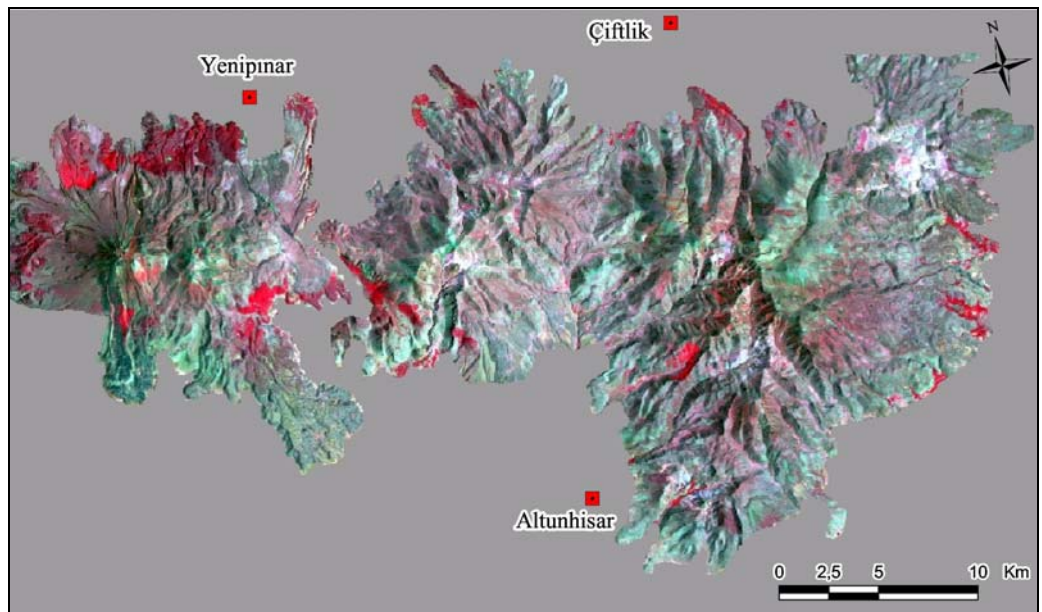


b. RGB of 476.

Figure 4.6. Color composites. a. RGB of 472, b. RGB of 476, c. RGB of 754, d. RGB of 475.



c. RGB of 754.



d. RGB of 475.

Figure 4.6 (Continued). Color composites. a. RGB of 472, b. RGB of 476, c. RGB of 754, d. RGB of 475.

4.2.2. Band Rationing

Band rationing is the selection of the bands, rationing to get the desired information and the meaningful order of display of these ratios. Spectral characteristics of the minerals are used for deciding the pairs of bands to be

rationed (Chapter 3). Prior to the process no correction has been made to the images unless stated.

Band ratio technique is based on highlighting the spectral differences that are unique to the materials being mapped. As the resulting image will have ratios instead of grey levels, the image is normalized contrast stretched to be able to display 256 grey levels.

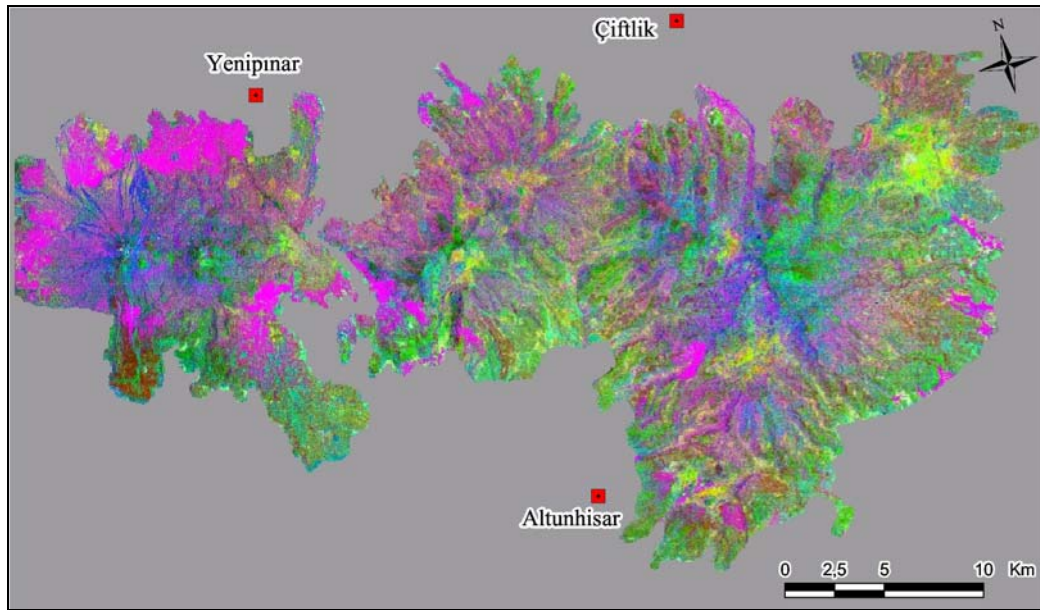
Band ratio of $5/7$ is expected to be high in clay minerals because they give high reflectance in band 5 and relatively low in band 7. Ratio of bands $3/2$ is high for iron oxide minerals and band ratio of $4/5$ is very low for iron oxides and nearly identical for clay minerals. Assigning respectively these ratios to the red, green and blue channels the image in Figure 4.7a is obtained. Simply the red pixel areas are clay-rich, green pixels are iron-oxide, blue pixels are both clay and iron-oxide dominated areas where dark blue areas have more FeO than clay minerals. Yellow pixels represent hydrothermally altered clay and FeO rich areas and mainly observed in and around volcanic centers of Tepeköy, Melendiz and Keçiboyduran.

Band ratio of $7/4$ is high for iron-oxides, $4/3$ is nearly identical for both mineral groups and $5/7$ is high for clay minerals. Therefore, the resulting RGB composite will display iron oxide rich areas in red (orange) and clay rich areas in blue and green will be background incapable of providing any distinct information. The pixels displayed as magenta are clay and iron oxide altered areas concentrated around the centers of Tepeköy, Melendiz and Keçiboyduran volcanics (Fig. 4.7b). Vegetation is displayed as cyan because both $4/3$ and $5/7$ have vegetation information.

Color composite of band ratio $3/4$, band 5 and band ratio of $5/7$ is an example that the ratio images can be displayed with the original bands. Ratio of $3/4$ is relatively high for iron oxides, band 5 and band ratio $5/7$ are both high for clay minerals. Therefore, the orange pixels near Melendiz complex represent FeO rich areas, cyan pixels mark the clay rich areas where both clay and FeO exist we see white pixels on the image (Fig. 4.7c).

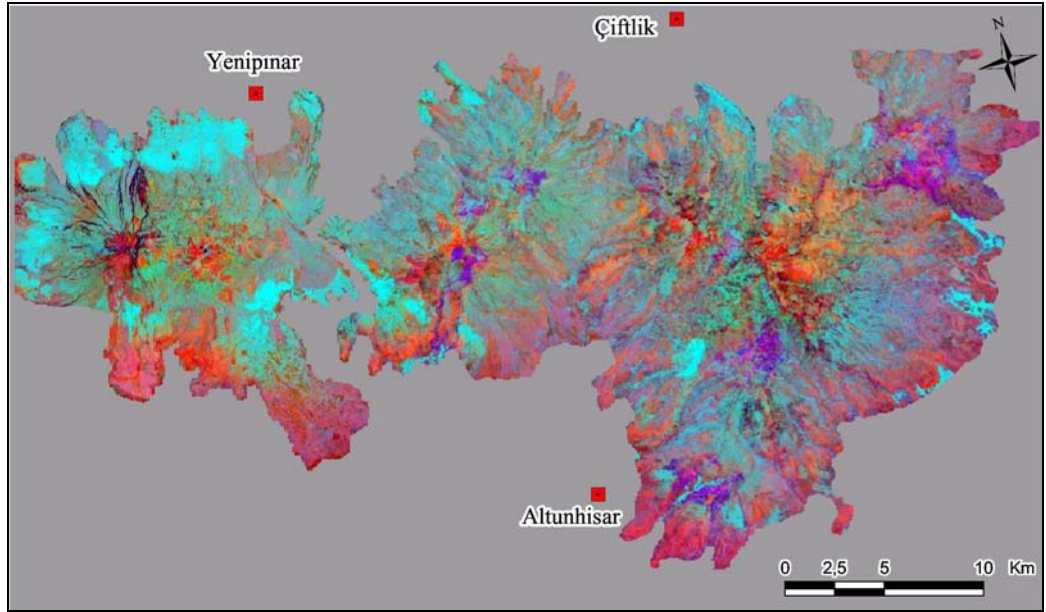
The RGB composite of 5/7, 5/4 and 3/1 is based on the ratios of haze removed bands of 1,3,4,5 and 7. The magenta pixels are the areas where both clay and iron oxide minerals are present. Cyan pixels are iron oxide rich areas and densely concentrated on the northeastern flanks of Melendiz volcanic center. Where there is high amount of iron oxide and clay minerals the white pixels are displayed. It is observed that magenta pixels outline the white pixel areas displaying a zonal pattern of alteration, highly altered zone in the center, less altered zone at the distal parts of the volcanic center (Fig. 4.7d).

The red pixels are iron oxide rich areas and displayed again in the north eastern flank of Melendiz complex, south western flanks of Keçiboyduran and a small area in the eastern part of Hasandağ complex. Ratio of 4/5 is low for iron oxides according to the spectral reflectance curve. Therefore the pixels having high red, high green and low blue; which makes orange-yellow; are intensely both clay and iron oxide altered areas (Fig. 4.7e).

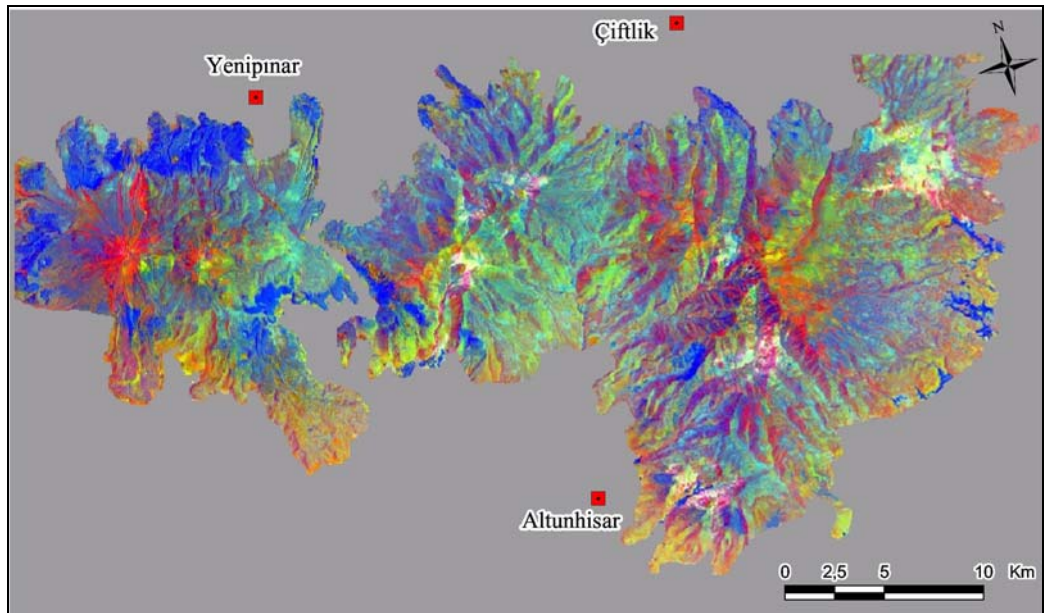


a. RGB of 5/7 : 3/2 : 4/5

Figure 4.7. Band ratio color composites. a. RGB of 5/7 : 3/2 : 4/5, b. RGB of 7/4 : 4/3 : 5/7, c. RGB of 3/4 : 5 : 5/7, d. RGB of 5/7 : 5/4 : 3/1, e. RGB of 3/1 : 5/7 : 4/5.

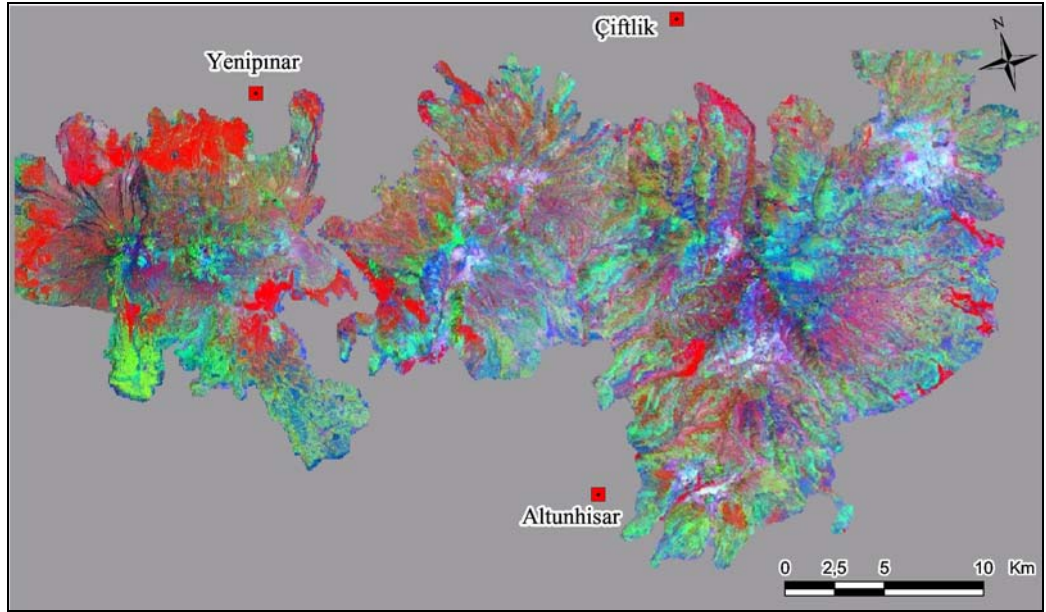


b. RGB of $7/4 : 4/3 : 5/7$.

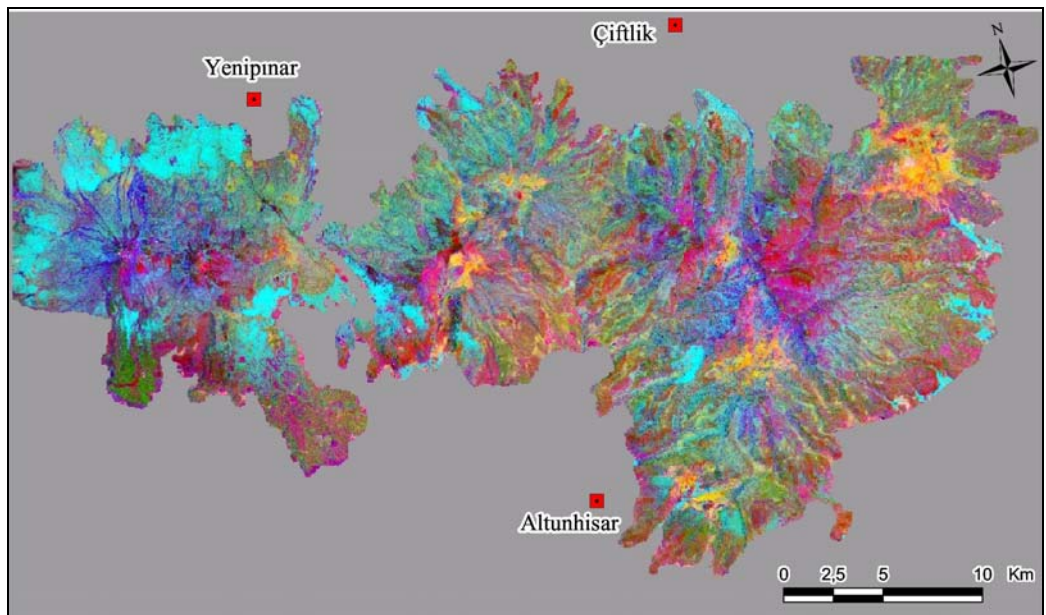


c. RGB of $3/4 : 5 : 5/7$.

Figure 4.7 (Continued). Band ratio color composites. a. RGB of $5/7 : 3/2 : 4/5$, b. RGB of $7/4 : 4/3 : 5/7$, c. RGB of $3/4 : 5 : 5/7$, d. RGB of $5/7 : 5/4 : 3/1$, e. RGB of $3/1 : 5/7 : 4/5$.



d. RGB display of 5/7 : 5/4 : 3/1.



e. RGB display of 3/1 : 5/7 : 4/5.

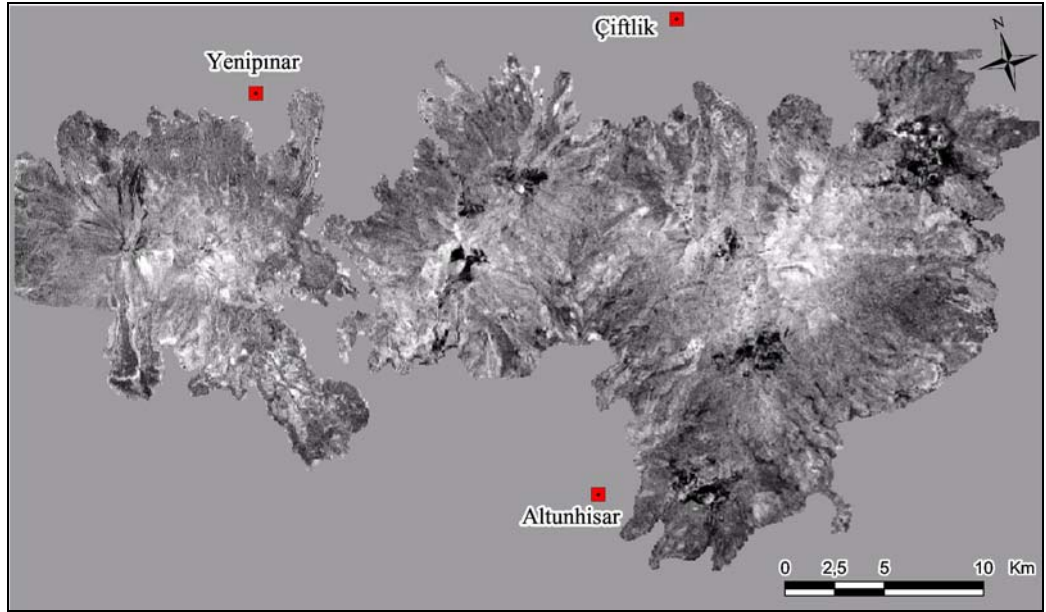
Figure 4.7. (Continued). Band ratio color composites. a. RGB of 5/7 : 3/2 : 4/5, b. RGB of 7/4 : 4/3 : 5/7, c. RGB of 3/4 : 5 : 5/7, d. RGB of 5/7 : 5/4 : 3/1, e. RGB of 3/1 : 5/7 : 4/5.

4.2.3. Crosta Technique

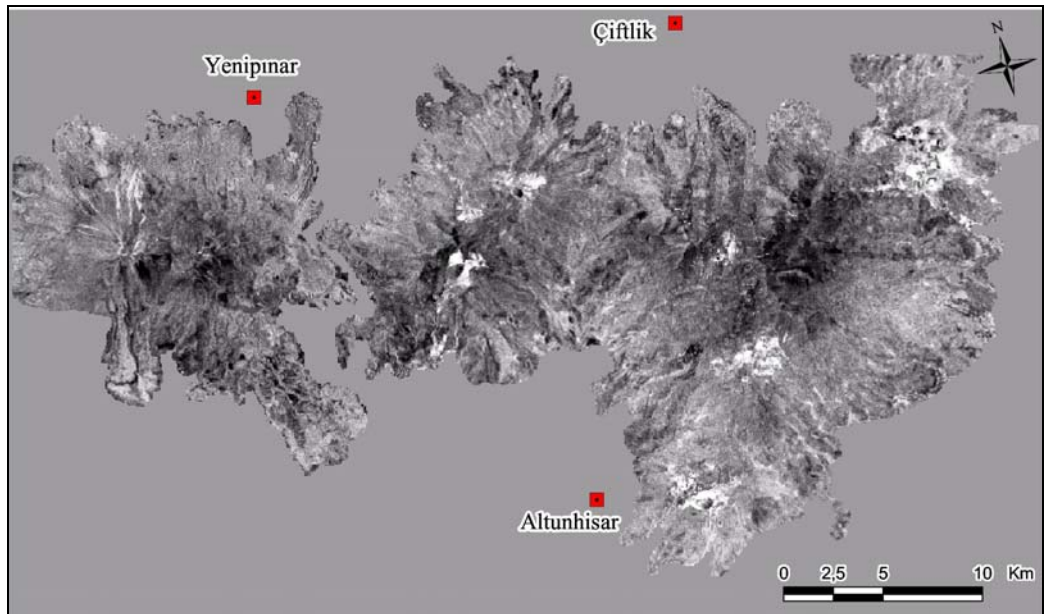
As discussed in the background chapter, the Crosta technique focuses on the information extraction of mainly the hydroxyls and the iron-oxides. Performing the analysis returns 3 output images which are hydroxyl (H), iron-oxide (F) and H+F images. No image correction has been made, raw data is used as input.

4.2.3.1. Hydroxyl Mapping

Here the PC4 of hydroxyl (TM1,4,5,7) analysis selected as the H image because the reflectance in PC3 is positive both from TM5 and TM7. As it is known from the spectral signatures that the hydroxyl minerals give high reflectance values in TM5 and low in TM7, we look for the principal component in which the difference of reflectance is large. The analysis results are tabulated in Table 4.2. Eigen values of bands 5 and 7 theoretically should be in opposite signs to reflect the spectral difference between them. In PC3 both of them are positive, meaning that the bright pixels in PC3 are both related with bands 5 and 7. To be able to differentiate the bands 5 and 7 we look for the principal component having opposite contributions by means of eigenvalues. In PC4, band 5 has negative and band 7 has positive eigenvalue. Therefore darkest pixels are responsible for the hydroxyl minerals in PC4, if it is negated the brightest pixels are hydroxyl minerals (Fig. 4.8).



a.



b.

Figure 4.8. Hydroxyl mapping. PC4, darkest pixels are responsible for the hydroxyl minerals, b. PC4, inverted (negated) bright pixels are hydroxyl minerals.

Table 4.2. Eigenvector Loadings for Hydroxyl Mapping

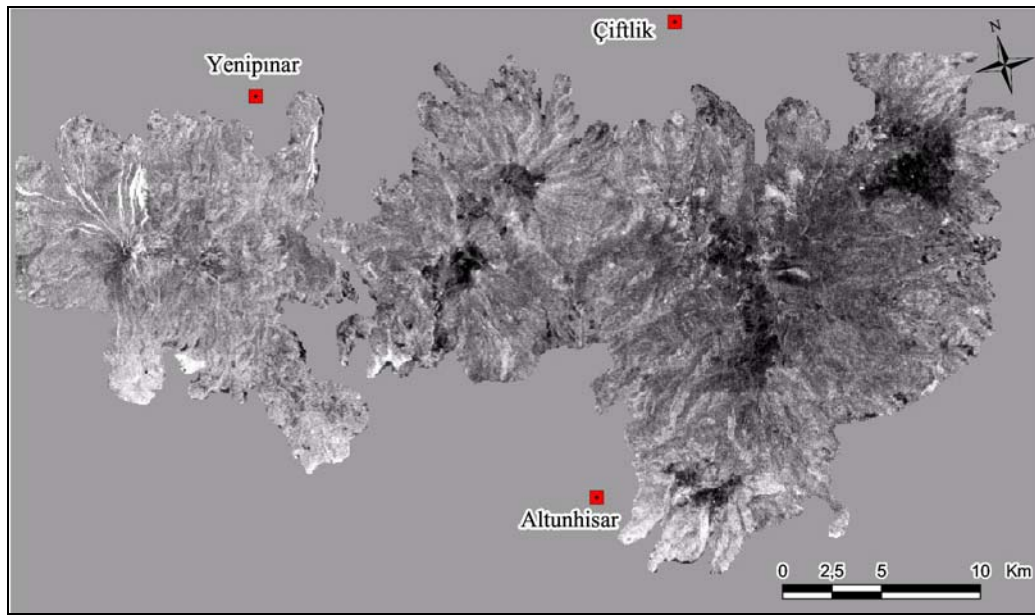
Axis	TM Band1	TM band4	TM band5	TM band7	% Variance
PC 1	0.3205	0.2845	0.7819	0.4527	85.9578
PC 2	-0.5464	0.7646	0.1291	-0.3165	8.3656
PC 3	-0.7371	-0.5223	0.3931	0.1711	4.8876
PC 4	-0.2353	0.2483	-0.4662	0.8158	0.7890

4.2.3.2. Iron Oxide Mapping

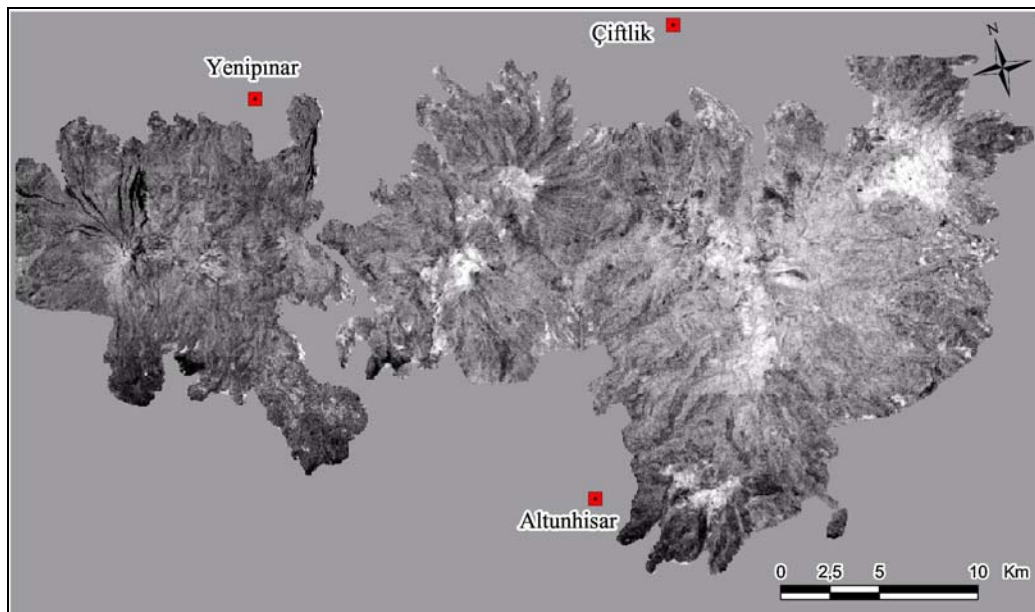
Here the PC4 of iron oxide (TM1,3,4,5) analysis is selected as the F image because the reflectance in PC3 is both from TM1 and TM3. As we know that the iron oxide minerals give high reflectance values in TM3 and low in TM1, we look for the principal component in which the difference of reflectance is large (Table 4.3). In PC3 both bands have positive eigenvalues that is not useful for separating the bands 1 and 3. The opposite eigenvalue signs of bands 1 and 3 in PC4 makes the bands separable. In PC4 the darkest pixels are responsible for the iron oxide minerals, if it is negated the brightest pixels are iron-oxide minerals (Fig. 4.9).

Table 4.3. Eigenvector Loadings for Iron-Oxide Mapping

Axis	TM band1	TM band3	TM band4	TM band5	% Variance
PC 1	0.3420	0.4551	0.2868	0.7705	83.3428
PC 2	-0.5548	-0.5465	0.4955	0.3846	10.8810
PC 3	0.2035	0.1825	0.8198	-0.5033	5.0467
PC 4	0.7306	-0.6789	0.0137	0.0716	0.7295



a.



b.

Figure 4.9. a. PC 4, darkest pixels represent the iron-oxide rich areas b. Inverted (negated) PC 4, brightest pixels display the iron-oxide rich areas.

4.2.3.3. H + F Mapping

The H and F images are summed up and the result is rescaled to 256 grey levels. The inverted H + F image displays the places where both iron oxide and hydroxyl minerals are present as brightest pixels.

Also another way to decide the H+F image is to perform PCA to H and F images selectively and the principle component having positive percentages from both input images is the H+F image (Table 4.4). PC2 having positive eigenvalues from both H and F images is selected as the H+F image. Originally the darkest pixels that are explained to be responsible for the H and F images, again in the H+F image the darkest pixels are responsible for the areas both having clay and iron oxide minerals. The final H+F image is negated to have the brightest pixels during mapping the hydrothermally altered areas (Fig. 4.10).

Table 4.4. Eigenvector Loadings for H + F Mapping

Axis	PC4 of Hydroxyl	PC4 of FeO	% Variance
PC 1	0.9121	-0.4100	60.2328
PC 2	0.4100	0.9121	39.7672

4.2.3.4. Color Composite of H, H+F and F images

After having the H, F and H+F images and the brightest pixels responsible for the hydroxyl and iron oxide minerals, it is easy to interpret the color composite of these. As the composite of H, H+F and F is displayed respectively in red, green and blue channels; the whitish pixels are intensely altered areas, both oxidized and argillized. Medium to dark bluish areas are oxidized and medium to dark reddish areas are dominated by hydroxyl, clay minerals (Fig. 4.11). Volcanic centers of Tepeköy, Melendiz and Keçiboyduran are mapped as highly altered whereas the outlying blue zone is the iron oxidized zone around these centers. Hasandağ volcanic complex displays different characteristics than the other volcanic complexes. As it is a younger volcanic complex it does not consist so much alteration but faint white in the center and bluish zone near to center indicates some hydrothermal activity has just started.

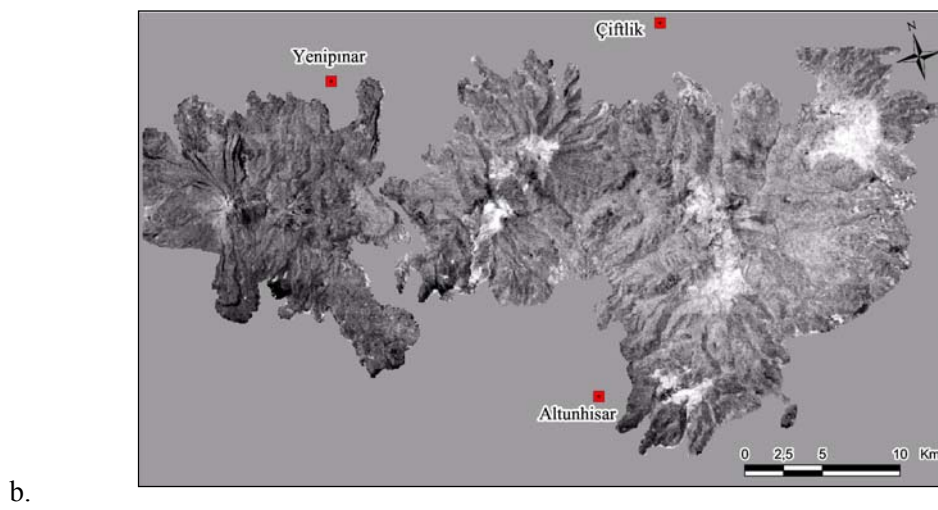
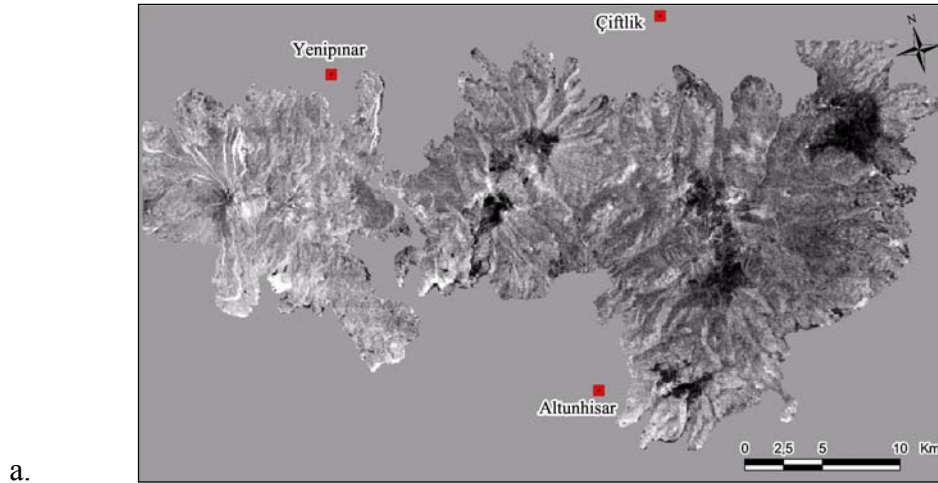


Figure 4.10. a. Darkest pixels represent both hydroxyl and iron oxide rich areas. b. H + F image, inverted and normalized. Brightest pixels represent this time both hydroxyl and iron oxide rich areas.

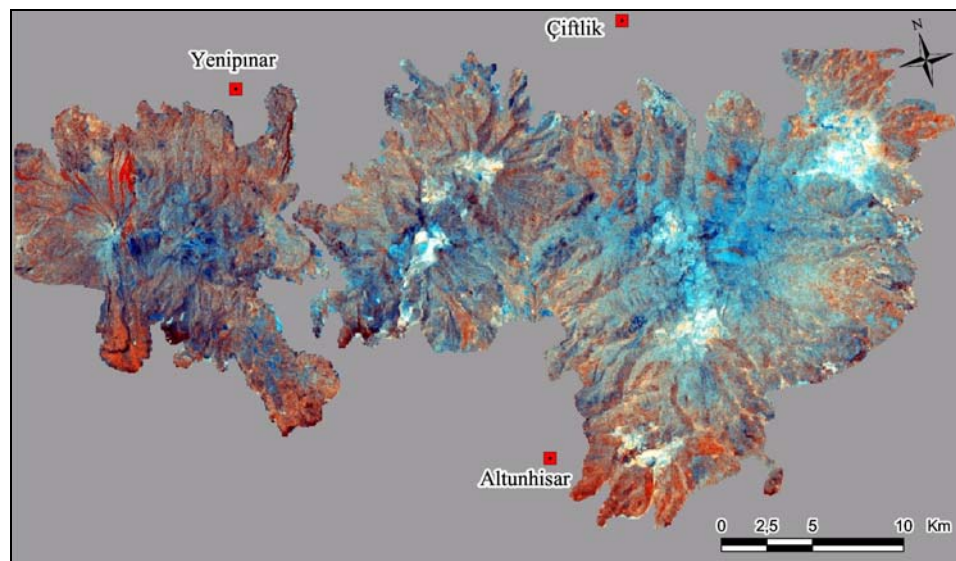


Figure 4.11 Color composite image of H: H+F: F.

4.2.4. Least Squares Fitting Method

The technique assumes that the bands used as input values are behaving as the variables of a linear expression. And the 'y' value of the equation gives us a calculated output value, namely the predicted band information. This predicted band is what that band should be according to the linear equation. The problem of having vegetation responsible of some reflectance in the bands that are used to map clay minerals, can therefore be omitted by using this technique. The vegetation is mapped in the predicted band with the values that are calculated just by using the reflectance information in the other bands. The minerals which are sensitive to a specific band are then differentiated from the features which are reflective to the other bands as well; just by taking the difference between the predicted values and the original values. Calling this difference, the residual, color composites are displayed with the specific anomalously reflective features and then interpreted.

$$y = mx + c$$

Table 4.5 represents the coefficients and constants obtained as a result of the multiple regression analysis. The formulae can be summarized as:

$$\text{Predicted Band} = a1*B1 + a2*B2 + a3*B3 + a4*B4 + a5*B5 + \text{Constant}$$

B1...n : independent or regressor variable

a1...n : regression coefficient for B1...n

Table 4.5. Coefficients and the constants of the sixth order polynomial function.

Raster	Const	band1	band2	band3	band4	band5	band7
band1 =	36,9442		1,5459	-0,0956	-0,0489	-0,0795	0,1542
band2 =	-1,0507	0,2244		0,395	0,0378	-0,0061	-0,0254
band3 =	-14,6677	-0,0583	1,6583		-0,0439	0,0276	0,1049
band4 =	27,9649	-0,2649	1,4088	-0,3905		0,7986	-0,9609
band5 =	12,7783	-0,2956	-0,1552	0,168	0,548		1,4506
band7 =	-5,7889	0,2046	-0,2322	0,2283	-0,2354	0,518	

The sixth order polynomial function is used to predict the bands according to the linear correlation between the input bands.

By using the residual band 3, residual band 7 and residual band 1 we can map hematite, clay and goethite. Here, it should be important to use Visible bands when calculating the residuals for these bands and to use IR bands when calculating the residuals of these bands. So it should be better to use Bands 1,2,3 for residuals of these bands and Bands 4,5,7 for residuals in the linear equations. Figure 4.12 is the composite of the residual band 3, residual band 7 and residual band 1 respectively in red, green and blue channels. As the iron oxide minerals are highly reflective in band 3 and clay minerals are highly reflective in band 7, the cyan pixels delineate both clay and iron oxide altered areas mainly located in the Tepeköy, Melendiz and Keçiboyduran volcanic centers. Magenta – dark blue pixels are mainly the iron oxide altered areas and they radially cover the outlines of the cyan areas indicating a zone of alteration coinciding the areas mapped in principal component analysis.

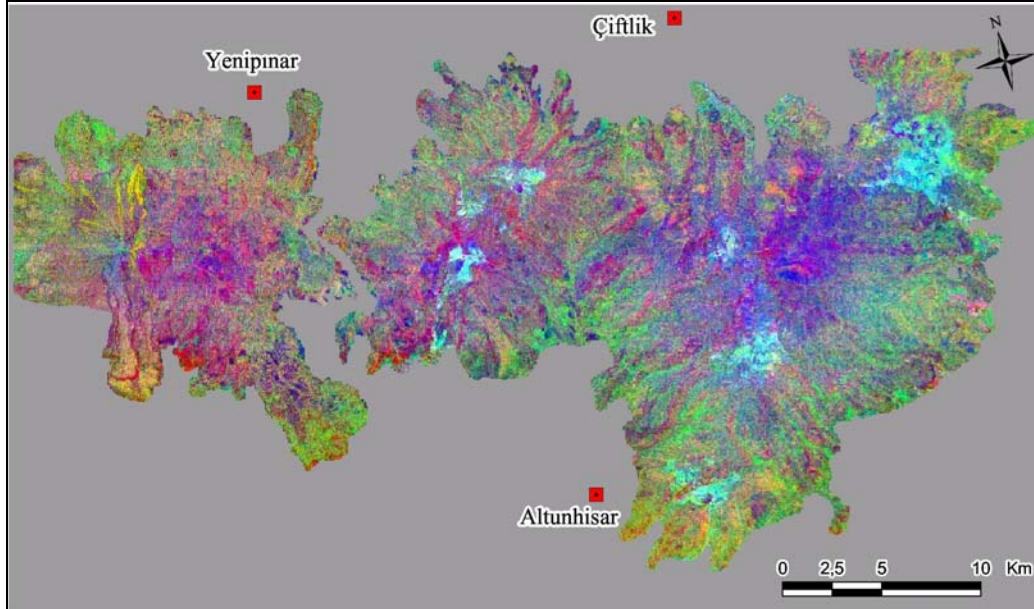


Figure 4.12. Res. Band3, Res. Band7, Res. Band1 as RGB. The pixels displayed as bright cyan are both iron-oxidized and clay altered regions.

4.3. Spectral Library Analysis

The analysis performed in this section includes the processing and filtering of selected alteration minerals which are Kaolinite, Illite, Montmorillonite, Pyrophyllite, Alunite, Orthoclase, Quartz, Epidote, Chlorite, Hematite, Goethite and Jarosite as explained in Chapter 3. Basically band ratio technique is applied and filtered according to the statistically calculated ratio intervals for these minerals. Band ratios are selected according to the spectral curves, band combinations that will give distinctive ratios (very high or very low) are preferred.

Spectral curve data of every mineral, which includes the reflectance values of the corresponding wavelengths, is divided into six wavelength interval classes. These wavelength intervals are selected as the corresponding spectral resolution of the Landsat 5 TM Bands of 1, 2, 3, 4, 5 and 7. The reflectance data in these classes are tested for identifying the statistical distribution type, by drawing the P-P and Q-Q plots. Descriptive statistical values are calculated and standard deviations are used to identify the filtering limits.

The following sections include the results of this spectral library analysis for every individual mineral used throughout the thesis. Note that the reference value is in percentage, not in digital number units.

4.3.1. Kaolinite Mapping

Spectral reflectance curve of kaolinite shows that it has high reflectance values in responding TM band intervals of 2,3,4,5 and relatively low reflectance in 7.

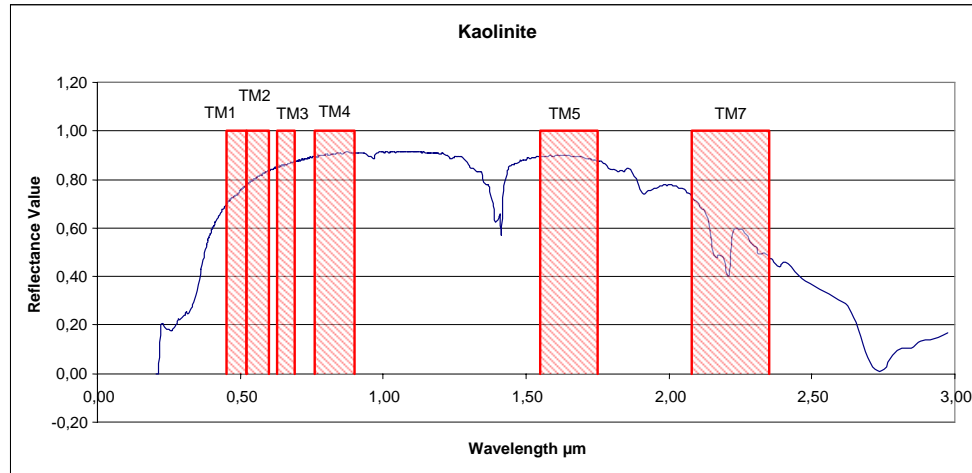


Figure 4.13. Spectral reflectance curve of kaolinite (USGS library).

Ratios of haze removed bands are filtered according to the statistically calculated upper and lower limits. The values that are passing the filter are statistically high probable kaolinite-rich pixels. While selecting the bands to be rationed, the bands tending to give relatively very high/low ratios, that are not close to 1, are selected as ratio pairs.

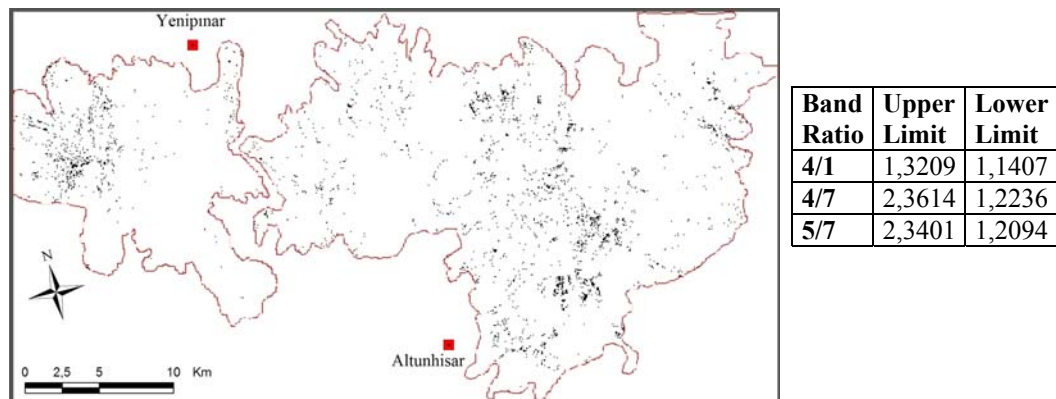


Figure 4.14. Band4/Band1 ; Band4/Band7 ; Band5/Band7 are filtered according to the upper and lower limits. Passed values are displayed as black pixels.

All Band Ratios are filtered according to the statistical limits and no value has passed.

4.3.2. Illite Mapping

Spectral reflectance curve of illite shows that it has high reflectance values in responding TM band intervals of 2, 5 and 7.

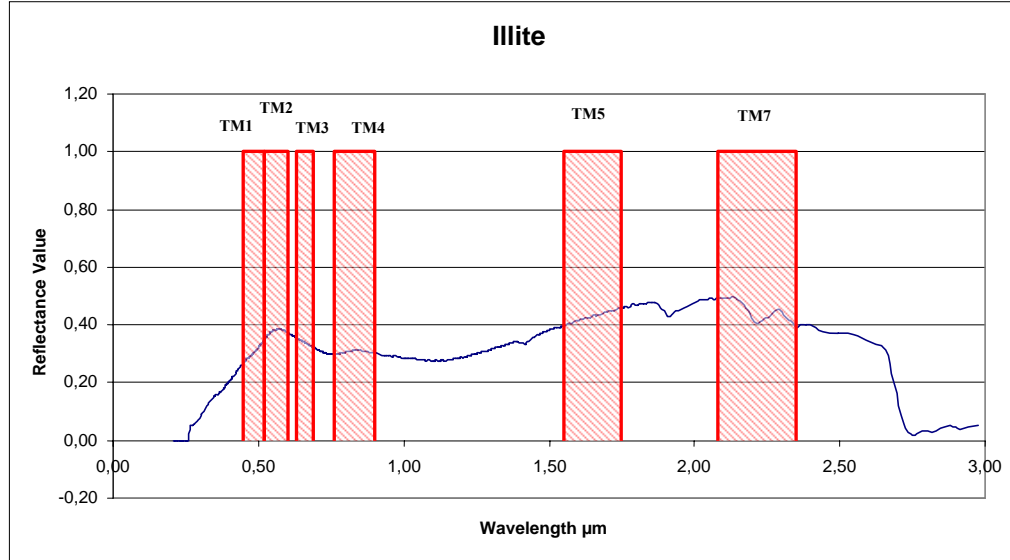


Figure 4.15. Spectral reflectance curve of illite (USGS library).

Illite is mapped along a linear attribute near center of Melendiz volcanic complex which corresponds to the buried fault between Keçiboyduran and Melendiz complexes. A few pixels are passed near Tepeköy region. Different combinations of band ratios are tried in the filtering process, 5/4-7/2-7/3, 2/1-5/4-7/1 and 1/2-1/7-4/5, and no pixel has passed the filters.



Figure 4.16. Band5/Band4, Band1/Band7, Band2/Band7 are filtered.

4.3.3. Montmorillonite Mapping

Spectral reflectance curve of montmorillonite shows that it has high reflectance values in responding TM band intervals of 3, 4 and 5.

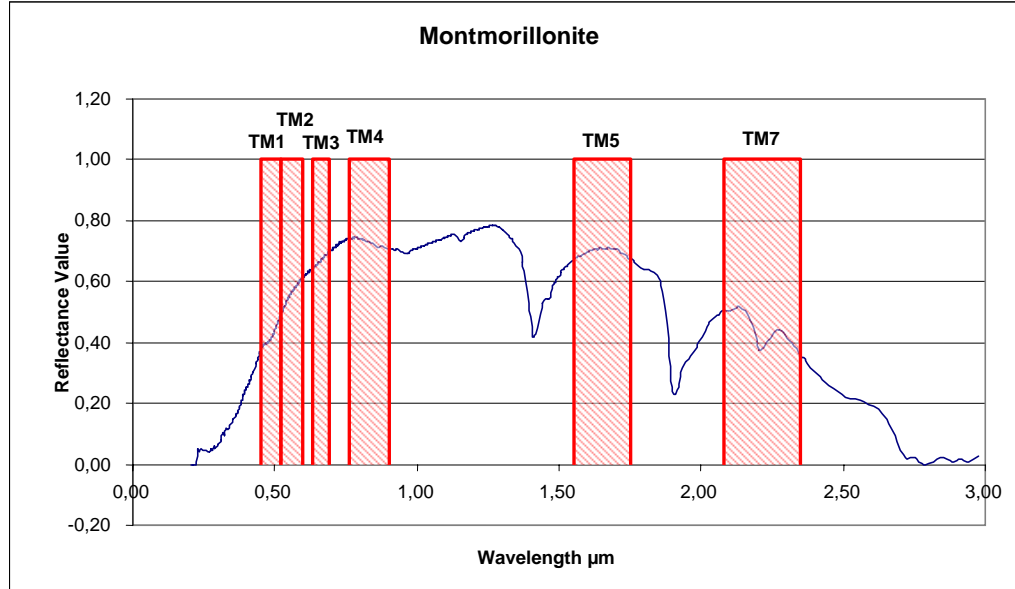


Figure 4.17. Spectral reflectance curve of montmorillonite (USGS library).

Montmorillonite is mapped around the Melendiz volcanic complex center displaying a radial pattern. A few pixels are passed in southwestern flanks of Keçiboyduran complex linear-like distributed, coinciding with the buried part of the Tuzgölü fault zone.

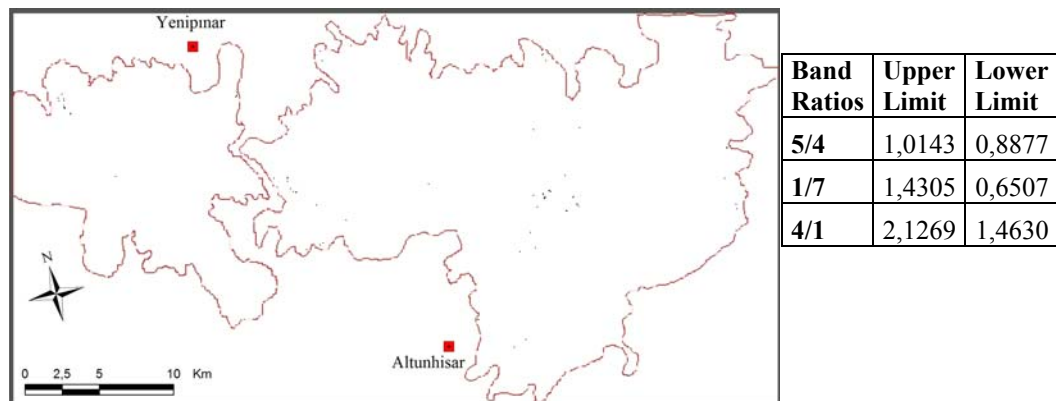


Figure 4.18. Band5/Band4, Band1/Band7, Band4/Band1 are filtered.

4.3.4. Pyrophyllite Mapping

Spectral reflectance curve of pyrophyllite shows that it has high reflectance values in responding TM band intervals of 3, 4 and 5.

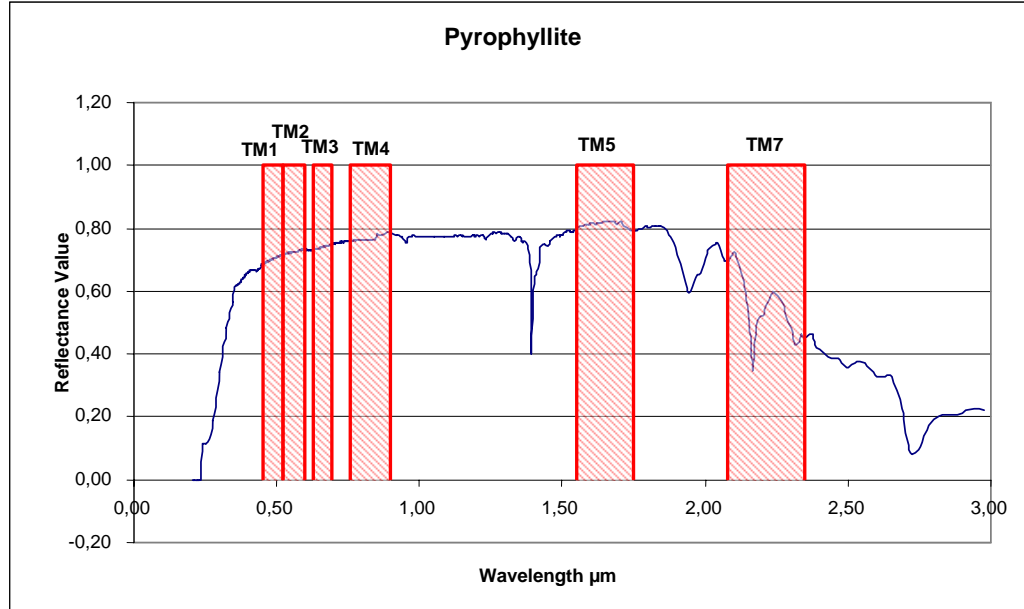


Figure 4.19. Spectral reflectance curve of pyrophyllite (USGS library).

Pyrophyllite is mapped around the Melendiz and Hasandağ volcanic complex centers displaying a radial pattern. Linear distribution on the southwestern flanks of Keçiboyduran is directed along the Tuzgölü fault zone. Pixels on the northern flanks of Hasandağ are mixed with vegetation. When band ratios 5/7 and 2/7 is added to the filtering formula, only the pixels near to the main volcanic centers are displayed.



Figure 4.20. Band5/Band4 and Band4/Band7 is filtered.

4.3.5. Alunite Mapping

Spectral reflectance curve of alunite shows that it has high reflectance values in responding TM band intervals of 3, 4 and 5.

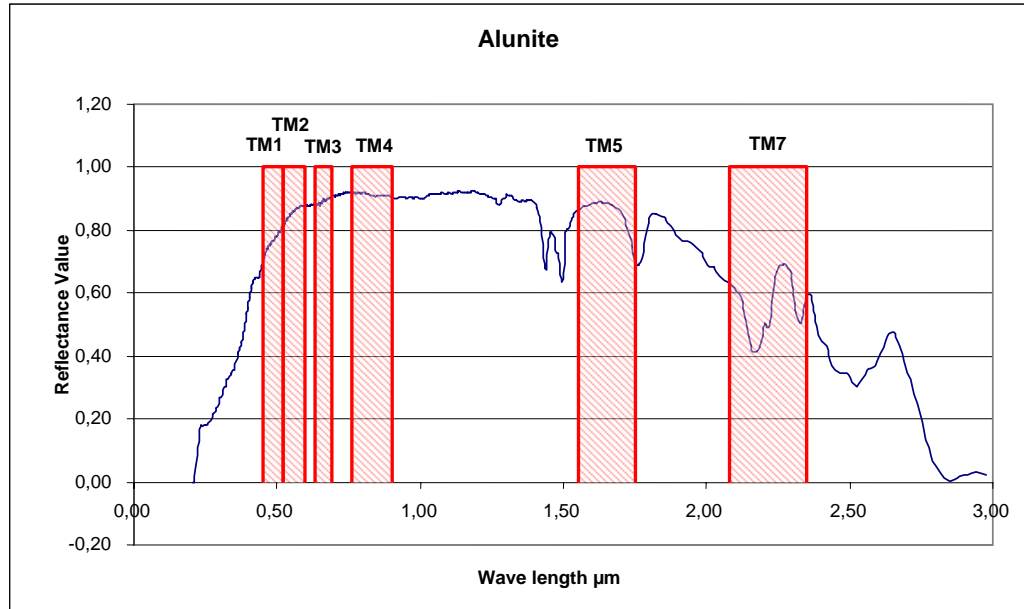


Figure 4.21. Spectral reflectance curve of alunite (USGS library).

Alunite is mapped around Hasandağ volcanic complex center and on the northern part of Melendiz volcanic complex in a very restricted zone. More bands in the filtering formula means more precise results, the probability of a real alunite pixel increases.



Figure 4.22. Band5/Band4, Band4/Band7, Band5/Band7, Band2/Band7 are filtered, when haze is removed.

4.3.6. Orthoclase Mapping

Spectral reflectance curve of orthoclase shows that it has high reflectance values in responding TM band intervals of 3, 4, 5 and 7. It has high reflectance in all of the six TM band intervals, which makes orthoclase difficult to be mapped.

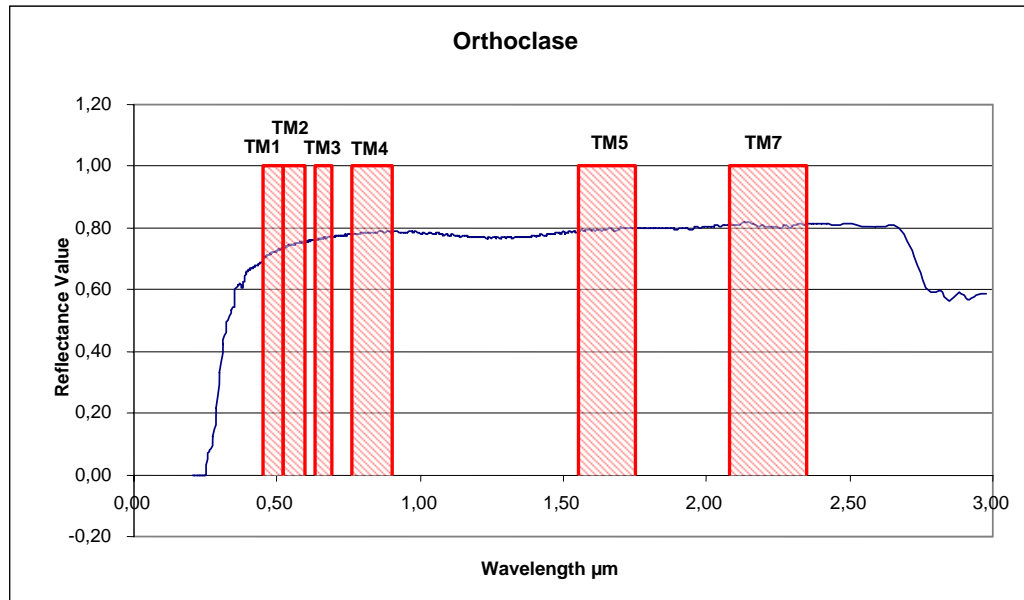


Figure 4.23. Spectral reflectance curve of orthoclase (USGS library).

Pixels that represent orthoclase seem to be distributed randomly. Concentrations observed in southeastern part of Hasandağ lava flows and southern part of Melendiz lava flows and less dense around the volcanic centers are instead of alteration product; look like the constituent of the fresh volcanics.

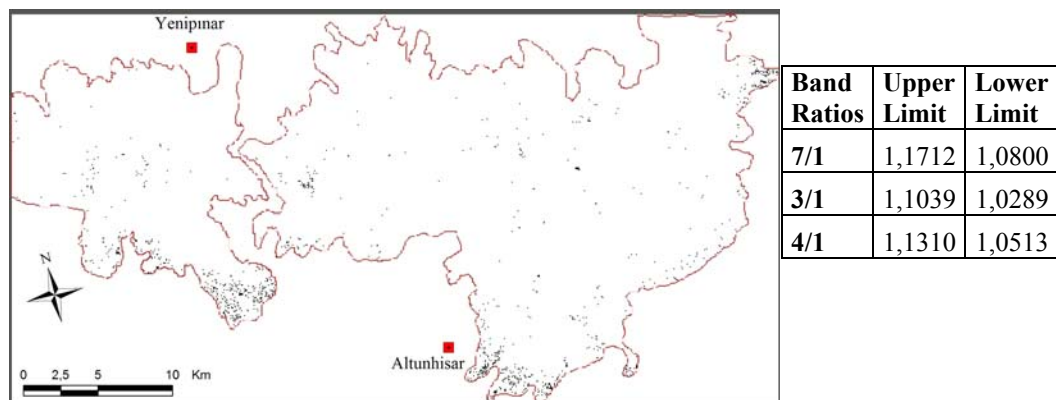


Figure 4.24. Band7/Band1, Band3/Band1, Band4/Band1 are filtered.

4.3.7. Quartz Mapping

Spectral reflectance curve of orthoclase shows that it has high reflectance values in responding TM band intervals of 4 and 5, low reflectance in band 2 and band 3.

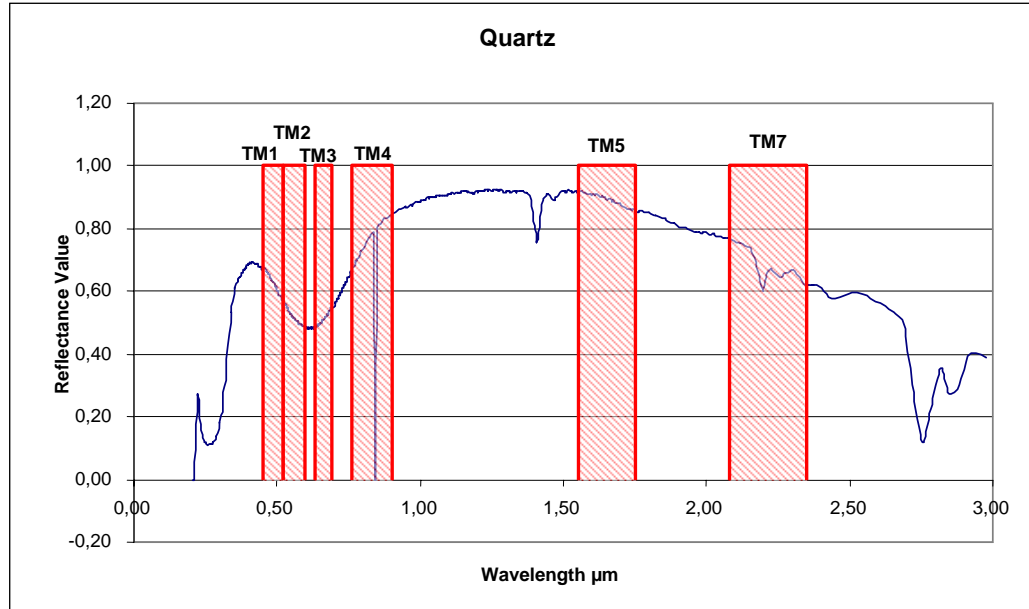


Figure 4.25. Spectral reflectance curve of quartz (USGS library).

Quartz is mapped in a zone on the northwestern flank of Hasandağ volcanic complex. It is a hard task to differentiate the alteration product quartz and the fresh rock quartz. The aim of the quartz mapping in this study is to try to get some information about the silicified areas.

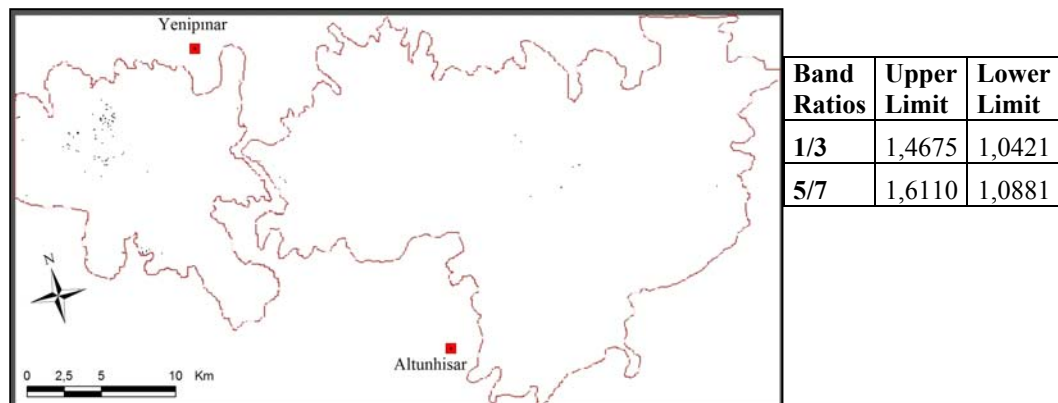


Figure 4.26. Band1/Band3 and Band5/Band7 is filtered.

4.3.8. Epidote Mapping

Spectral reflectance curve of epidote shows that it has high reflectance values in responding TM band interval of 5, very low reflectance in band 1, 2 and 3.

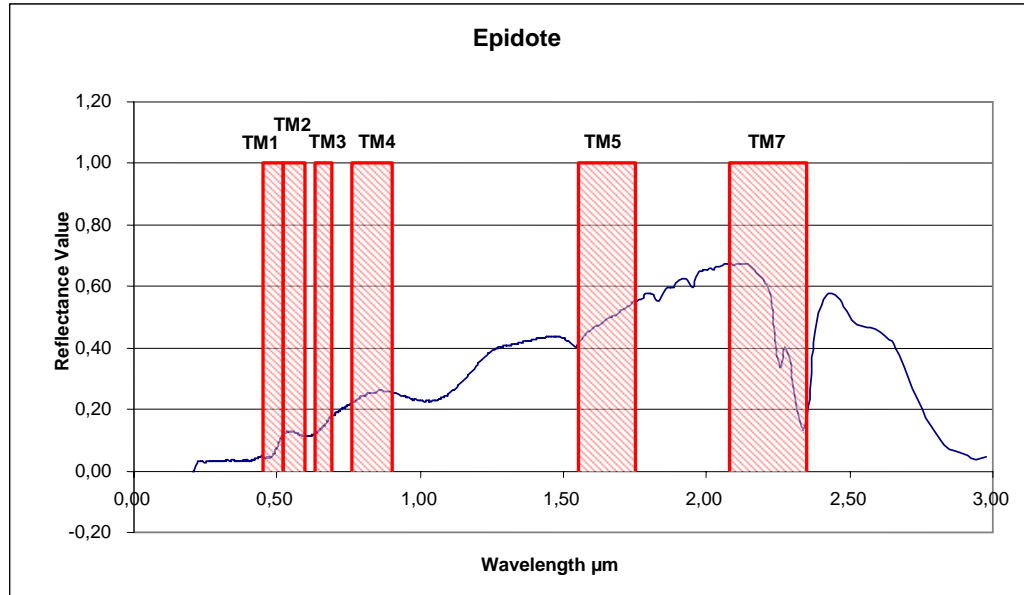


Figure 4.27. Spectral reflectance curve of epidote (USGS library).

At a first glance epidote is mapped with the vegetation in this filtering combination. Radial distribution is very well observed just around Keçiboyduran and Melendiz volcanic centers. When 5/7, 5/4 and 4/1 ratios are added to the filtering formula the resulting image is vegetation free and the epidote distribution seems like random.

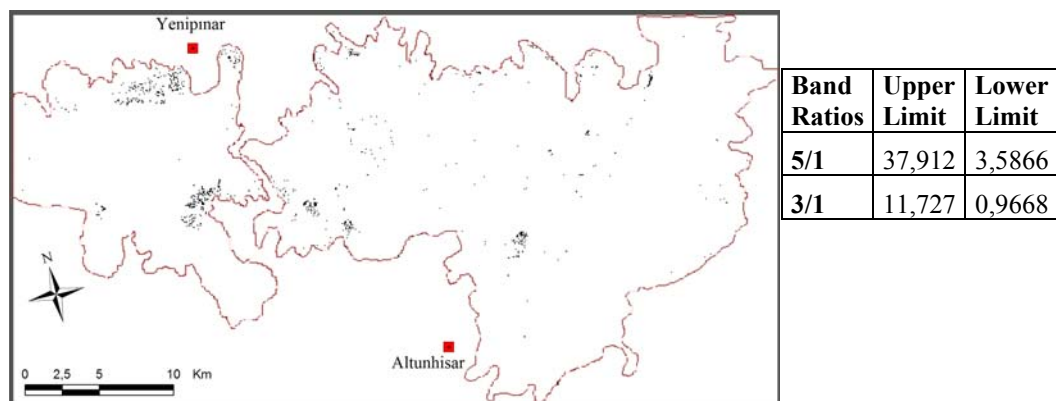


Figure 4.28. Band5/Band1 and Band3/Band1 is filtered.

4.3.9. Chlorite Mapping

Like epidote spectral reflectance curve of chlorite also has high reflectance values in responding TM band interval of 5 and 7, very low reflectance in band 1, 2 and 3.

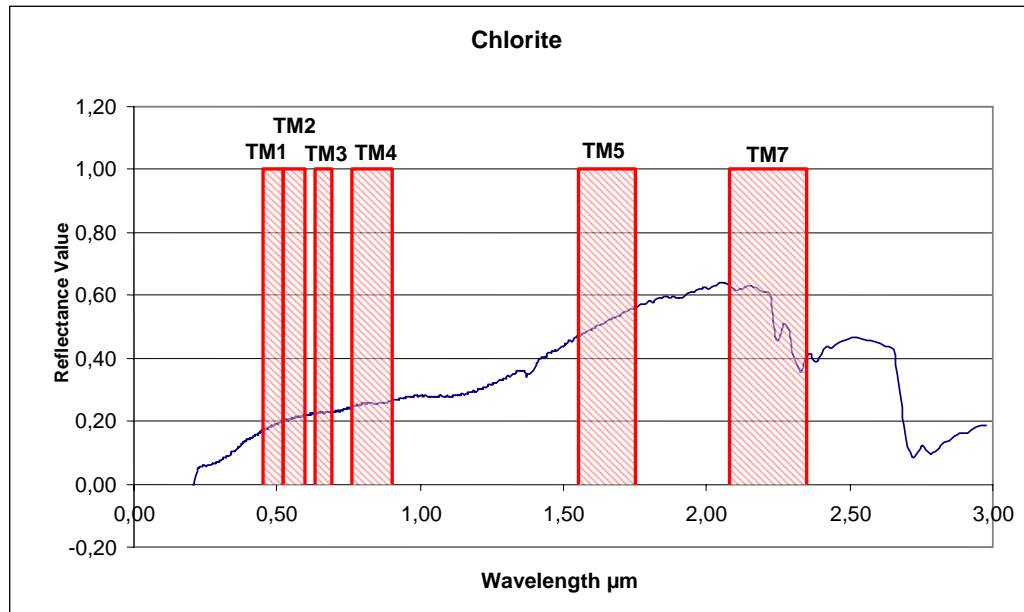


Figure 4.29. Spectral reflectance curve of chlorite (USGS library).

Chlorite is found to be radially distributed close to the volcanic centers of Hasandağ, Keçiboyduran and Melendiz. The filtering formula is well masked the vegetation which makes the result more reliable. A few pixels mapped in the Tepeköy region, which is known to be altered which makes the result more precise.

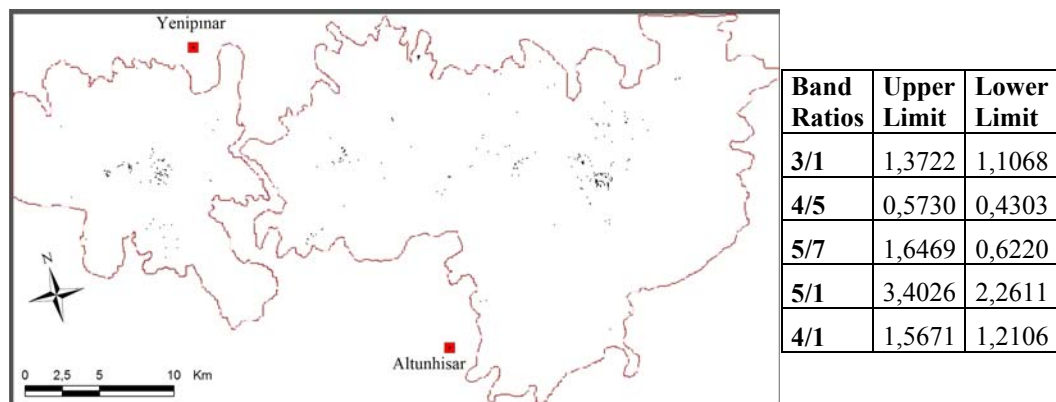


Figure 4.30. Band3/Band1, Band4/Band5, Band5/Band7, Band5/Band1, Band4/Band1 are filtered, when haze is removed.

4.3.10. Hematite Mapping

Ferric oxides have similar spectral reflectance curve which is very low in band 1, moderately high in band 3 and very high in bands 5 and 7. Band ratio of 3/1 is used mostly instead of band 5 and 7, to avoid the contribution of clay minerals.

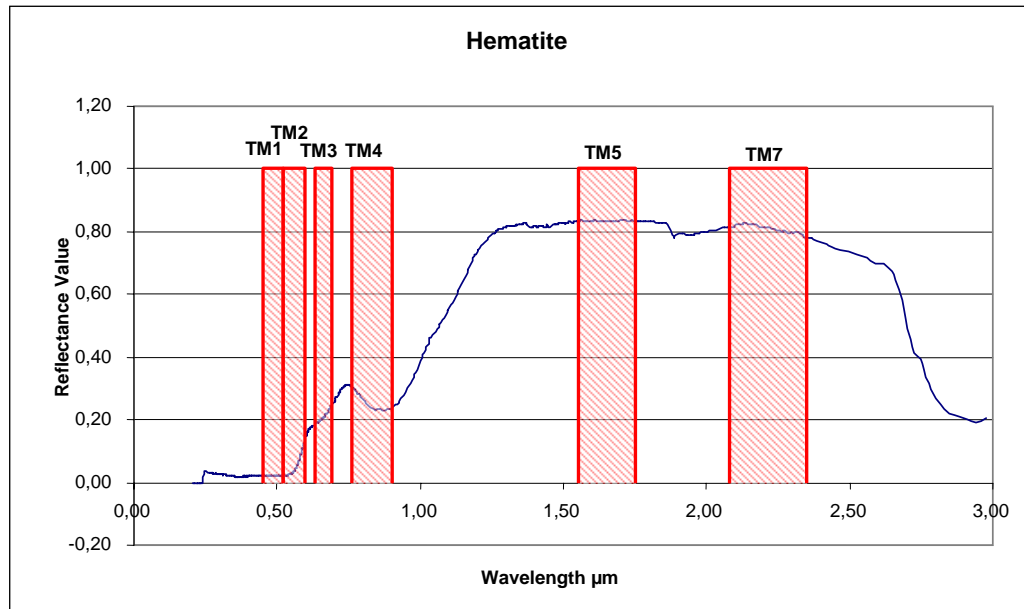


Figure 4.31. Spectral reflectance curve of hematite (USGS library).

Hematite is mapped on the northern flanks of Keçiboyduran complex and in the area between the Melendiz volcanic center and Tepeköy area. The classical methods have also indicated that this area is rich of ironoxide minerals. Also when band ratios of 3/5, 3/2 and 5/2 are filtered the vegetation is mapped with a few pixels approving the prior filter.

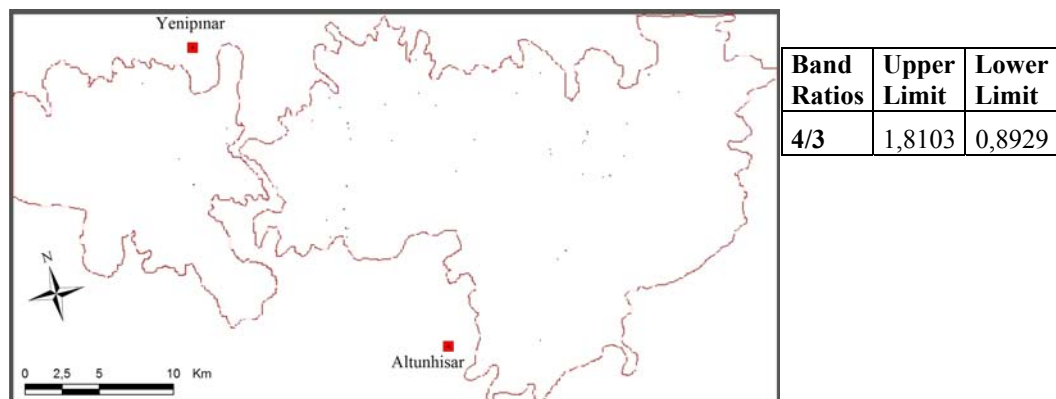


Figure 4.32. Band4/Band3 is filtered, when haze is removed.

4.3.11. Goethite Mapping

Goethite, as a ferric hydroxide has relatively lower reflectance in corresponding bands of 5 and 7 than hematite and jarosite.

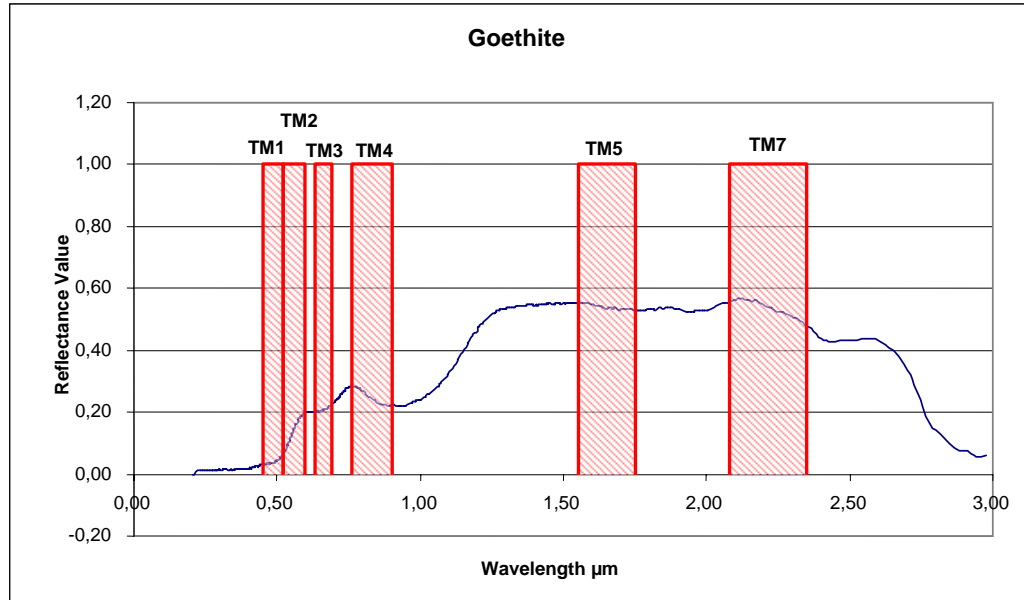


Figure 4.33. Spectral reflectance curve of goethite (USGS library).

Goethite is mapped on the western flanks of Keçiboyduran complex and like Hematite; in the area between the Melendiz volcanic center and Tepeköy area, also around the Melendiz volcanic center. Also when band ratios of 3/5, 3/2 and 5/2 are filtered noisy image with the vegetation is mapped, far from a precise result.



Figure 4.34. Band2/Band1 is filtered, when haze is removed.

4.3.12. Jarosite Mapping

Jarosite is highly reflective in band 5 interval and as the other iron-oxide minerals low reflectance in band 1 and moderate in band 3 intervals.

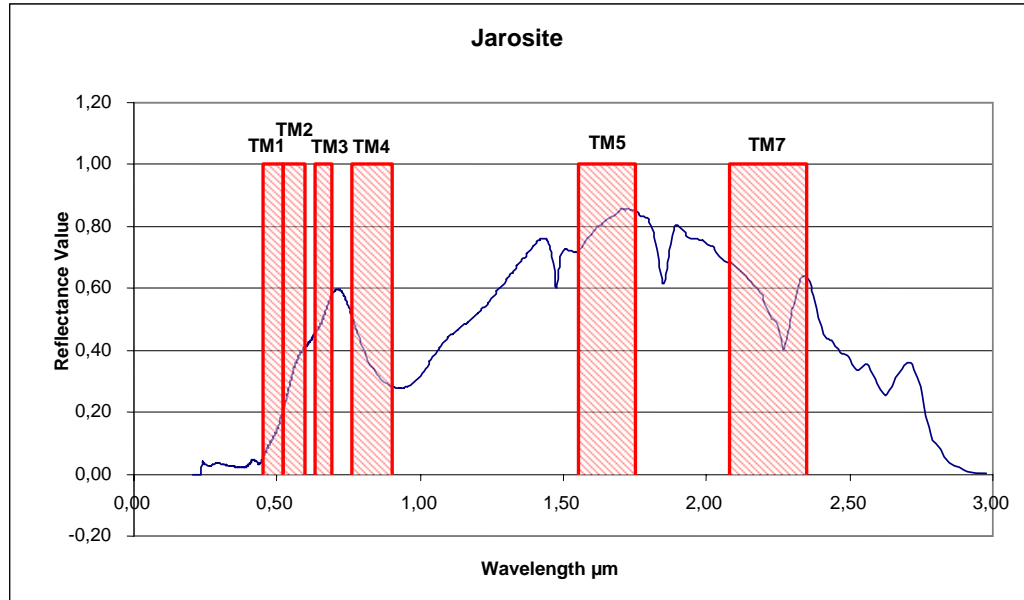


Figure 4.35. Spectral reflectance curve of jarosite (USGS library).

Jarosite is mapped on the southwestern flanks of Keçiboyduran complex and in a small area near the Melendiz volcanic center. Unlike the hematite and goethite jarosite couldn't be mapped by this filter combination. When ratios of 3/5, 3/2, 3/4, 4/1, 5/2, 4/5 are filtered very noisy image is obtained, like 3/4 of the area is covered with jarosite.



Figure 4.36. Band1/Band7 and Band1/Band5 are filtered.

4.3.13. Vegetation Mapping for Accuracy Assessment

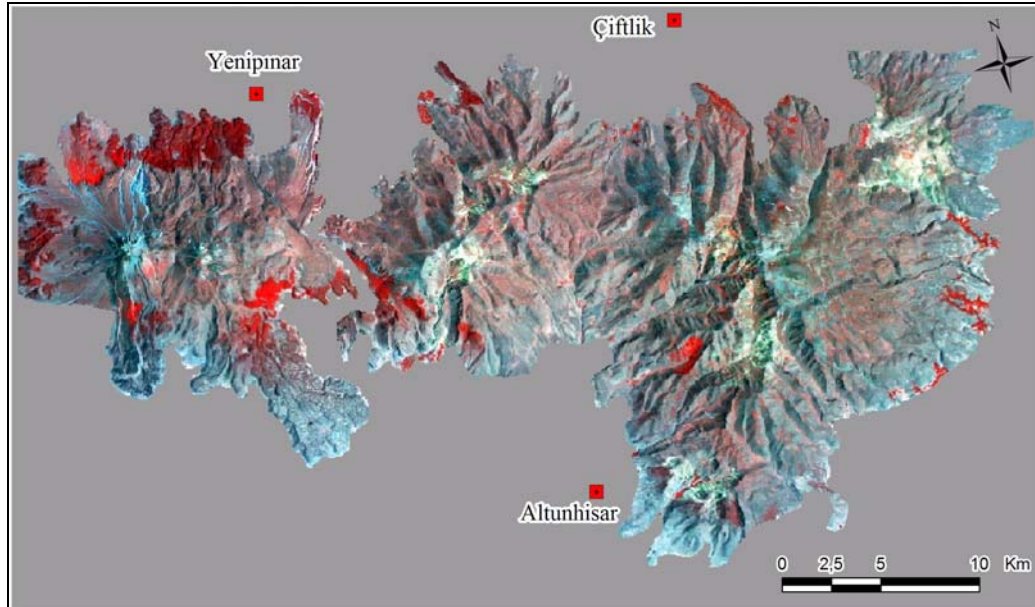
The quantitative way to explain the ability of the spectral analysis method is performed by an accuracy assessment procedure.

The color composite of bands 4, 2 and 1 is used as the reference data for the accuracy assessment procedure because visually the best differentiation of vegetation in the red channel is obtained (Fig. 4.37a). The RGB color composite of bands 4, 2 and 1; displays the vegetated areas in dark-medium red pixels. This reference color composite is filtered according to the pixel values in the vegetated areas. Pixel values between 80 and 160 for band 4, values between 43 and 30 for band 2, and values between 94 and 73 for band 1 are assigned to an output value of 1. Values, outside these ranges are assigned to 0. The resulting image is a binary map of vegetation derived from the original data (Figure 4.37b).

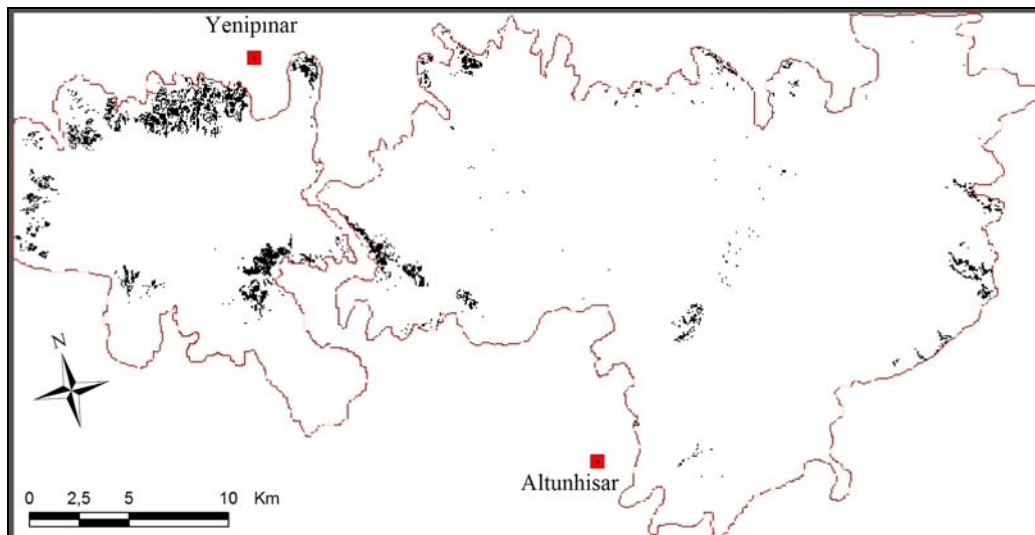
Cheat grass is selected from the USGS spectral library in order to perform an accuracy assessment process (Fig. 4.38a). Wide variety of vegetation types gives high reflectance in band 4 interval.

Band ratio of 1/4 is filtered by spectral analysis method that is explained in section 3.3.3 and resulting vegetation map is shown in Figure 4.38b. The red pixels in the color composite, fit perfectly to the black pixels (output is inverted) of the filtering output image. As known from principal component analysis only around %5 of the variance is vegetation. The filtering technique therefore filters the little vegetation information that is present in the image with a very high visual accuracy.

The pixels in the reference image and the image obtained after spectral analysis method are correlated to calculate the percentage accuracies (Table 4.6). Counted pixel values are shown in the table. Accordingly the (1,1) value is the pixels both mapped in the original data and in the spectral analysis result; (0,1) is the pixels displayed by original and missed by the analysis; (1,0) pixels are displayed only by analysis result and not exist in the original data and value of (0,0) are the pixels both did not displayed by original data and analysis result.

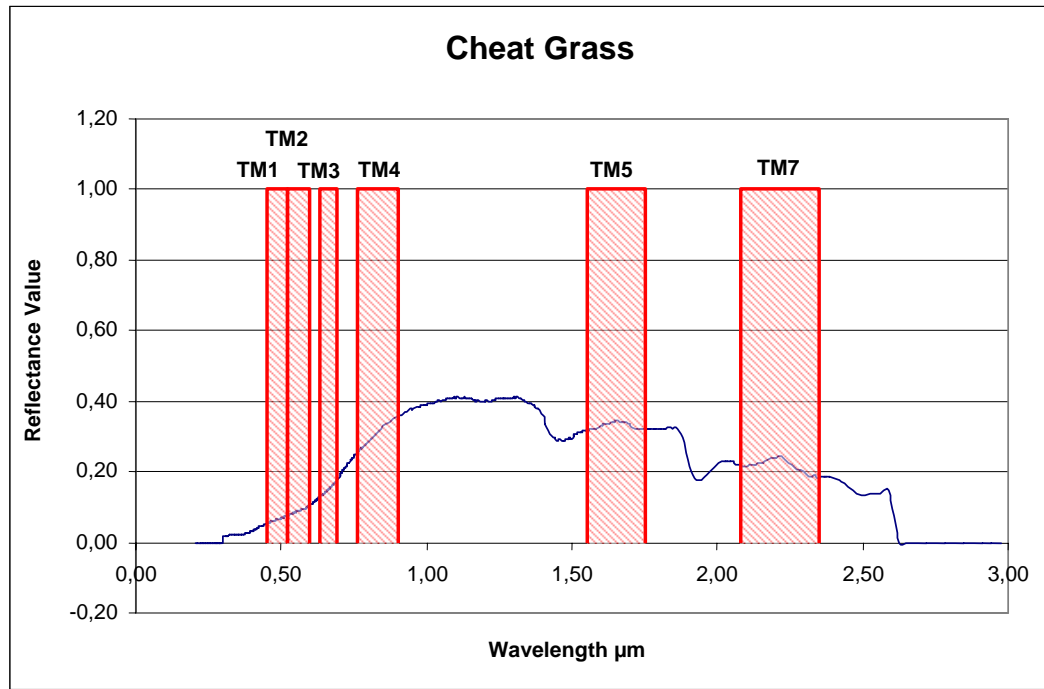


a.

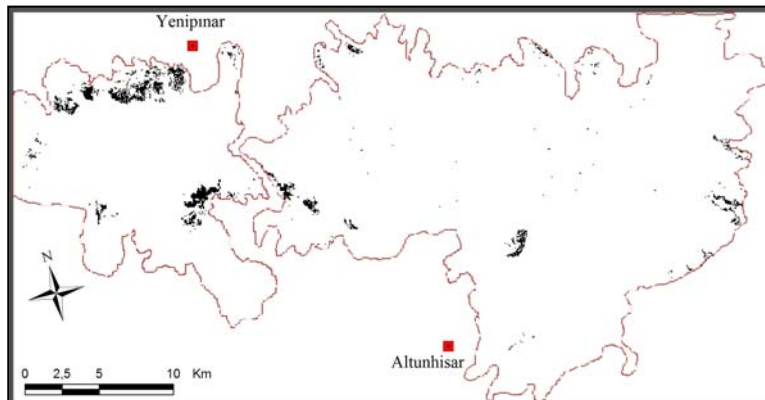


b.

Figure 4.37. Reference data. a. Color composite of band4, band2 and band1 as RGB b. Binary map of vegetation, filtered from the reference data.



a.



b.

Band Ratio	Upper Limit	Lower Limit
1/4	0,3310	0,1449

Figure 4.38. Spectral analysis data. a. Spectral reflectance curve of cheat grass (USGS) b. Band1 / Band4 is filtered with the statistically generated formula, black pixels are cheat grass.

Table 4.6. Accuracy assessment matrix

Correlation Matrix		Original Data		Total	Error of Commission		User Accuracy	
		1	0					
Spectral Analysis Result	1	10000 px (1,1)	5814 px (1,0)	15814	36,76	63,24		
	0	13428 px (0,1)	65535 px (0,0)	65535	17	83		
Total		23428	71349	94777				
	Error of Omission	57,32	8,15					
	Producer Accuracy	42,68	91,85					

Therefore, the pixel counts of values (1,1) and (0,0) give the number of correctly mapped pixels, hence accuracy. Total number of pixels (excluding nulls) is 94777, so the percentage calculations are as follows;

$$\text{Overall Accuracy} : \frac{10000 + 65535}{94777} \times 100 = 79,70$$

$$\text{Error of Omission}(0,1) : \frac{13428}{23428} \times 100 = 57,32$$

$$\text{Error of Commission}(1,0) : \frac{5814}{15814} \times 100 = 36,76$$

The error of omission percentage refers to the pixels that are omitted in the analysis results and the error of commission percentage refers to the pixels incorrectly mapped by the analysis. Corollary of omission error is ‘Producer Accuracy’ and refers to the probability of a displayed pixel to have the same value as the original data. ‘User Accuracy’ is the probability of the original pixel to be mapped correctly by the analysis method and is the corollary of commission error.

The accuracy of the filtering technique can be increased with the increasing number of band ratios being filtered at the same time.

CHAPTER 5

DISCUSSION AND CONCLUSIONS

Processing the images returned a number of output maps directly or indirectly related with alteration. Literally known methods will be discussed separately from the proposed ‘spectral filtering’ method. The result of merging of these separate outputs will be discussed to state the final conclusions.

5.1. Data

The alteration mapping is mainly the mapping of alteration minerals. As the focused point is the minerals within a rock unit, the size of these minerals is defined in centimeters. The TM data used in this study has spatial resolution of 30 m, which is one pixel represents a 30 x 30 m area on the surface. Spatially the desired information does not exist in the image we have. But in the case of alteration minerals, the wide colorful distribution gives way to a chance to be mapped. Likewise clay altered area with dimensions of 5 x 5 km in normal conditions should be mapped by TM data.

As discussed in Chapter 3, it is not only the spatial resolution but also the spectral resolution of the satellite system equally important in alteration mineral mapping. Landsat TM 5 has 7 bands one of which is in thermal infrared region. Most of alteration minerals have spectrally speaking, small scale signatures in their reflectance patterns. Abrupt changes occur in reflectance spectra within a nanometer (0,001 μm) wavelength range. With band intervals like 0.45 – 0.52 (TM band 1) it is unlikely to catch those important signatures.

5.2. Conventional Techniques of Alteration Mapping

Generally all of the four literally publicized methods are found to be effective for obtaining generalized information about the alteration of the image area. But none of them is found to be capable of displaying the mineral-based alteration maps. The reason of this expected result is just because of the data type we are using.

Color composites are found to be fast and accurate in general mapping of alteration. Among the all methods applied in this study the color composite method requires the least data transformation. They are incapable of displaying detailed map of alteration and the precision of the output maps are very low.

Band ratios are relatively successful in generating precise alteration zones.

Principal component analysis, especially the feature oriented PCA returned very accurate results that are overlapping with the ancillary alteration data of the study area. The method is effective in delineating the borders of clay and iron oxide altered areas but ineffective in mapping the mineral based alteration areas (Fig. 5.1). The method is incapable of differentiating the hematite and jarosite or kaolinite and illite.

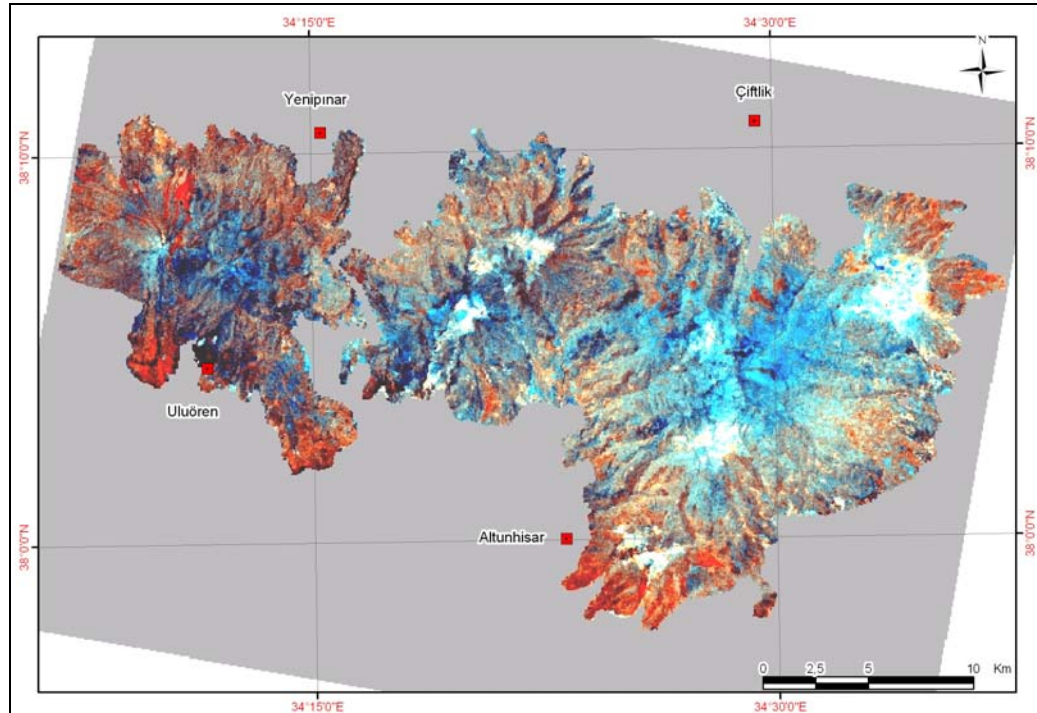


Figure 5.1. Color composite of Crosta H, H+F and F as RGB.

Least squares fitting method has the similar precision with PCA. General outlines of alteration are mapped with Ls-fit. technique (Fig. 5.2).

All of the conventional methods agree that the volcanic eruption centers of Tepek y, Ke iboyduran and Melendiz volcanic complexes are highly altered having both clay and iron oxide minerals and away from the centers, iron oxide zone is mapped in PCA and Ls-fit. techniques.

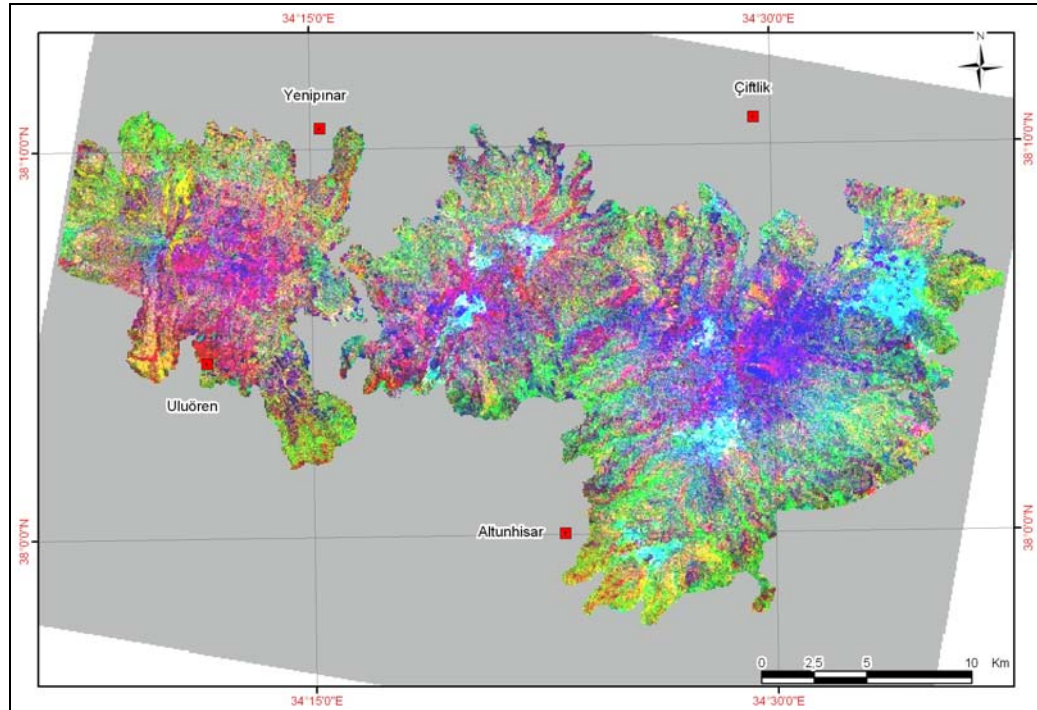


Figure 5.2. Color composite of residual bands 3, 7 and 1 as RGB.

5.3. Mineral mapping by using spectral reflectance data

The proposed method aimed to map the alteration minerals individually. Statistical method of filtering the band ratios is tested and found to be very accurate with the vegetation data. For every mineral 30 combinations of band ratios are present. Bands that are likely to give high ratios are selected for the filtering process. Although some of the previously known clay altered areas could not be mapped, in general the results were coincident with the previously applied methods. Detailed mineral maps are obtained as outputs of this method. The resulting mineral maps are grouped for ironoxide minerals and clay minerals separately (Fig. 5.3, Fig. 5.5). In Figure 5.3, main ironoxide-rich areas are mapped in Tepek y, Melendiz and Ke iboyduran volcanic centers and along a

north-south trending linear path in the west of Keçiboyduran volcanic center. This linear concentration overlaps with the buried fault in the same area by Toprak, 1998 (Fig. 2.2).

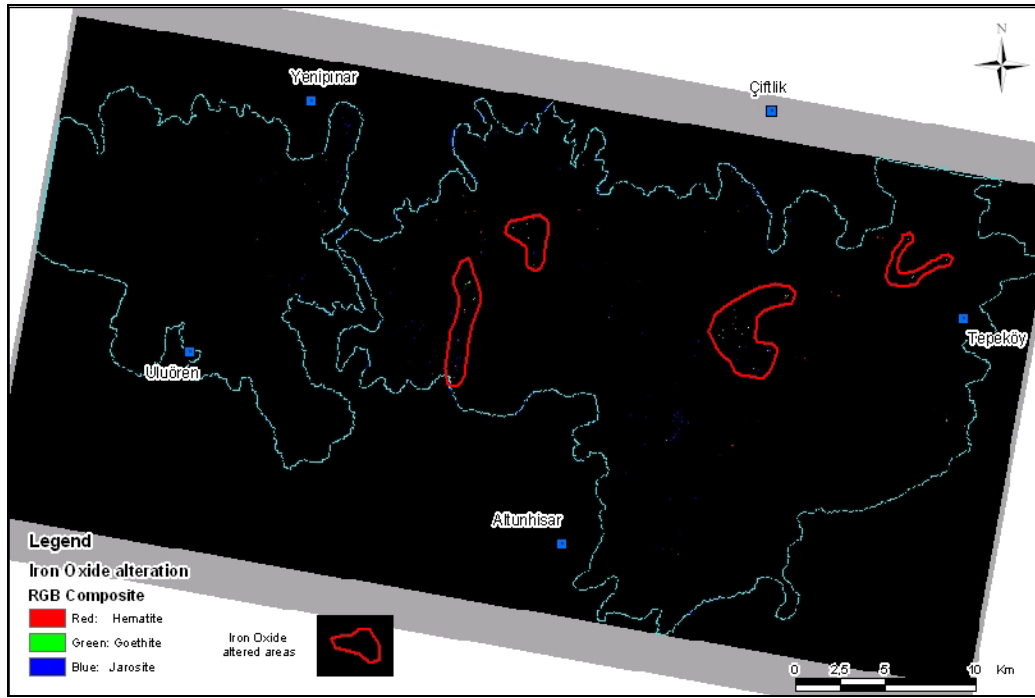


Figure 5.3. Ironoxide-rich areas obtained by spectral library analysis.

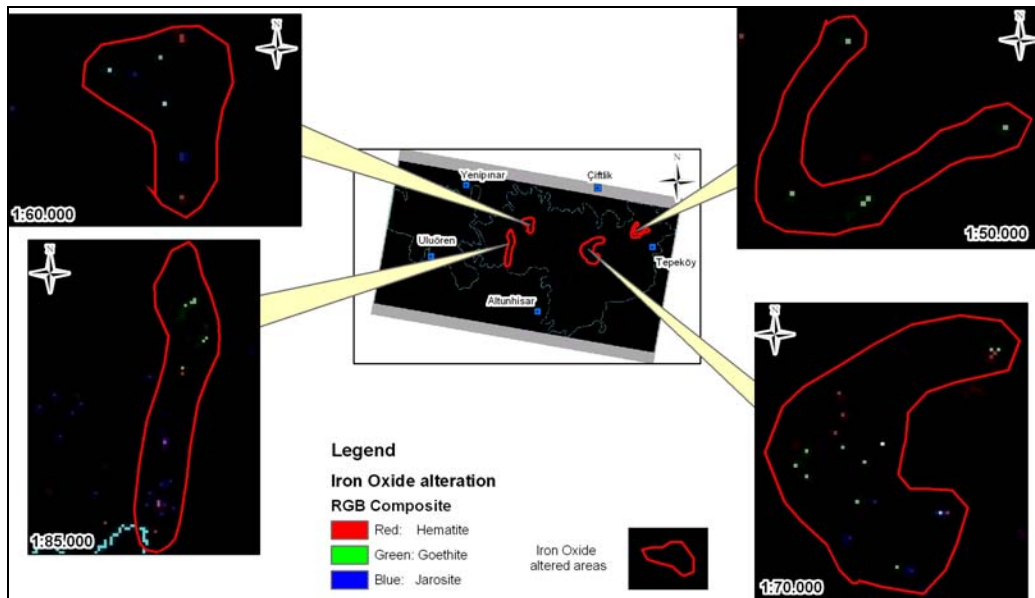


Figure 5.4. Close up views of ironoxide-rich pixels.

Clay-rich areas in Figure 5.5 are mapped in Melendiz volcanic center, in the Tepeköy volcanic center, in the northwest flanks of Hasandağ complex and a

small area between Keçiboyduran and Hasandağ volcanic complexes directed along Tuzgölü fault zone (Fig. 2.2).

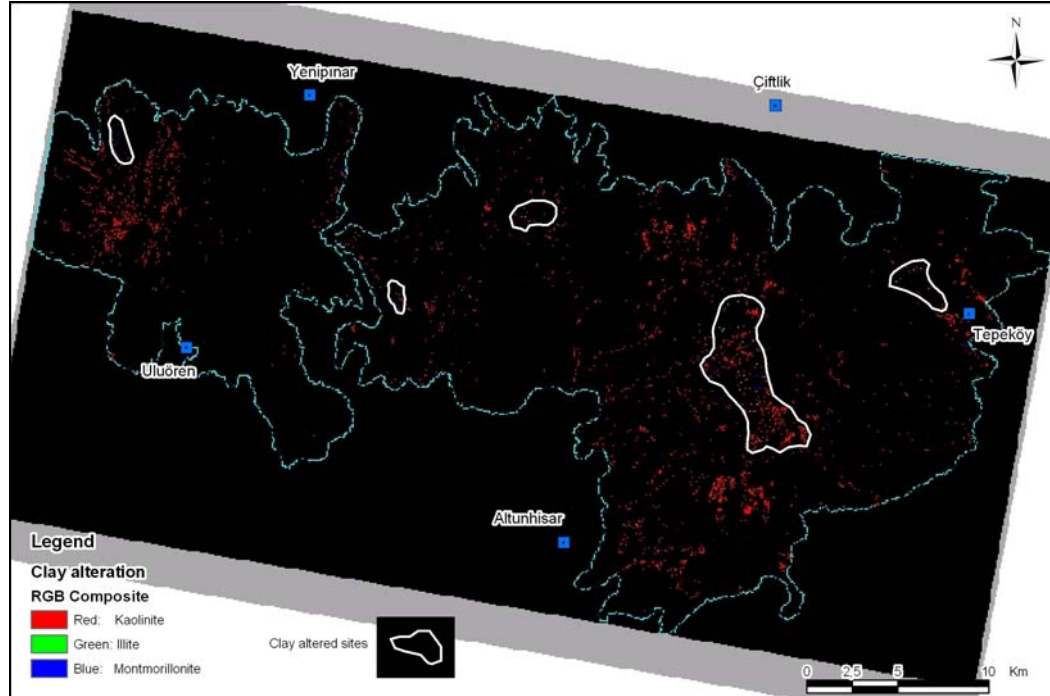


Figure 5.5. Clay minerals-rich areas obtained by spectral library analysis.

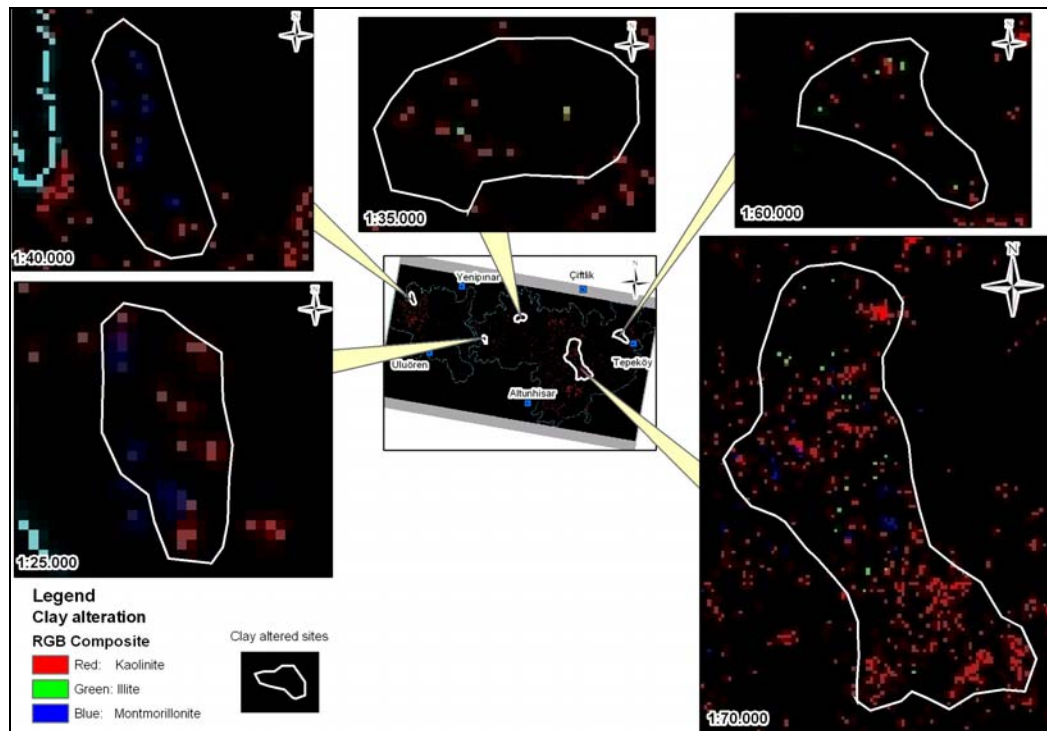


Figure 5.6. Close up views of clay-rich pixels.

Melendiz volcanic center is mapped as both clay and ironoxide altered, where small areas of Tepek y and Hasandağ volcanic complexes are mapped as ironoxide altered only.

However there are significant intersections with the conventional methods' outputs and mineral mapping method outputs, Tepek y volcanic center, mapped as both clay and ironoxide rich in classical ways, is mapped as more fresh by the spectral analysis method (Fig. 5.7).

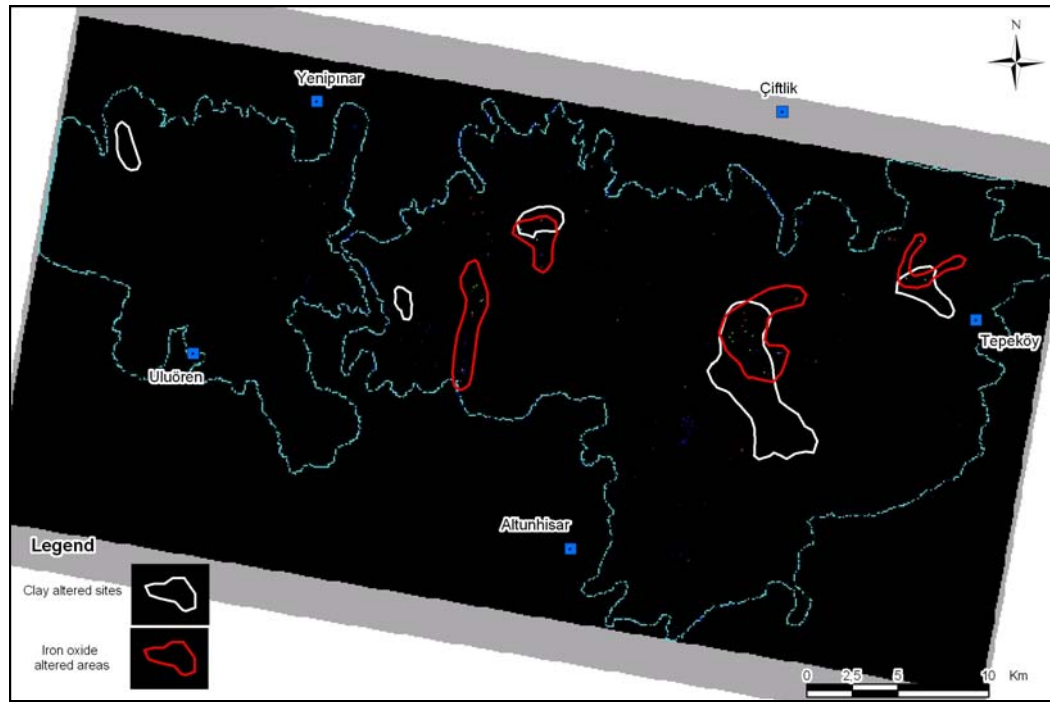


Figure 5.7. Areas that are both clay and iron oxide altered.

5.4. Further Recommendations

Instead of the ancillary alteration data that is used for accuracy assessment, a field study should be carried on and this study should include the systematic rock sampling to reveal the geochemistry of the area, thus clarifying the accuracy of the mineral maps and alteration maps generated by conventional methods.

The methods applied in this study should be revised and used with the hyperspectral data.

REFERENCES

- Abdelhamid G. and Rabba I., 1994. An investigation of mineralized zones revealed during geological mapping, Jabal Hamra Faddan-Wadi Araba, Jordan, using Landsat TM data. *Int. J. Remote Sensing*, vol. 15, No. 7, 1495 – 1506.
- Abrams J. Michael, 1983. Remote Sensing for Porphyry Copper Deposits in Southern Arizona. *Economic Geology* vol. 78, 1983, pp. 591-604.
- Amos, B. J., Greenbaum, D., 1989. Alteration detection using TM imagery. The effects of the supergene weathering in an arid climate. *Int. J. Remote Sensing*, vol. 20, No. 3, 515-527.
- Aydar, E., Gündoğdu, N., Bayhan, H. and Gourgaud, A., 1994. Volcano-structural and petrological investigation of the Cappadocian Quaternary volcanism, *TUBİTAK Yerbilimleri Dergisi*, 3: 25-42.
- Beane, R.E., 1982, Hydrothermal alteration in silicate rocks, southwestern North America *in* Titley, S. R., ed., *Advances in Geology of the Porphyry Copper Deposits, Southwestern North America*: Tucson, Univ. Ariz. Press, Chapter 6.
- Beekman, P.H., 1966. The Pliocene and Quaternary volcanism in the Hasan Dağ-Melendiz Dağ region. *Bulletin of Mineral Resources and Exploration Institute, Ankara*, 66, 90-105.

- Besang, C., Eckhardt, F.J., Harre, W., Kreuzer, H., Müller, P., 1977. Radiometrische Alterbestimmungen an Neogenen Eruptivgesteinen der Türkei. Geol. Jb. B 25, 3-36.
- Chica-Olmo M., Abarca F., 2002. Development of a Decision Support System based on remote sensing and GIS techniques for gold-rich area identification in SE Spain. International Journal of Remote Sensing, 23, 22, 4801-4814.
- Chavez, Pat. S., 1989. Extracting spectral contrast in Landsat Thematic Mapper image data using selective principal component analysis. Photogrammetric Engineering and Remote Sensing, vol. 55, No. 3, pp. 339 – 348.
- Clark, R. N., Gallagher, A. J., & Swayze, G. A. (1990). Material absorption band depth mapping of imaging spectrometer data using a complete band shape least-squares fit with library reference spectra. In R. O. Green (Ed.), Proceedings of the second airborne visible/infrared imaging spectrometer (AVIRIS) workshop. JPL Publication, 90-54, 176-186.
- Deniel, C, *et al.*, 1998, The Hasan Dağı stratovolcano Central Anatolia, Turkey : evolution from calc-alkaline to alkaline magmatism in a collision, Journal of Volcanology and Geothermal Research 87, 275–302.
- Dhont, D., Chorowicz, J., Yürür, T., Froger, J-L, Köse, O., Gündoğdu, N., 1998, Emplacement of volcanic vents and geodynamics of Central Anatolia, Turkey, Journal of Volcanology and Geothermal Research 85, 33–54.
- Ercan, T., Tokel, S., Matsuda, J., Ul, T., Notsu, K. and Fujitani, T., 1992. New geochemical, isotopic and radiometric data of the Quaternary volcanism of Hasandağı-Karacadağ (Central Anatolia), TJK Bülteni, 7: 8-21 (In Turkish with English abstract).

- Ercan, T., Fujitani, T., Matsuda, J.I., Tokel, S., Notsu, K., Ul, T., Can, B., Selvi, Y., Yıldırım, T., Fişekçi, A., Ölmez, M. and Akbaşlı, A., 1990. The origin and evolution of the Cenozoic volcanism of Hasandağı-Karacadağ area (Central Anatolia), *Jeomorfoloji Dergisi*, 18: 39-54 (In Turkish with English abstract).
- Faruqi, S. A., 1991. Remote sensing studies for identification of exploration targets around Malanjkhand copper deposit of central India. *Proceedings of 8th Thematic Conference on Geologic Remote Sensing*, Denver, Colorado, USA, April 29 – May 2, 1991.
- Ferrier G., White K., Griffiths G., Bryant R., Stefouli M., 2002. The mapping of hydrothermal alteration zones on the island of Lesvos, Greece using an integrated remote sensing dataset. *International Journal of Remote Sensing*, 23, 2, 341-356.
- Froger, J-L, Lenat, J-F, Chorowicz, J., Le Penneç, J-L, Bourdier, J-L, Köse, O, Zimitoğlu, O., Gündoğdu, N.M., Gourgaud, A., 1998, Hidden calderas evidenced by multisource geophysical data; example of Cappadocian Calderas, Central Anatolia, *Journal of Volcanology and Geothermal Research* 185, 99–128
- Goossens, M. A., and Kroonenberg, S. B., 1994. Spectral discrimination of contact metamorphic zones and its potential for mineral exploration, province of Salamanca, Spain. *Remote Sensing of the Environment*, 47, 331-344.
- Göncüoğlu, M. C. and Toprak, V., 1992. Neogene and Quaternary Volcanism of Central Anatolia: A Volcano-Structural Evaluation. *Bulletin de la Section de Volcanologie, Societe Géologique de France*, 26, 1 – 6.
- Guilbert, M. John, Park, F. Charles, 1986. *The Geology of Ore Deposits*. W.H. Freeman, New York.

- Innocenti, F., Mazzuoli, R., Pasquare, G., Radicatti Di Brozolo, F., Villari, L., 1975. The Neogene calcalkaline volcanism of Central Anatolia: geochronological data on Kayseri-Niğde area. *Geol. Mag.* 112(4), 349-360.
- Jensen, R. John, 1996. *Introductory Digital Image Processing A Remote Sensing Perspective* 2nd edition, Upper Saddle River, Prentice Hall, New Jersey.
- Jingyuan Y., Xucman W., 1991. The Application of Remote Sensing Techniques for Gold Prospecting in the North Fujian Province. *Proceedings of 8th Thematic Conference on Geologic Remote Sensing*, Denver, Colorado, USA, April 29 – May 2, 1991.
- Kaufmann, H., 1988. Mineral Exploration Along the Auaba-Levant Structure by Use of TM-data. Concepts, Processing and Results. *Int. J. Remote Sensing*, vol. 9, No. 10 and 11, 1639-1658.
- Le Pennec, J.-L., Bourdier, J.-L., Froger, J.-L., Temel, A., Camus, G., Gorgaud, A., 1994. Neogene Ignimbrites of Nevşehir Plateau (central Turkey): Stratigraphy, Distribution and Source Constraints. *J. Volcanol. And Geotherm. Res.* 63, 59-87.
- Loughlin, W. P., 1991. Principal Component Analysis for Alteration Mapping. *Proceedings of 8th Thematic Conference on Geologic Remote Sensing*, Denver, Colorado, USA, April 29 – May 2, 1991.
- Mather, M. Paul, 1989. *Computer Processing of Remotely Sensed Images: An Introduction*. John Wiley and Sons, Great Britain.
- Vincent, K. Robert, 1997. *Fundamentals of Geological and Environmental Remote Sensing*. Prentice Hall, Upper Saddle River, New Jersey.

- Pasquare, G., 1968, Geology of the Cenozoic Volcanic Area of the Central Anatolia, *Atti Accad. Naz. Lincei*, 9, 53-204.
- Pasquare, G., Poli, S., Vezzoli, L., Zanchi, A., 1988. Continental Arc Volcanism and Tectonic Setting in Central Anatolia, Turkey. *Tectonophysics* 146, 217-230.
- Rothery, D. A., 1987. Improved discrimination of rock units using Landsat Thematic Mapper imagery of the Oman ophiolite. *Journal of the Geological Society, London*, vol. 144, 587-597.
- Rowan, L.C., Crowley J.K., Schmidt R.G., Ager C.M., Mars J.C., 2000. Mapping hydrothermally altered rocks by analyzing hyperspectral image (AVIRIS) data of forested areas in the Southeastern United States. *Journal of Geochemical Exploration* 68, 145–166.
- Sabins, F.F., 1999. Remote sensing for mineral exploration. *Ore Geology Reviews* 14, 157–183.
- Tangestani, M.H. and Moore F., 2002. Porphyry copper alteration mapping at the Meiduk area, Iran. *International Journal of Remote Sensing*, 23, 22, 4815-4825.
- Temel, A., Gündoğdu, M.N., Gourgaud, A., Le Pennec, J.-L., 1998. Ignimbrites of Cappadocia (Central Anatolia, Turkey): petrology and geochemistry. *Jour. of Volc. And Geotherm. Res.* 85, 447-471.
- Toprak, V., Göncüoğlu, M.C., 1993. Tectonic control on the development of the Neogene-Quaternary Central Anatolian Volcanic Province, Turkey. *Geological Journal* 28, 357-369.

Toprak, V., 1994. Central Kızılırmak fault zone: Northern margin of Central Anatolian Volcanics.

Toprak, V., 1996. Kapadokya Volkanik Çöküntüsünde Gelişmiş Kuvaterner Yaşlı Havzaların Kökeni, Orta Anadolu. Jeoloji Müh. Böl. 30. yıl sempozy. Bildirileri.

Toprak, V. and Göncüoğlu, M.C., 1993. Keçiboyduran – Melendiz Fault and its regional significance (Central Anatolia). Yerbilimleri 16, 55 – 65.

Toprak, V., 1998. Vent distribution and its relation to regional tectonics, Cappadocian Volcanics, Turkey. Journal of Volcanology and Geothermal Research 85, 55 – 67.

USGS Spectral Library Data. <http://speclab.cr.gov/>